FINNISH METEOROLOGICAL INSTITUTE
CONTRIBUTIONS

No. 80

# ELECTROMAGNETIC SIGNATURES OF LIGHTNING NEAR THE HF FREQUENCY BAND

JAKKE MÄKELÄ

DEPARTMENT OF PHYSICS
FACULTY OF SCIENCE
UNIVERSITY OF HELSINKI
HELSINKI, FINLAND

ACADEMIC DISSERTATION in physics

To be presented, with the permission of the Faculty of Physics of the University of Helsinki, for public examination in auditorium A110 of the Chemicum building (A.I.Virtasen aukio 1), on the 25th of January 2010, at 12 o'clock noon.

Finnish Meteorological Institute
Helsinki, 2009

ISBN 978-951-697-703-7 (paperback)
ISBN 978-951-697-704-4 (PDF)
ISSN 0782-6117

Yliopistopaino
Helsinki, 2009

FINNISH METEOROLOGICAL INSTITUTE

Series title, number and report code of publication
Contributions 80, FMI-CONT-80

Published by Finnish Meteorological Institute
(Erik Palménin aukio 1) P.O. Box 503
FI-00101 Helsinki, Finland

Date
December 2009

Author
Jakke Mäkelä

Title

Electromagnetic signatures of lightning near the HF frequency band

Abstract

The dissertation deals with remote narrowband measurements of the electromagnetic radiation emitted by lightning flashes. A lightning flash consists of a number of sub-processes. The return stroke, which transfers electrical charge from the thundercloud to to the ground, is electromagnetically an impulsive wideband process; that is, it emits radiation at most frequencies in the electromagnetic spectrum, but its duration is only some tens of microseconds. Before and after the return stroke, multiple sub-processes redistribute electrical charges within the thundercloud. These sub-processes can last for tens to hundreds of milliseconds, many orders of magnitude longer than the return stroke. Each sub-process causes radiation with specific time-domain characteristics, having maxima at different frequencies. Thus, if the radiation is measured at a single narrow frequency band, it is difficult to identify the sub-processes, and some sub-processes can be missed altogether. However, narrowband detectors are simple to design and miniaturize. In particular, near the High Frequency band (High Frequency, 3 MHz to 30 MHz), ordinary shortwave radios can, in principle, be used as detectors. This dissertation utilizes a prototype detector which is essentially a handheld AM radio receiver. Measurements were made in Scandinavia, and several independent data sources were used to identify lightning sub-processes, as well as the distance to each individual flash.

It is shown that multiple sub-processes radiate strongly near the HF band. The return stroke usually radiates intensely, but it cannot be reliably identified from the time-domain signal alone. This means that a narrowband measurement is best used to characterize the energy of the radiation integrated over the whole flash, without attempting to identify individual processes. The dissertation analyzes the conditions under which this integrated energy can be used to estimate the distance to the flash. It is shown that flash-by-flash variations are large, but the integrated energy is very sensitive to changes in the distance, dropping as approximately the inverse cube root of the distance. Flashes can, in principle, be detected at distances of more than 100 km, but since the ground conductivity can vary, ranging accuracy drops dramatically at distances larger than 20 km. These limitations mean that individual flashes cannot be ranged accurately using a single narrowband detector, and the useful range is limited to 30 kilometers at the most. Nevertheless, simple statistical corrections are developed, which enable an accurate estimate of the distance to the closest edge of an active storm cell, as well as the approach speed. The results of the dissertation could therefore have practical applications in real-time short-range lightning detection and warning systems.

Classification (UDK)
551.594, 551.94.2, 551.584.221, 551.501.7

Keywords
Lightning, electromagnetic radiation, narrowband measurements, lightning ranging

ISSN and series title
0782-6117 Finnish Meteorological Institute Contributions

ISBN 978-951-697-703-7 (paperback)
ISBN 978-951-697-704-4 (pdf)

Language
English

Sold by
Finnish Meteorological Institute
PO Box 503, FI-00101 HELSINKI

Pages
152

Price

ILMATIETEEN LAITOS

Julkaisun sarja, numero ja raporttikoodi
Contributions 80, FMI-CONT-80

Julkaisija Ilmatieteen laitos (Erik Palménin aukio 1)
PL 503, 00101 Helsinki

Julkaisuaika
Joulukuu 2009

Tekijä
Jakke Mäkelä

Nimeke

Salamaprosessien sähkömagneettinen säteily HF-taajuusalueella

Tiivistelmä

Tässä tutkimuksessa tarkastellaan salamoiden aiheuttaman sähkömagneettisen säteilyn etämittauksia. Salama koostuu useista aliprosesseista, joilla kaikilla on erilaiset säteilyominaisuudet. Pääsalama, joka siirtää sähköistä varausta ukkospilvestä maahan, on impulsiivinen ja laajakaistainen prosessi. Se säteilee lähes kaikilla sähkömagneettisen spektrin taajuuksilla, mutta sen kesto on vain kymmeniä mikrosekunteja. Varaukset siirtyvät ukkospilven sisällä myös ennen ja jälkeen pääsalaman, ja nämä aliprosessit aiheuttavat pitkäkestoisempaa säteilyä. Näiden aliprosessien kesto voi olla kymmeniä tai satoja millisekunteja, eli satoja kertoja pidempi kuin pääsalaman, ja kukin säteilee voimakkaimmin eri taajuuksilla. Jos säteilyä siis mitataan yhdellä kapealla taajuuskaistalla, yksittäisiä aliprosesseja on vaikea tunnistaa, ja jotkin aliprosessit saattavat jäädä kokonaan havaitsematta. Kapeakaistaisia mittauksia voidaan kuitenkin tehdä yksinkertaisilla ja pienikokoisilla laitteilla. Erityisesti HF-taajuusalueella (High Frequency, 3 MHz-30 MHz) voidaan periaatteessa käyttää tavallista lyhytaaltoradiota. Työssä on käytetty prototyyppilaitetta, joka perustuu AM-radion toimintaperiaatteisiin. Mittauksia suoritettiin Skandinaviassa, käyttäen useita riippumattomia vertailumittauksia. Näiden avulla pystytään tunnistamaan salaman aliprosessit, sekä arvioimaan salamaniskun etäisyys mittauspisteestä.

Tutkimuksessa osoitetaan, että useat aliprosessit aiheuttavat voimakasta säteilyä HF-taajuuksilla. Pääsalaman säteily on erityisen voimakasta, mutta pääsalama on vaikea tunnistaa pelkän aikasignaalin pohjalta. Käytännössä kapeakaistaisesta signaalista voidaan arvioida salaman säteilemä kokonaisenergia koko salamaniskun ajalta. Tutkimuksessa selvitetään, millä edellytyksillä tätä kokonaisenergiaa voidaan käyttää salaman etäisyyden arviointiin. Iskujen välillä on suuria eroja, mutta salamaniskujen kokonaisenergia muuttuu nopeasti etäisyyden funktiona. Salamaniskuja voidaan periaatteessa havaita yli sadan kilometrin etäisyydeltä, mutta maanpinnan johtavuuserojen takia etäisyysarvion tarkkuus heikkenee huomattavasti, kun etäisyys on yli 20 kilometriä. Näiden rajoitteiden perusteella voidaan todeta, että yhdellä kapeakaistaisella vastaanottimella ei voida realistisesti arvioida yksittäisten salamaniskujen etäisyyttä. Tutkimuksessa kehitetään kuitenkin yksinkertainen tilastollinen menetelmä, jolla voidaan riittävän tarkasti arvioida etäisyys myrskysolun lähimpään reunaan. Myös solun etenemisnopeus voidaan arvioida tällä menetelmällä. Tutkimuksessa havaittuja tuloksia voidaan soveltaa aktiivisten ukkosmyrskyjen reaaliaikaiseen havaitsemiseen ja niistä varoittamiseen.

Luokitus (UDK)
551.594, 551.94.2, 551.584.221, 551.501.7

Asiasanat
Salama, sähkömagneettinen säteily, kapeakaistainen mittaus, salaman etäisyys

ISSN ja avainnimike
0782-6117 Finnish Meteorological Institute Contributions

ISBN 978-951-697-703-7 (paperback)
ISBN 978-951-697-704-4 (pdf)

Kieli
Englanti

Myynti
Ilmatieteen laitos
PL 503, FI-00101 HELSINKI

Sivumäärä
152

Hinta

## Errata

Paper I: The headings of the subplots in Figures 3-6 should read “Flash 27”.

Paper IV: The first sentence of Section 4 should read “The analysis in Section 3 was based…”

Paper IV: Equation (6) should read $E_0 = \sqrt{1/\alpha\beta}\sqrt{E_1 E_2 R_1^{\,k} R_2^{\,k}}$ .

# Acknowledgements

It was a dark and stormy night, most memorably the night of the overhead storm of July 24, 2006, when some of the best measurements for this thesis were made, a man and his oscilloscope alone against the violent forces of nature; but, as always in science, the real work was done within a large and variegated team. My advisors, Dr Vernon Cooray and Dr Tapio Tuomi, were always available when needed, and always quiet when not needed; such steering is what a graduate student most appreciates. At Nokia, the core team of Niko Porjo, Joni Jantunen, and Tom Ahola did most of the work that actually required knowing what one was doing, with Ari Hämäläinen and Simo Apell pitching in at crucial times. Anyone who has observed my Mr Bean-like approach to all things electronic will appreciate that this dissertation would not exist without them. Terho Kaikuranta, Seppo Nissilä, and Kari Pitkäranta are thanked for their help within the dark world of Corporate Management, giving the project life support over the years. The coffee-hour team in Salo (Juhola, Östergård, Parikka, Naula, Salminen) helped minimize the general misery of working in Salo. At FMI, Antti Mäkelä helped understand the bizarre quirks of lightning detection networks. The dissertation was painstakingly reviewed by Dr Risto Pirjola and Dr Farhad Rachidi, forcing considerable reworking of some of the text. I thank the Finnish Meteorological Institute for financial support with the printing of the dissertation. The University of Uppsala provided a much-needed island of academic eccentricity in an ocean of business-minded conformity; thanks go in particular to Raul Montaño, Marley Becerra, Mahbubur Rahman, Zikri Baharuddin, Linda Ahmad, and Mahendra Fernando. I thank my parents and sisters (Jaakko, Maija, Mirkka, and Maria), not least for babysitting when lightning took me where children could not go, but also for showing general interest in the project. Perhaps counterintuitively, I note with gratitude that my wife and children showed very little general interest the project. A family is meant to be a family, not a logistical support function for a PhD program. So thank you Hanna, Hilla, Ilona, and Artturi, for holding my obsession to a somewhat manageable level, and keeping me cognizant of the ancient folk wisdom: lightning is transient, but family is permanent.

# Contents

## List of original publications

This thesis is based on the following publications:

I (Mäkelä et al (2007)) Mäkelä, J.S., Edirisinghe, M., Fernando, M., Montaño, R. and Cooray, V., 2007. HF radiation emitted by chaotic leader processes. Journal of Atmospheric and Solar-Terrestrial Physics 69, Issue 6, 707-720.

II (Mäkelä et al (2008b)) Mäkelä, J.S., Porjo, N., Jantunen, J., Ahola, T. and Hämäläinen, A., 2008. Using full-flash narrowband energy for ranging of lightning ground strokes. Journal of Atmospheric and Solar-Terrestrial Physics 70, Issue 1, 156-168.

III (Mäkelä et al (2008c)) Mäkelä, J.S., Porjo, N., Mäkelä, A., Tuomi, T. and Cooray, V., 2008. Properties of preliminary breakdown processes in Scandinavian lightning. Journal of Atmospheric and Solar-Terrestrial Physics 70, Issue 16, 2041-2052.

IV (Mäkelä et al (2009)) Mäkelä, J.S., Porjo, N., Jantunen, J., Ahola, T., Mäkelä, A., Tuomi, T. and Cooray, V., 2009. Single-station narrowband ranging of active storm cells without lightning-type discrimination. Journal of Atmospheric and Solar-Terrestrial Physics 71, Issues 8-9, 911-922.

The publications are referred to in the text by their Roman numerals. The author of the thesis is the first author in all four papers, and is therefore responsible for overall planning of the papers, all data analysis, and interpretation of the results. The measurements of Paper I were perfomed by the co-athors. The measurement devices used in Papers II-IV were designed primarily by the co-authors, but the measurements were also performed by the author.

Detailed technical information on the narrowband devices is presented as a separate Appendix. Most of the practical design work was done by the co-authors of papers II-IV, and therefore this information is not presented as part of the main thesis. The information is, however, important for understanding and validating the results discussed in the thesis.

## Abbreviations

| | |
|---|---|
| AM | Amplitude Modulation |
| CG | Cloud-to-Ground (flash, lightning) |
| DF | Direction Finding |
| LF | Low Frequency (30 kHz-300 kHz) |
| HF | High Frequency (3 MHz-30MHz) |
| FFT | Fast Fourier Transform |
| IC | Intra-cloud (flash, lightning) |
| MF | Medium Frequency (300 kHz -3MHz) |
| MW | Medium Wave (approximately 520 kHz-1610 kHz) |
| NPBP | Narrow Positive Bipolar Pulse |
| PBP | Preliminary breakdown Process |
| RMS | Root-mean-square |
| SL | Stepped leader |
| VHF | Very High Frequency (30 MHz-300 MHz) |

# 1 Introduction

The purpose of this thesis is to evaluate the amount of physical information that can be determined by measuring lightning at a narrow frequency band. Lightning is electromagnetically a wideband phenomenon that radiates at all electromagnetic frequencies from near DC to X-ray. In addition, a lightning flash consists of a large number of sub-processes, each of which radiates with its own particular characteristics. There are three main types of lightning flash: negative cloud-to-ground (CG) flashes, which transport negative charge from the cloud to the ground; positive CG flashes, which transport positive charge; and intra-cloud (IC) flashes, which transport charge within the cloud without ever reaching the ground. Of these three types of lightning discharge, negative cloud-to-ground flashes are by far the best understood. The description below is based on generally accepted models of negative lightning flashes, although even in this case some details are still controversial.

As charges separate within a thundercloud, the static electric field grows until it reaches a level at which an electrical breakdown can occur. The terminology with respect to the very earliest stages of the breakdown is still not completely standardized. It is, however, accepted that there a negative CG flash typically begins with a preliminary breakdown process (PBP). The detailed sub-processes which occur within the PBP are still under active study. The duration of the PBP is not always well defined, but the time duration between the first breakdown and the return stroke is typically some tens of milliseconds. Before the return stroke, a stepped leader (SL) is formed, consisting of segments which propagate in discrete jumps and can be seen visually. A clearly identifiable SL stage lasts between 10 and 20 milliseconds (although there may be some overlap with the PBP stage). The return stroke occurs when the downward stepped leader becomes connected with an upward leader from the ground; the risetime of the return stroke can be a microsecond or less, and the whole duration is some tens of microseconds. The peak current is typically some tens of kiloAmperes. In some cases, the return stroke is followed by a continuing current of up to 200 A, lasting some tens of milliseconds. The continuing current produces little radiation, and is therefore typically difficult to observe remotely. More typically, there is no current to the ground for some tens of milliseconds, after which a subsequent stroke can be launched. A subsequent stroke is typically preceded by a dart leader that radiates much less than the stepped leader before the first return stroke. The multiplicity (number of subsequent strokes) can sometimes be more than ten, and the overall flash process can last up to a second or even longer.

In practice, the radiation produced by a lightning flash does not behave as simply as described above. The sub-processes may radiate very differently depending on the frequency. For example, the return stroke radiates at all frequencies from near DC to above optical, but is most intense in the LF band (30-300kHz). Stepped leaders, on the other hand, radiate predominantly at VHF (30-300MHz). In addition to the well-defined processes described above, there are numerous poorly understood in-cloud processes during the flash, which can radiate strongly at particular frequencies. These have been classified into groups such as J-, K-, and M-processes. Additionally, negative flashes are only one type of discharge mechanism. Positive flashes have different leader mechanisms than negative flashes. There is little high-frequency

radiation before a positive return stroke but strong radiation just after it. In the case of intra-cloud flashes, the above model may not be valid at all. Due to ambiguity in the definitions, as well as measurement limitations, separating these various processes has been left outside the scope of this paper. All processes that do not fit into the simplified model above are therefore called simply "in-cloud processes".

The choice of the specific frequency band was driven by a practical interest in designing the simplest possible remote lightning detector, with minimal size, complexity, cost, and power consumption. As a result, the frequencies of interest span both the Medium Frequency band (MF, 300 kHz – 3 MHz) and the High Frequency band (HF, 3 MHz – 30 MHz). For simplicity, the single term "HF band" will be used in this thesis to cover the whole range.

A prototype system was designed and tested during the project. The focus of the thesis however is not on the prototype technology, but on the physics that must be understood in order to develop a reliable detection system. The experiments with the prototype system enabled the measurement of natural lightning, and hence the collection of information which is not adequately covered in the existing literature or theoretical models.

It has been known from the very beginning of radio technology that lightning is a source of interference in amplitude-modulated (AM) radio reception. In fact, Popov (1896) showed that lightning causes distinctive noise in a radio channel; this occurred before manmade radio transmissions were demonstrated, so that in this sense lightning detection can be said to pre-date other uses of the radio. Radio measurements of lightning were made extensively until the 1960's, although mainly with the purpose of improving radio transmissions; see e.g. Le Vine (1987) and Nanevicz et al (1987) for reviews. Taylor (1973) observed increased radio noise near tornados at 3 MHz, an observation which Johnson et al (1977) extended by studying storm-related radio noise at a wider range of frequencies, from 10 kHz to 74 Mhz. Johnson et al (1977) found that noise in the MHz range is the best general indicator of thunderstorm intensity; this is the frequency range that is also used in this thesis. A narrowband device operating near 500 kHz, described by Kohl (1980), appears to be one of the few to have been in operational forecast use. A specific comment about this technique by Johnson et al (1982) deserves to be quoted in full:

> "*The sferics counter appears to be useful in the sense that it will indicate when lightning exists within the detection range of the sensor. It is pointed out that this same detection capability has been achieved by using inexpensive transistor radios.*"

This is of interest because the device used in this thesis is essentially a (slightly modified) transistor radio in the sense mentioned above. The basic principle has, therefore, been in informal use at least for decades, even if the above paragraph is the only explicit mention in a peer-reviewed paper. AM radios are also commonly used by amateur storm chasers as rudimentary detection devices (author's personal observation). In the scientific community, after the 1980's, occasional narrowband measurements in the HF band have been performed, mainly in Sweden and Sri Lanka (Cooray and Pérez (1994b); Gomes et al (1998); Gomes et al (2004)). Fernando and Cooray (2008) give a recent review of narrowband measurements between 1 MHz and 15 MHz.

Currently, a number of very small devices are on the market which appear to operate on narrowband detection principles. However, the lightning research community has been unable to verify the functionality of such devices, and therefore there is no official opinion on them by professional organizations (e.g. American Meteorological Society (2002)). Although little or nothing has been

described in the open literature, some information about the operating principles can be gleaned from patent publications, and is presented in this thesis. Nevertheless, no open literature seems to exist on the performance of such devices.

A central claim of this thesis is that a significant part of the problem is due to insufficiently defined physical parameters. Narrowband devices typically claim to measure the "distance to the storm", without specifying what this physically means. There is a very large difference between trying to measure the distance to the center of a storm and to the closest edge of a storm, for example. The detection efficiency and ranging accuracy of narrowband devices is even more difficult to ascertain. Very little information (peer-reviewed or otherwise) has been published by the manufacturers of such devices that would allow a theoretical analysis of the devices, or enable the devices to be compared quantitatively against other devices. In this sense, it is not a major exaggeration to say that at present, narrowband devices are essentially unfalsifiable; in other words, there are no tests which could unequivocally pass or fail such devices.

The thesis shows that narrowband devices have characteristics which make it unrealistic to base such a test for example on a flash-by-flash comparison with another device (such as a lightning detection network). The ranging of storms by narrowband methods is, by nature, statistical. As in any statistical method, the definition of "good" or sufficient performance depends largely on the requirements of the application. However, the thesis proposes five hypotheses which need to be satisfied before a narrowband method can claim to be validated at all. A data set is presented for which the hypotheses are valid, but the data set is relatively small and restricted to one geographical location. Full validation will thus require more independent measurements. The hypotheses are:

**Hypothesis 1**. In an HF signal, the energy emitted by cloud processes can be as large as or larger than the emission from ground return strokes. When the emitted energy is measured for the entire duration of the flash, IC processes may dominate. This is in contrast to the broadband electric field, in which the return stroke almost always contributes the highest peak.

**Hypothesis 2**. The intensity of an HF signal can be used for ranging. This requires two phenomena: the intensity drops sufficiently fast as a function of distance, and the source intensities have a narrow or at least well-defined distribution. The distance can then be statistically estimated from the emitted intensities alone, as long as a sufficiently large sample is available. An empirical formula to determine the distance can be developed, although the scatter in the data is likely to be large.

**Hypothesis 3.** The main processes that radiate in the HF range are common to both cloud-to-ground (CG) and intra-cloud (IC) lightning. Therefore, the intensities radiated by IC and CG flashes at comparable distances are approximately equal. If there is enough similarity, there is no need for IC/CG differentiation, and all flashes can be used for statistical ranging.

**Hypothesis 4.** Although ground conductivity affects the results, its effects can be neglected at least under some specific circumstances. The thesis presents measurements from a case in which the propagation can be neglected in this way, but in general, ground conductivities will need to be considered.

**Hypothesis 5.** If Hypotheses 1-4 are valid, the distance to the closest edge of a cell can be estimated statistically from the full-flash energy of all lightning flashes, using a simple floating average. This is demonstrated in one sample case in Finland.

This thesis evaluates the hypotheses by describing and expanding on original research in four peer-reviewed publications by the author. The papers contain data analysis from two sets of measurements: one performed in Sri Lanka measuring the vertical electric field, and the other done in Finland using a radio receiver designed for this purpose.

Paper I describes direct measurements of HF radiation in lightning in Sri Lanka. For detection purposes, the main significance of the work is that it shows that the radiation emitted in subsequent strokes is usually insignificant, but can increase dramatically if there is a "chaotic leader", associated with IC events during the leader phase. The paper primarily addresses Hypothesis 1.

Paper II describes a narrowband detection system which is based on the analysis of amplitude-modulated radio interference. Measurements made in Finland are presented, using a lightning detection network and broadband electric field measurements to provide a ground truth for the ranging. An empirical formula is derived to support Hypothesis 2.

Paper III presents measurements in Finland of the preliminary breakdowns preceding first return strokes. It is shown that the energy of a preliminary breakdown (a purely in-cloud process) can be comparable to the energy of the return stroke, which supports Hypothesis 1. Paper III also shows that the electromagnetic radiation from close preliminary breakdowns propagates primarily as a space-wave (for which the attenuation is not dependent on the ground conductivity), while the radiation from the return stroke at any distance propagates largely as a ground-wave (which attenuates as a function of ground conductivity). This is used in Paper IV to justify Hypothesis 4.

Paper IV presents data in support of Hypotheses 3-5. The paper provides a framework for quantifying and evaluating the reliability of local narrowband detectors.

The hypotheses are shown to be essentially valid at least for Scandinavian lightning. The results cannot be considered the type of independent validation demanded by the American Meteorological Society (2002), especially since no fully functional alarm system has been built. However, they are used to propose a methodology by which narrowband devices could be verified in a fair and realistic way; conversely, they show the limitations of what can be claimed for a local narrowband detector. A single-station narrowband device can realistically be expected to determine whether the closest edge of a storm cell is within a specified radius, and to accurately estimate transitions across this radius. Because of source and propagation variations, this radius can in practice be between 10 and 20 km. At much larger distances, accurate ranging depends on knowledge of the conductivity of the ground.

Section 2 of the thesis analyzes the existing literature relevant for understanding narrowband detection. Although Papers I-IV are cited where relevant, the focus is on describing the background; the new results of this thesis are discussed in the later chapters. Section 3 describes the devices and methods which were used for data capture in Papers II-IV; more detail is given than was possible in the space of the peer-reviewed papers. Each of the working hypotheses is then analyzed in Sections 4 to 8. In a few cases, the hypothesis relies on analyses which have been already extensively discussed in Section 2; in such cases, the section is kept brief rather than duplicating the material. Most of the analysis is based on materials published in Papers I-IV, but some additional unpublished material has been added to broaden the arguments. Section 9 then evaluates whether the method can be considered to be validated based on these results, and proposes a general methodology by which devices of this type could be validated in a rigorous yet fair way. Final conclusions and future steps are drawn in Section 10.

A separate Appendix describes the design of the narrowband system in detail. Since the practical design work was done largely by co-authors of papers II-IV, the material is not presented as part of the main thesis. However, the author believes that this information should be in the public domain, as it is necessary for evaluating the validity of the measurements.

# 2 Background

## 2.1 Methods for remote lightning detection

Although the focus of this thesis is on physics, a key driver for the research is the development of a practical lightning detection system. For this purpose, an overview of remote detection methods is made.

Lightning risk may be globally underestimated because much of the damage occurs at small scales, affecting only a few individuals or buildings at a time. Holle et al (1996) demonstrated such under-reporting in the United States by comparing official lightning damage statistics from the official NOAA publication *Storm Data* (which mainly records large losses) to results that were extrapolated from small individual lightning-damage insurance claims. The official statistics suggested annual losses of about 30 million USD in the USA, whereas the extrapolation gave a figure ten times larger, with 300,000 lightning-related insurance claims, mainly related to lightning overvoltages.

Personal injuries and deaths, as recorded in *Storm Data,* were studied in more detail by Curran et al (2000). There were very large variations within the United States, with an average of 0.42 lightning deaths per million per year countrywide but almost 5 deaths per million per year in Florida. Curran et al (2000) cited other literature which shows that *Storm Data* systematically underestimates deaths and injuries. In general, damage related to convective phenomena (lightning, tornados, thunderstorm-related winds, and hail) in 1992-1994 annually caused about 40 deaths and 700 injuries, and overall resulted in 400 million USD in damage. If the economic underreporting is as serious as Holle et al (1999) suggest, the small-scale thunderstorm damage may exceed the billion-dollar level annually. Results from Poland (Loboda (2008)) suggest casualty rates of about 0.8 per million per year (between 1/1000 and 1/10,000 flashes).

It must be noted that in the case of the United States, the figure is this large even though the population is well-educated about lightning risks, lightning protection is taken seriously in the most affected areas, and thunderstorm forecasts are high-quality and readily available in the media. The United States therefore represents a society which is protecting its infrastructure well. It is far from clear whether more complete protection is even realistic in the United States (for example, little can realistically be done about hail damage). However, other societies appear to be less well protected, but in their case the underreporting is even more difficult to analyze. Conditions in the general society and infrastructure clearly do have an effect on lightning risk; Holle et al (2005) analyzed temporal changes in the United States lightning casualties, and observed that better protection of houses and infrastructure have decreased indoors casualties radically. Most casualties now occur during outdoors recreational activities.

There is more or less a general consensus in the lightning research community that complete safety can only be achieved by lightning protection and grounding of the structures that need to be protected. The majority of the literature falling under “lightning protection” deals with such passive systems. For

personal protection, the most widely accepted receommendation (Holle et al (1999), American Meteorological Society (2002)) is that individuals should protect themselves by going indoors into a protected building.

Remote lightning detection is commercially relevant when the information can be used to direct activities to diminish damage that may be caused by lightning flashes. It is known that for electrical utilities, prediction of lightning activity can help find damage points (Cummins et al (1998)). The impact of forest fires may be diminished if strike points can be found quickly before they ignite the whole forest (Krider et al (1980)).

Lightning detection techniques can also be used to actually predict lightning risk and launch protective actions before the storms are overhead. The work of Gulyás et al (2008) aims to quantify preventative lightning protection, dividing it into three components: information gathering, forecasting, and preventative actions. In aviation, real-time lightning detection and radar information can be used to direct airplanes around active thunderstorms. It is also possible to use real-time lightning detection systems to determine when to stop or start ramp activities in airports; at present, different airports have very different procedures for doing so (Heitkemper et al (2008)). Idone and Orville (1990) describe an application in which real-time data are used to define thunderstorm watch periods for power utilities. Remote detection has also been proposed as concrete part of a stadium safety protocol (Gratz and Noble (2006)), which includes protected areas to which viewers can be collected in case of an active danger (defined as lightning activity within ten miles or 16 km of the stadium). An expert system methodology for similar open air mass performances has been proposed by Németh et al (2008).

The simple charge moment approximation is sufficient for a general-level understanding of the radiated fields from lightning. As discussed by McLain and Uman (1971), if the height $H$ of the return stroke is much smaller than the distance $R$, then the vertical electric electric field $E$ and horizontal magnetic field $B_\varphi$ can be written as

$$E = -\frac{1}{4\pi\varepsilon_0}\left(\frac{M}{R^3} + \frac{dM/dt}{cR^2} + \frac{d^2M/dt^2}{c^2R}\right) \quad \textbf{(1)}$$

$$B_\varphi = \frac{\mu_0}{4\pi}\left(\frac{dM/dt}{R^2} + \frac{d^2M/dt^2}{cR}\right) \quad \textbf{(2)}$$

where $\varepsilon_0$ is the permittivity and $\mu_0$ the permeability of free space. $M$ is the vertical dipole moment, defined in the first approximation as a function of the vertical charge line density $\rho$ at retarded time $t$-$R/c$ as

$$M(t) = 2\int_0^H \rho(z, t - \frac{R}{c}) z dz \quad \textbf{(3)}$$

with the factor 2 coming from the inclusion of the mirror charge. Thus $dM/dt$ is the current moment. This separates the fields into static ($1/R^3$), inductive ($1/R^2$), and radiative ($1/R$) components. Although more accurate formulations of the fields have been suggested e.g. by Thottappillil and Rakov (2001), Equations (1) and (2) are sufficiently exact to use in comparing different types of detectors.

Lightning detection networks are currently considered the highest-quality (and also most expensive) option. The technology is based on using a wideband magnetic field direction finding system (Krider et al (1976)) or on the time-of-arrival or most typically both (Cummins et al (1998)). The sensors in the network respond to the microsecond-scale changes of the radiative electromagnetic fields at the point of attachment to the ground. The US National Lightning Detection Network (NLDN) is perhaps the most closely documented of such networks (see e.g. Idone et al (1998a); Idone et al (1998b)).

An older and simpler technology, lightning flash counters, measure the number of flashes within a given geographical radius (flash density) by measuring abrupt electric field changes $\Delta E$ due to lightning. They were prevalent approximately from the 1950's to the 1980's, but large statistical datasets of flash density still continue to be published (e.g. Kuleshov et al (2006)). Flash counters usually have additional circuitry that enable cloud-to-ground and intra-cloud flashes to be separated (Mackerras (1985)). The effective range of a flash counter is the range at which all flashes are on average observed; for practical applications, this range should be between 10 km and 30 km. Flash counters may work either by predominantly responding to the electrostatic field with its $1/R^3$ drop-off, or to the radiation field with its $1/R$ drop-off (Equation (1). Pierce (1956) (cited in Cooray (1986b)) noted that electrostatic counters are therefore more robust, since they are more sensitive to changes in the distance than to changes in the flash intensity. Thus, for single-station measurements, a fast drop-off is advantageous.

One family of lightning detectors relies on electromagnetic measurements at a single narrow band. Taylor (1973) noted a correspondence between noise at 3 MHz and the proximity of tornados, but did not propose a specific warning device. Narrowband detection of thunderstorm electric noise at 500 kHz was actively researched in the 1960's (Kohl and Miller (1963); Kohl (1964); Kohl (1969); Stanford (1971)). An operational system is described by Kohl (1980). The system did not rely specifically on Equations (1) and (2) but instead used the number and intensity of individual pulses at 500 kHz to determine distance and also development level of a storm. The system was verified against radar data and appears to have been in active operational use. However, Johnson et al (1982), referring to a device of this type, found that the device required continual recalibration due to variations in the ambient noise, and therefore was not very reliable in practice.

Peer-reviewed information on the very simplest narrowband devices is scattered. Rafalsky et al (1995) reviewed some of the literature on single-station direction-finding (DF) systems. Direction-finding requires measurement of the horizontal magnetic field vector; the location of the source can then be determined, if it can be assumed that the current source is vertical. This is not necessarily true of the return stroke channel in general, but is usually assumed to be approximately true at the attachment point of the return stroke channel. High-quality DF devices like that of Krider et al (1976) or Rafalsky et al (1995) are generally wideband. Rafalsky et al (1995) noted that narrowband devices tend to be inefficient because they utilize only a small amount of the energy available in the lightning flash, and also because the spectral amplitudes of electromagnetic radiation from lightning flashes can be very different at different frequencies (a fact that is further analyzed by Nanevicz et al (1987) and Le Vine (1987)). If only magnetic field information is available, Rafalsky et al (1995) pointed out that the detection scheme requires that all flashes be assumed to have the same intensity, which is clearly not the case; however, aside from the measurements of Paper IV at 1 MHz, no measurements are known to have been made of these source variations. Ortéga (2007) described a system that has been in satisfactory operational use in Tahiti, consisting of a network of commercial narrowband magnetic detectors (bandwidth 40-100 kHz).

There is essentially no peer-reviewed information on the portable devices which the American Meteorological Society (2002) refers to. The only publicly available information can be gleaned from patents. Patents should be treated with great care as sources, as they do not necessarily reveal all the details that are needed to understand the principles, nor, more critically, does a granted patent in any way suggest that the invention actually works as promised. However, where no other information is available, patents can at least reveal the working principles and assumptions which have been made.

Ostrander (1989) proposed to use a narrowband detector at about 50 kHz to isolate the radiation field pulses, and a wideband filter from 250 Hz to 250 kHz to isolate the inductive field component, and calculate the distance from the ratio of the two. Breitmeier et al (1993) described a device which compares the outputs at two or more low frequencies (700-1400 Hz), and estimates the distance based on their ratios. At these frequencies the electrostatic ($1/R^3$) term dominates. The ranging scheme appears to rely on the fact that if the charge density is written as a harmonic $M(t) = M(\omega)e^{i\omega t}$, the ratio $M(\omega_1)/M(\omega_2)$ is approximately constant across all flashes. Murtha and Skinner (1999) described an extremely simple detection scheme in which the system is triggered by any impulsive event that exceeds a given threshold, and which tries to eliminate man-made interference, but makes no real ranging attempt. Hed et al (2001) described a system which appears to be related to the observations of Taylor (1973): a lightning detection system is proposed which separates near-continuous tornado noise from lightning noise. Very little detailed information is given, however.

## 2.2 Theory of narrowband detection

As defined by Le Vine (1987), the parameter that should be used to quantify the intensity of any individual lightning process is the spectrum (the magnitude of the Fourier transform of the electric field time domain measurement). In many studies (e.g. Cooray and Lundquist (1985); Cooray and Pérez (1994b); Jayaratne and Cooray (1994)), the peak electric field has been used to quantify the intensity of various processes. As discussed in paper IV, this method of comparison is strictly speaking physically justified only for highly impulsive processes such as return strokes.

There are two methods to determine the spectrum of a lightning process. Direct calculation of the Fourier transform requires an electric field measurement with a wide bandwidth and a high dynamic range, since the intensities drop off quickly at high frequencies. A technically simpler solution is to use a narrowband filter and detection system tuned to a specific frequency; this can be done with standard radio receivers. A stand-alone narrowband system cannot, however, identify the lightning process which is causing the signal, as can be seen in Figure 1.

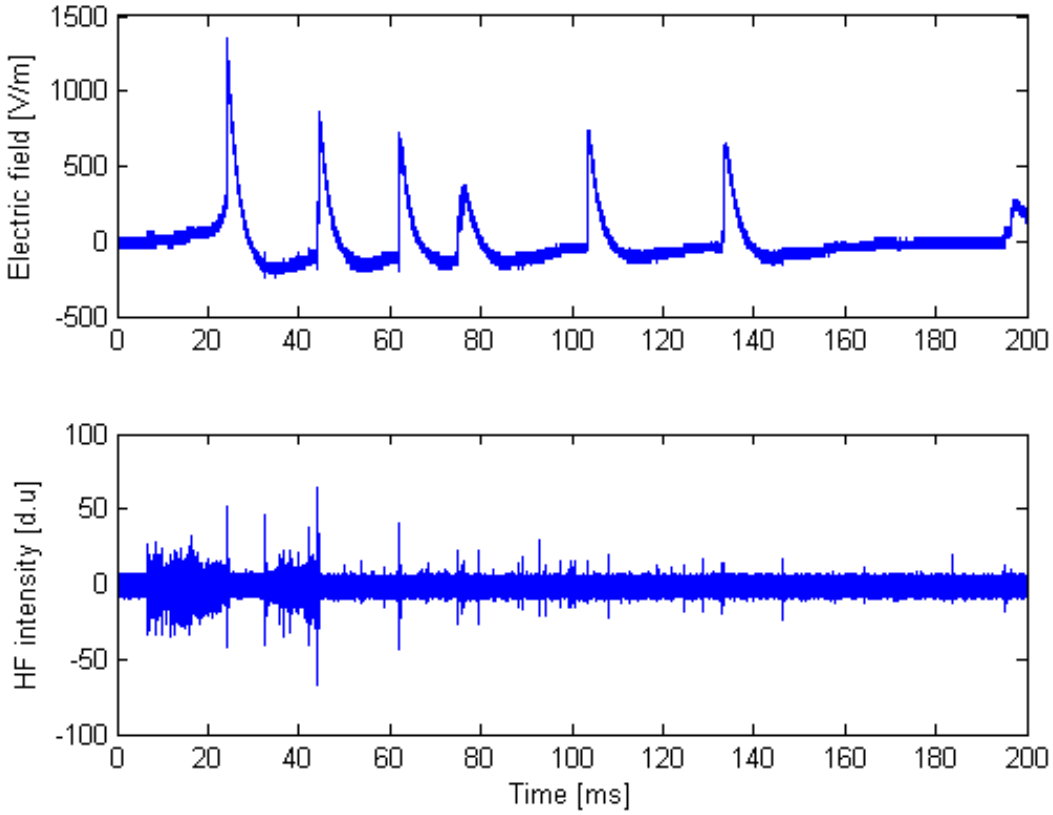


**Figure 1: Comparison between the wideband electric field (top panel) and the narrowband field at 3 MHz field (bottom panel) for a signal including a first return stroke and five subsequent return strokes. The difficulty in identifying the processes from the narrowband signal is readily apparent, as is the high noise level in the narrowband signal.**

For measurements at a single resonant frequency, the definitions of Le Vine (1987) can be followed. The system in this case consists of an antenna connected to a standard AM radio receiver, followed by a post-detection filter (Figure 2). This model assumes that the signal is not downconverted to the intermediate frequency. Such a downconversion was made in the devices of Papers II-IV, and the effect of the downconversion is analyzed in Section 3.

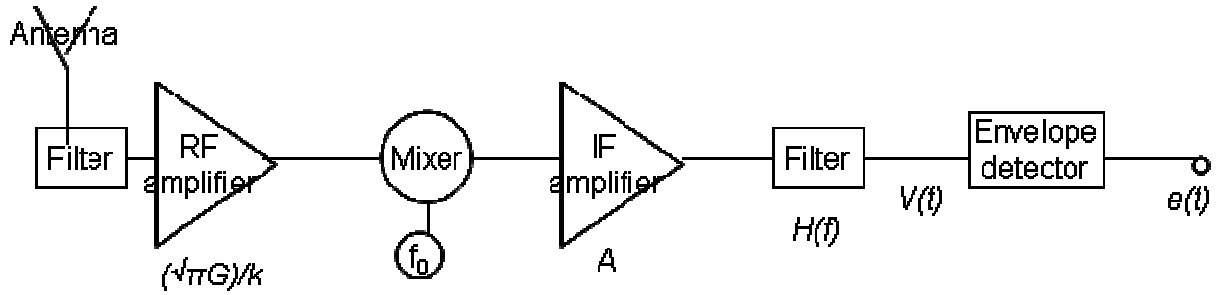


**Figure 2: Schematic of a general narrowband receiver, with definitions used by Le Vine (1987).**

For impulsive events in which the signal can be validly broken down into harmonic components, the voltage out of the antenna at a given frequency $\omega = 2\pi f$ is proportional to the vertical electric field, with a proportionality constant $\sqrt{\pi G}/k$, where $G$ is the gain of the antenna and $k = \omega\sqrt{\mu\varepsilon} = 2\pi/\lambda$. Le Vine (1987) then writes the vertical component of the electric field in its complex analytic representation as

$$E(t) = \mathrm{Re}\left\{\int_0^\infty 2E(f)e^{-i2\pi ft}\,df\right\} \quad \textbf{(4)}$$

with *E(f)* being the Fourier transform of *E(t)*. The voltage out of the antenna can then be written as

$$V(t) = \mathrm{Re}\left\{\int_0^\infty 2a(f)H(f)E(f)e^{-i2\pi ft}\,df\right\} \quad \textbf{(5)}$$

where *H(f)* is the Fourier transform of the filter *h(t)* and $a(f) = (A/k)\sqrt{\pi G}$, combining the gains of the antenna and the amplifier with gain *A*. The equivalent filter *H(f)* is assumed to have a bandpass that is very narrow around the center frequency $f_0$, i.e. *H(f)* is nonzero only very near the center frequency $f_0$ and zero elsewhere. A change of variables $z = f - f_0$ is then made. The integration limits can be mathematically extended to infinity because the equivalent filter is assumed zero outside the bandpass. Equation (5) then becomes

$$V(t) = \mathrm{Re}\left\{e^{-i2\pi f_0 t}\int_{-\infty}^\infty 2a(f_0+z)E(f_0+z)H(z)e^{-i2\pi zt}\,dz\right\} = \left|e(f_0,t)\right|\cos(2\pi f_0 t + \varphi) \quad \textbf{(6)}$$

$$e(f_0,t) = \int_{-\infty}^\infty 2a(f_0+z)E(f_0+z)H(z)e^{-i2\pi zt}\,dz \quad \textbf{(7)}$$

which describes amplitude modulated sinusoid at frequency $f_0$ (with an unknown phase $\varphi$). The output of the detector is therefore just the envelope of this signal

$$e_0(t) = \left|e(f_0,t)\right| = \left|\int_{-\infty}^\infty 2a(f_0+z)E(f_0+z)H(z)e^{-i2\pi zt}\,dz\right| \quad \textbf{(8)}$$

With a narrow enough bandpass, it is possible to make the approximations $a(f_0 + z) \approx a(f_0)$ and $E(f_0 + z) \approx E(f_0)$, simplifying Equation (8) to

$$e_0^2(t) = |E(f_0)|^2 h^2(t) \quad \textbf{(9)}$$

in which the first term is the magnitude of the electric field spectrum at $f_0$, and the second term is the impulse response of the system defined as

$$h(t) = \int_{-\infty}^{\infty} 2a(f_0)H(z)e^{-i2\pi zt}dz \quad \textbf{(10)}$$

Both sides of Equation (10) are then integrated, and Parseval's theorem is used to get

$$\int_{-\infty}^{\infty} e_0^2(t)dt = \int_{-\infty}^{\infty} |E(f_0)|^2 h^2(t)dt = 4|E(f_0)|^2 \int_{-\infty}^{\infty} |a(f_0)H(z)|^2 dz \quad \textbf{(11)}$$

The spectrum is then given by the equation

$$|E(f_0)| = \frac{1}{2\sqrt{\Delta}} \sqrt{\int_{-\infty}^{\infty} e_0^2(t)dt} \qquad \textbf{(12)}$$

where

$$\Delta = |a(f_0)H(0)|^2 \int_{-\infty}^{\infty} \frac{H^2(z)}{H^2(0)} dz \equiv G^2 B \qquad \textbf{(13)}$$

where G is the gain of the system and B is the bandwidth. The equation simplifies further if the system can be modeled as an ideal bandpass filter, with $H(z)$ being a constant $H_0$ when $|z| < B/2$ and zero elsewhere. Equation (8) can then be written as

$$e_0(t) = 2\left|a(f_0)E(f_0)H_0 \int_{-B/2}^{B/2} e^{-i2\pi ft} df\right| = 2|a(f_0)E(f_0)H_0 B|snc(\pi Bt) \equiv e_p snc(\pi Bt) \quad \textbf{(14)}$$

where $e_p$ is the peak value of the output signal and $snc(x) = \sin(x)/x$. Squaring and integrating gives

$$\int_{-\infty}^{\infty} e_0^2(t) = e_p^2 \int_{-\infty}^{\infty} snc^2(\pi Bt) = e_p^2 / B \quad \textbf{(15)}$$

Combining Equations (12) and (15) finally gives

$$\left|E(f_0)\right| = \frac{e_p}{2GB} \qquad \textbf{(16)}$$

The practice of calculating the spectrum from the field peak is therefore valid, but only under the large number of idealizations defined above. In particular, Equation (16) is only valid if the signal consists of discrete impulses, separated by a time duration that is larger than the response time of the system. Le Vine (1977) further extends the analysis into the case of a sequence of pulses with random arrival times or amplitudes. However, the idealizations break down when the signal is noiselike and continuous. In such a case, Le Vine (1987) defines the spectrum to be the Fourier transform of the autocorrelation function over a time period [-T,T]. In the general form, this results in the equation

$$\left|E_r(f_0)\right| = \frac{1}{2\sqrt{\Delta}} \sqrt{\frac{1}{2T} \int_{-T}^{T} e_0^2(t)dt} \qquad , \textbf{(17)}$$

which is dimensionally equivalent to Equation (12), because the time T appears explicitly in the denominator, and implicitly in the numerator. As shown in Paper I, when the signal is discrete, this spectrum becomes

$$\left|E_r(f_0)\right| \approx \frac{1}{2\sqrt{\Delta}} \sqrt{\frac{1}{2N} \sum_{k=-N}^{N} e_k^2} = \frac{\sigma}{2\sqrt{\Delta}} = \frac{\sigma}{2G\sqrt{B}} \qquad \textbf{(18)}$$

where $\sigma$ is the standard deviation of the sample. In an ideal case, the two definitions should give the same result, and hence the peak and standard deviation should be linearly related by the formula

$$e_p = \sigma\sqrt{B} \quad \textbf{(19)}$$

The intensity derived from peak energy should thus be linearly related to the intensity from the standard deviation, and could be used as an intensity value (assuming that the antenna response is fast enough to capture the peak accurately).

An alternative method was defined by Willett et al (1990): for continuous signals, it may be preferable to use the power spectral density (PSD), rather than the energy spectral density (ESD). In principle, the ESD can be derived by performing the Fourier transform of the broadband signal. The most commonly cited parameter in the literature is the energy spectral density ESD, with units of $(V/m/Hz)^2$. This is the correct measure for impulsive processes. However, for continuous processes, the power spectral density PSD with units of $(V/m)^2/Hz$ is considered, by Willett et al (1990), to be more relevant. The PSD in Willett et al (1990) is simply defined by the formula *PSD(f)=k*ESD(f)/W*, where *W* is the time period

and $k$ is a dimensionless constant to account for windowing. This is exactly correct for a step function, as long as the time window is within the step. However, for non-impulsive and irregular signals, it will be necessary to revert to the time domain.

In both Paper I and Paper III, a key problem is that continuous events are being compared to impulsive ones (continuous chaotic leaders or preliminary breakdowns to impulsive return stroke signals). The solution in Paper I was to calculate the root-mean-square (RMS) sum of the narrowband electric field from the chaotic leader (in effect, the power spectral density), and compare it to the narrowband intensity at the moment of the return stroke (in effect ,the energy spectral density). Strictly speaking, this means that two parameters that have different dimensions were compared. This was justified in Paper I by considering the ratio to be empirical. However, there is in fact no dimensional mismatch, since the "RMS sum" of a single peak is equal to the peak itself. For return strokes, the RMS and peak methods give well-correlated results (see Figure 3).

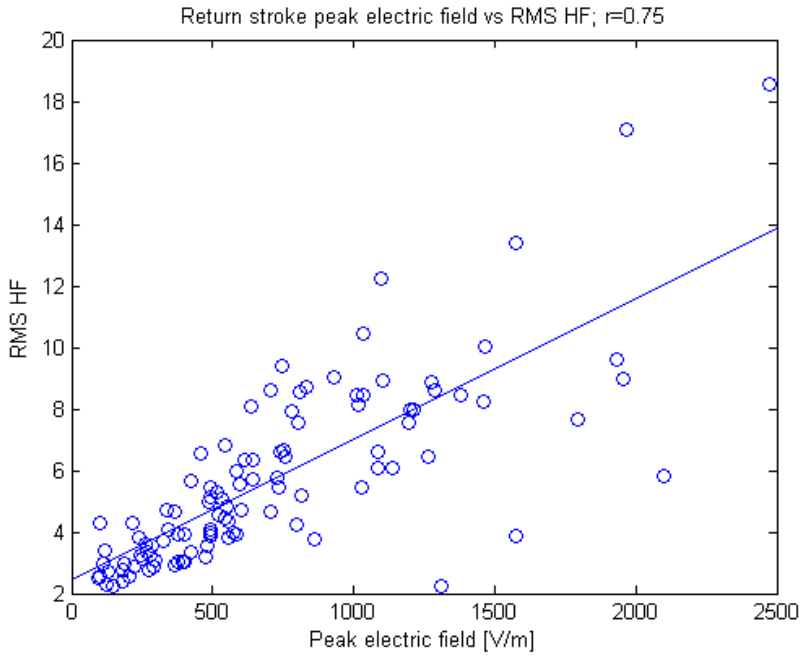


**Figure 3: Correlation of peak energy and narrowband RMS energy for return strokes (from data set of Paper I)**

The use of 1 MHz for the measurements was dictated largely by practical considerations related to antenna size, component cost, and overall simplicity (see Appendix). In practical terms, the measurement frequency is within the Medium Wave band (MW, 520-1610 kHz) on which commercial AM radio broadcasts also take place. This in turn is a subset of the medium frequency band (MF, 300 kHz to 3 MHz). Most of the earlier narrowband measurements have been in the High Frequency band (HF, 3 MHz to 30 MHz). The bands are defined in terms of radio propagation characteristics, specifically the possibility of very long transmission paths due to refraction from the E-layer of the ionosphere (skywave propagation). In principle, in the MF band, skywave transmission is only possible at night when the D

layer in the ionosphere weakens and does not absorb the signal. In the HF band, in principle the day/night difference is much smaller since the D layer does not absorb waves at these frequencies. In practice, there is no well-defined frequency at which this change occurs; for example, Pierce (1977) classifies both MF and HF to be essentially identical in terms of source signals and propagation characteristics. For close lightning flashes, which are the focus of this thesis, the phenomenon is irrelevant (or at least has been left outside the scope of this thesis). In this thesis, it is assumed that existing measurements at 3 MHz also characterize the expected signal at 1 MHz.

A well-known property of narrowband radiation is shown in Figure 4: the intensity of emitted radiation is empirically known to decrease as an *1/f* (the inverse of the frequency), at least in the range from some tens of kHz to some MHz. This result was criticized by Nanevicz et al (1987) as being misleading. It has been derived from a relatively small number of different experiments, using different instruments and different normalizations for distance. For example, Oh (1969) assumed a simple inverse dependence on distance, an assumption that Paper II shows to be incorrect at least at 1 MHz. Nanevicz et al (1987) also pointed out that after about 10 MHz, the data points appear to drop off more rapidly than 1/f. This was directly confirmed by Willett et al (1990), using FFT measurements of different lightning processes (see Figure 5). Sonnadara et al (2006) observed a change at about 2 MHz, with a $1/f^2$ drop-off above that frequency.

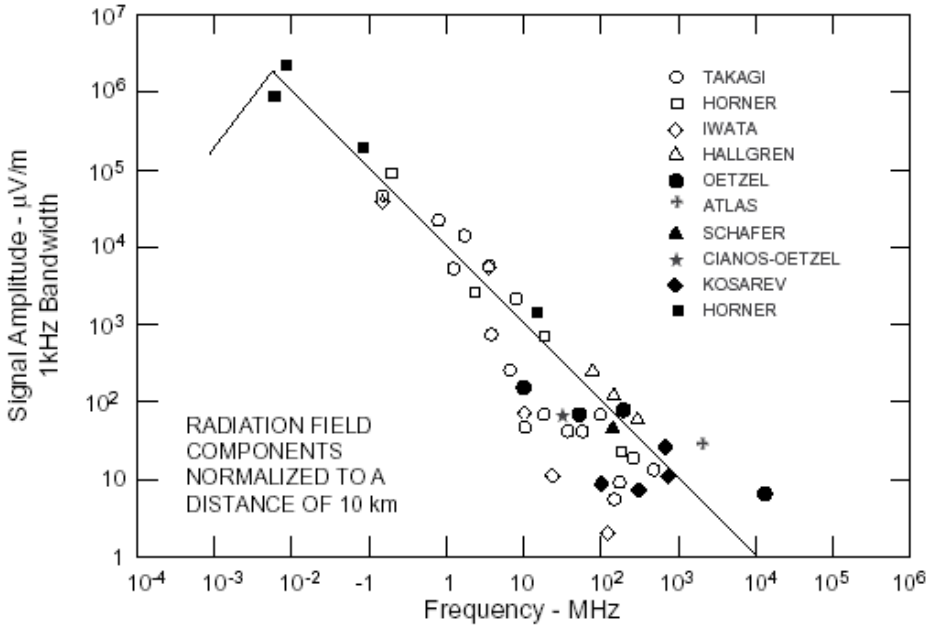


**Figure 4. Frequency spectrum of electric field radiated by lightning (from Nanevicz et al (1987)). A *1/f* curve has been fitted to the data points. Above 10 MHz, the drop-off may be faster.**

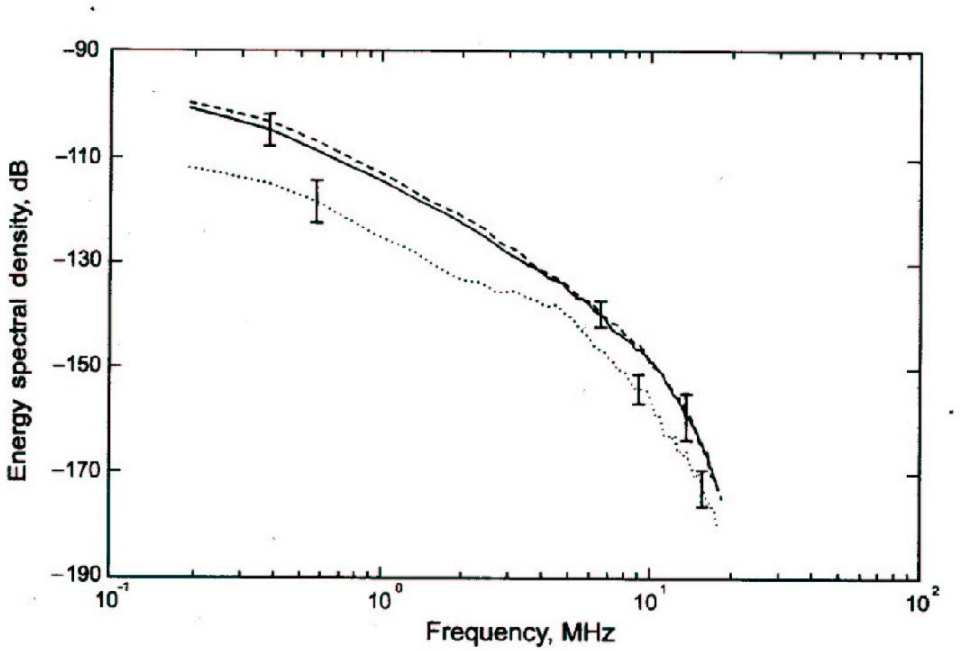


**Figure 5. Spectra measured by FFT, from Willett et al (1990). Emissions from 74 return strokes (solid). Dashed for subsequent strokes, dotted for preliminary breakdowns (more specifically, "characteristic pulses" which Willett et al (1990) observed to occur after the first preliminary breakdown and before the onset of the stepped leader). Normalized to 50 km. The dB scale of the vertical axis is relative to V/m/Hz. The faster drop in intensity after 10 MHz is clearly seen.**

The studies above analyzed fast transients in the electromagnetic field; an alternative approach is to analyze the more steady-state noise caused by lightning. Zonge and Evans (1966) described measurements in which the steady-state RF noise at various frequencies between 1 MHz and 1 GHz was measured for developing thunderstorms. Similar results were reported at 500 kHz by Kohl (1966), but it was also noted that an increase in noise did not always result in actual thunderstorms. The intensities were normalized to the square root of the bandwidth, and averaging the voltages over one minute. A rise in the RF noise level was observed at all frequencies up to 15 minutes before the first return stroke in the cell. Zonge and Evans (1966) noted that the noise level was very near the atmospheric noise level, and additionally the presence of multiple storm cells made the results unreliable. Continuous RF noise from thunderstorms at a range of frequencies from 10 kHz to 74 MHz was also studied by Johnson et al (1977), who found that the MHz range is the best general indicator of storm intensity, even though the signal as such is stronger near 10 kHz.

## 2.3 Sources of HF radiation

The various lightning processes have been analyzed for HF content in a variety of papers, but the different papers should be compared with care. There are differences in the devices and methodologies. In particular, Paper I and Paper III point out difficulties in comparing the intensities of processes which have very different durations. The return stroke has a duration of a few microseconds, while preliminary breakdowns may last many milliseconds. This means that the very concept of ”intensity” can be problematic when different types of processes are compared.

Qualitatively, first return strokes are very strong emitters of RF radiation (Weidman et al (1981); Beasley et al (1982); Willett et al (1990); Cooray and Pérez (1994b)), while Le Vine and Krider (1977) and Jayaratne and Cooray (1994) found subsequent strokes to emit significantly less. The intensity of the stepped-leader phase is inconclusive. Jayaratne and Cooray (1994) found that stepped leaders before the first return stroke can emit almost as strongly as the return strokes. In Paper I, 34 Sri Lankan flashes (with 74 subsequent strokes) are studied in detail using two different parameterizations for the intensity (the highest peak and the RMS intensity). The two parameterizations give somewhat different results, but both consistently show that the return strokes emit more strongly than normal leader processes (either stepped leaders before the first return stroke, or dart leaders before subsequent strokes). However, a class of leaders called “chaotic leaders” emits in some cases more intensely than the return strokes.

The preliminary breakdown that precedes stepped leaders has been studied by a few authors, but with inconclusive results. Weidman et al (1981) and Cooray and Pérez (1994a) found breakdowns to be strong RF emitters. However, Willett et al (1990) analyzed the spectra of the characteristic pulses, which they usually found to follow the preliminary breakdown, and precede the stepped leader phase, in Florida lightning, and found that these characteristic pulses have intensities about 10dB lower than the return stroke. Jeyanthiran et al (2008b) measured lightning flashes in Sri Lanka, and found that the ratio of the return stroke to the breakdown intensity is about 5.6 in the peak broadband electric field, and 2-3 in the peak HF signal at frequencies of 3, 5, and 10 MHz. Gomes et al (1998) showed that the breakdown has very different behavior at different latitudes, being very weak in the tropics, and strong in Scandinavia. In semi-tropical Florida, breakdowns do not seem to have consistent structure, and therefore their intensity may be difficult to quantify at all (Beasley et al (1982)). This variation is in contrast to the signatures from return strokes, which do not appear to be significantly different at these different locations (Cooray and Jayaratne (1994)). This means that the full-flash HF energetics of lightning flashes may have significant climatological variations.

In Paper III, preliminary breakdown processes (PBP) in Finnish lightning are studied, with the distances to the flashes known. It is shown that the results depend on the definition of “HF intensity”. In most of the earlier studies, intensity has been defined as the highest peak in the signal. Paper IV points out that this definition is physically somewhat arbitrary, when a continuous process (PBP) is compared to an impulsive one (RS), and therefore the RMS energy should be used instead. Using the peak field method, the RS-PBP ratio is found to be about 4, although in 25% of the cases the PBP is actually more intense. However, when the RMS energy is used, the PBP and RS intensities are almost identical at short distances. It is possible that some of the inconsistencies in the earlier literature are, therefore, due to inconsistent definitions of intensity. It is also seen that defining the beginning and particularly the end of a breakdown is arbitrary. The narrowband signal could be used to define the process more accurately, but the question of defining the most intense process has still not been answered in a satisfying manner.

Cloud flashes have been directly studied by several authors, but these cannot be directly compared to the ground flashes due, for example, to the difficulty in ranging the cloud flash. HF radiation in cloud flashes was measured by Jeyanthiran et al (2006), who found high HF intensities associated specifically with the onset of cloud flashes. Jeyanthiran et al (2008a) confirmed this result, but noted that in 15% of the cloud flashes HF maxima are seen later in the flash. Krider et al (1979) noted that, qualitatively, the RF radiation from IC processes does not appear to differ significantly from radiation due to the cloud processes associated with CG flashes.

Amongst the few in-cloud processes that have been explicitly studied from this perspective, Le Vine (1980) showed that narrow positive bipolar pulses (NPBP) are particularly strong HF emitters. Cooray and Lundquist (1985) compared peak electric field intensities from NPBP's and return strokes, and found that NPBP's were weaker by a factor of 0.2 to 0.5. Willett et al (1989) quantitatively compared NPBP and return stroke spectra from a single storm cell at a distance of 45 km. They found the spectra to be equal up to about 8 MHz; above 8 MHz the NPBP had a larger intensity. Willett et al (1989) found that NPBP's have very short duration (full width half maximum of ~2 μs compared to ~13 μs for return strokes) and are uncommon (only 18 NPBP's within 85 CG flashes for one storm). Therefore, their contribution to the full-flash energy will not be very large.

Particularly lacking are long measurements of full flashes, which would indicate what the contributions to the overall integrated energy are. The integrated energy is the most significant parameter for this thesis, since it is used for ranging (Papers II-IV). As noted in Paper III, a weak but long-lasting preliminary breakdown can contribute as much energy as an intense but short return stroke. It is, therefore, at present open what the dominating phenomenon is. There are some measurements of HF duration associated with various processes; this parameter, although practically not as significant as the intensity, has the advantage of being more quantitatively measurable. Cooray and Pérez (1994b) found that the HF emitted by a negative return stroke has a duration from 60 to 600 μs after the return stroke, while the average duration after positive return strokes is 5 to 25 ms (i.e. almost two orders of magnitude longer). They also found that negative flashes often have a "quiet period" just after the return stroke, with HF radiation reappearing some milliseconds later. Such quiet periods were observed earlier at 10 MHz e.g. by Clegg and Thomson (1979), who noted that the distribution of such gaps was consistent with the distribution of K-change events in the cloud. Edirisinghe et al (2006) also observed such quiet periods in negative ground flashes.

## 2.4 Physical lightning processes that cause HF radiation

There are many possible causes for the HF radiation. Understanding those causes is important to validate at least Hypotheses 1 and 4. In an early study, Brook and Kitagawa (1960) observed that there was a delay of 10-500 μs between the return stroke and the onset of RF radiation, also observed by Le Vine and Krider (1977). Such a delay could have been attributable to branching after the formation of the return stroke channel. However, the delay was shown by Cooray (1986a) to be most likely due to differential attenuation of the high-frequency signals from the lowest part of the return stroke channel, which means that the whole return stroke channel radiates immediately. This was also supported by the measurements of Jayaratne and Cooray (1994).

Tortuosity in the return stroke channel was proposed as an HF source by Le Vine et al (1986), but this was suggested to be an inadequate answer, since subsequent strokes do not radiate as intensely, even when they pass through the same tortuous channel. Cooray and Orville (1990) showed that in addition to tortuosity, it is necessary to consider variations in the waveform, its rise time, and any variations in the velocity along the channel. Cooray and Pérez (1994b) suggested that an important cause of HF radiation in a return stroke could be the ionization of virgin air in the corona sheath that surrounds the conductive return stroke channel. Such ionization also occurs in the stepped leaders as well as the streamers that precede the leaders. Cooray and Fernando (2008) modeled the relative importance of branches, charge irregularities, and tortuosity in the channel, and suggest that the main source of HF radiation is charge irregularities and branches in the channel, rather than its tortuosity.

# 3 Measurements used in this thesis

This section describes the devices and measurements used in all of the papers. In particular, many of the idealizations described in Section 2.2 are not valid with the system used, and the effect of these non-idealities is analyzed. These effects seem to be fundamental, and will be present in any device that operates by these principles.

The experimental work of this thesis was done in two locations. The experiments for Paper I were performed Sri Lanka, at the campus of the University of Colombo, in 2005. The experiments were vertical electric field measurements performed with a plate antenna and a vertical antenna. The devices and setup used in Sri Lanka were standard devices of the type which have also been used in earlier studies (Cooray and Pérez (1994b); Jayaratne and Cooray (1994); Jeyanthiran et al (2006)).

The experiments of Papers II-IV were performed using the same standard measurement devices as in Paper I, but in addition, included a narrowband system that has not been described earlier in the literature. Therefore, more detailed information is presented here that did not fit in the scope of Papers II to IV. The narrowband devices are described in detail in a separate Appendix.

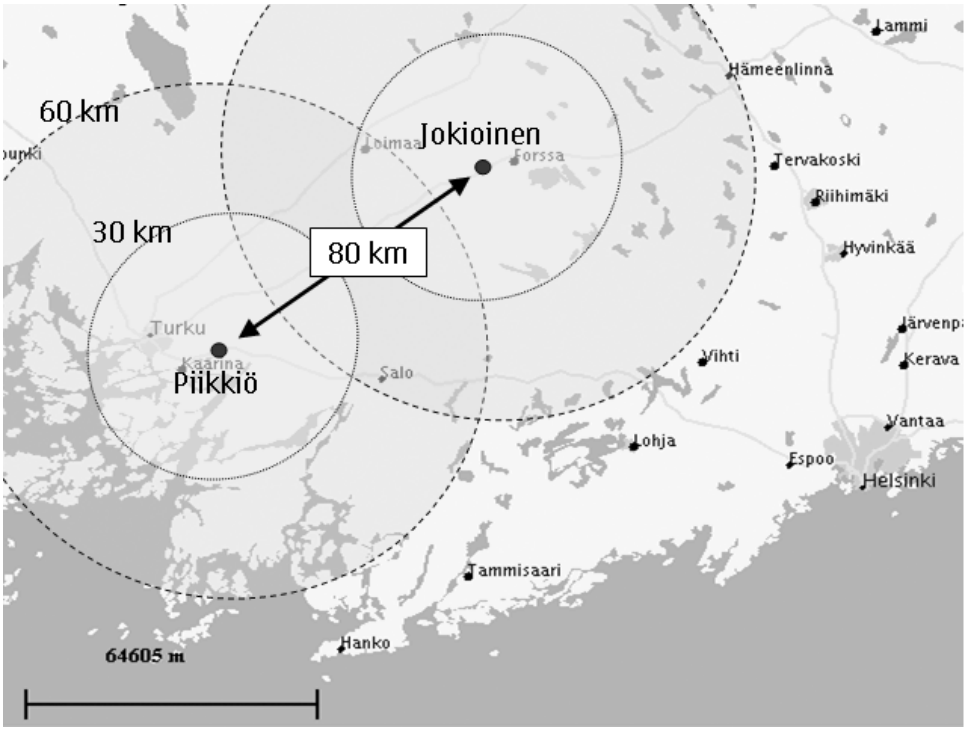


**Figure 6: Measurement sites in Finland.**

The experiments in Papers II-IV were performed in 2006 at two locations in Finland. The site in Piikkiö, Finland (EUREF coordinates 60.4198N, 22.4714W) was located on the premises of a private home. The site is located near the coast, but free access to the sea was largely blocked by islands. There is a small sector to the southwest, which was almost unobstructed. The antenna site is located in a

sparsely built detached residential area, about 10 m from the corner of the house in which the oscilloscope was placed. There were seven other one-story houses within about 150 m of the antennas. The other site was located at the meteorological observatory of the Finnish Meteorological Institute in Jokioinen, Finland (EUREF coordinates 60.8138N, 23.4979W). The site is about 80 km northeast from Piikkiö, and is surrounded by clay ground in all directions. There are no major lakes in the area, and all propagation is thus over ground.

Because of the non-linearities discussed below, no absolute calibration was made. Instead, the data were compared to lightning detection information from the NORDLIS network provided by the Finnish Meteorological Institute. The network is described by Tuomi and Mäkelä (2007); although the network accuracy has not been independently evaluated, the data have been used in this work as the absolute ground truth. Representative data outputs are shown in Figure 7 (CG flashes) and Figure 8 (IC flashes). The data capture length is one second.

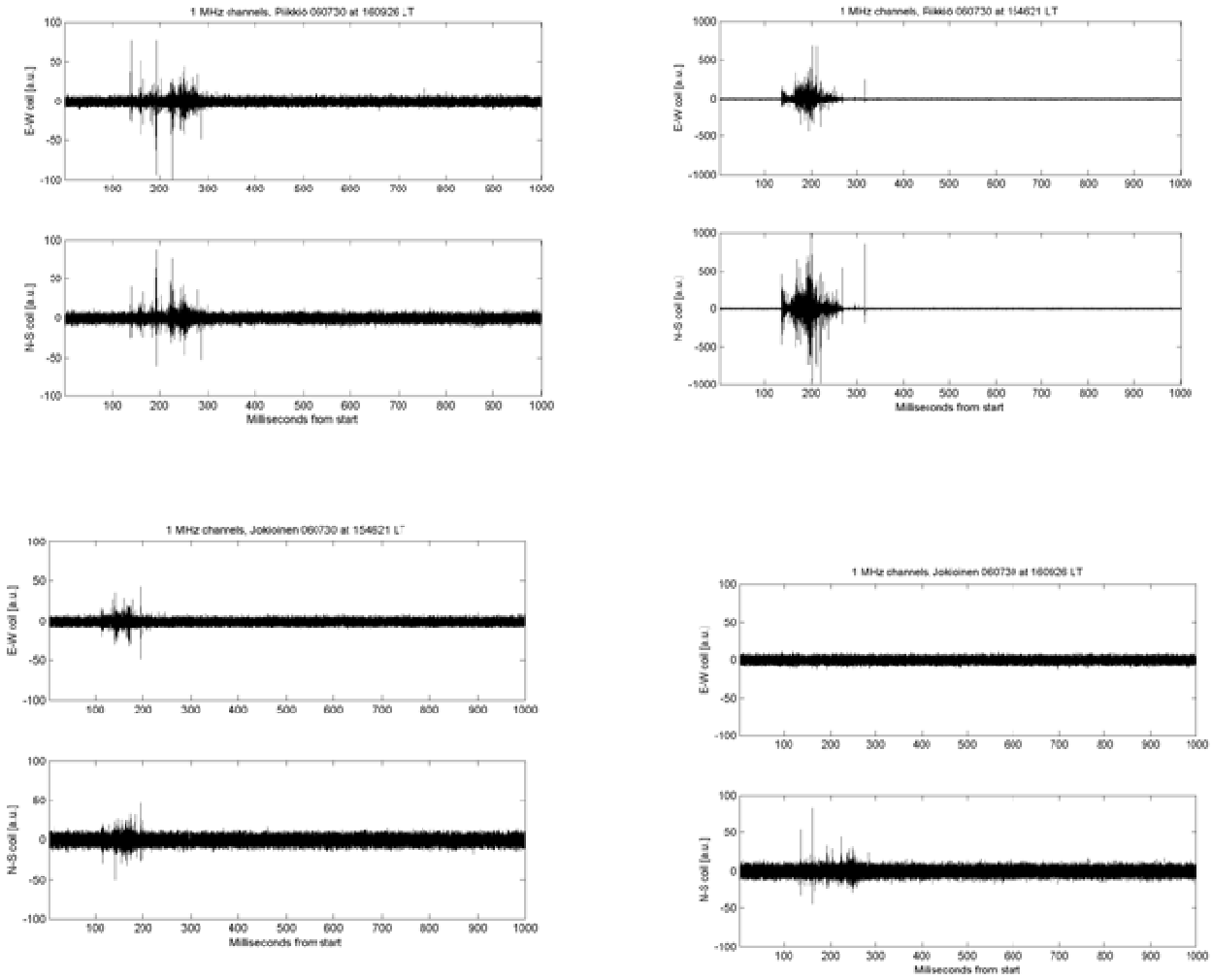


**Figure 7: Narrowband signals from four intra-cloud flashes, using the narrowband devices of papers II-IV. The signals from two orthogonal coils are shown in each plot. The x-axis has dimensions of millisecond; each capture lasted 1 second. The y-scale is in arbitrary units; the top right flash has a scale that is ten times larger than the others, and is from a very close flash. The directionality is particularly apparent in the bottom right flash, in which the distant flash is not seen at all in one of the channels.**

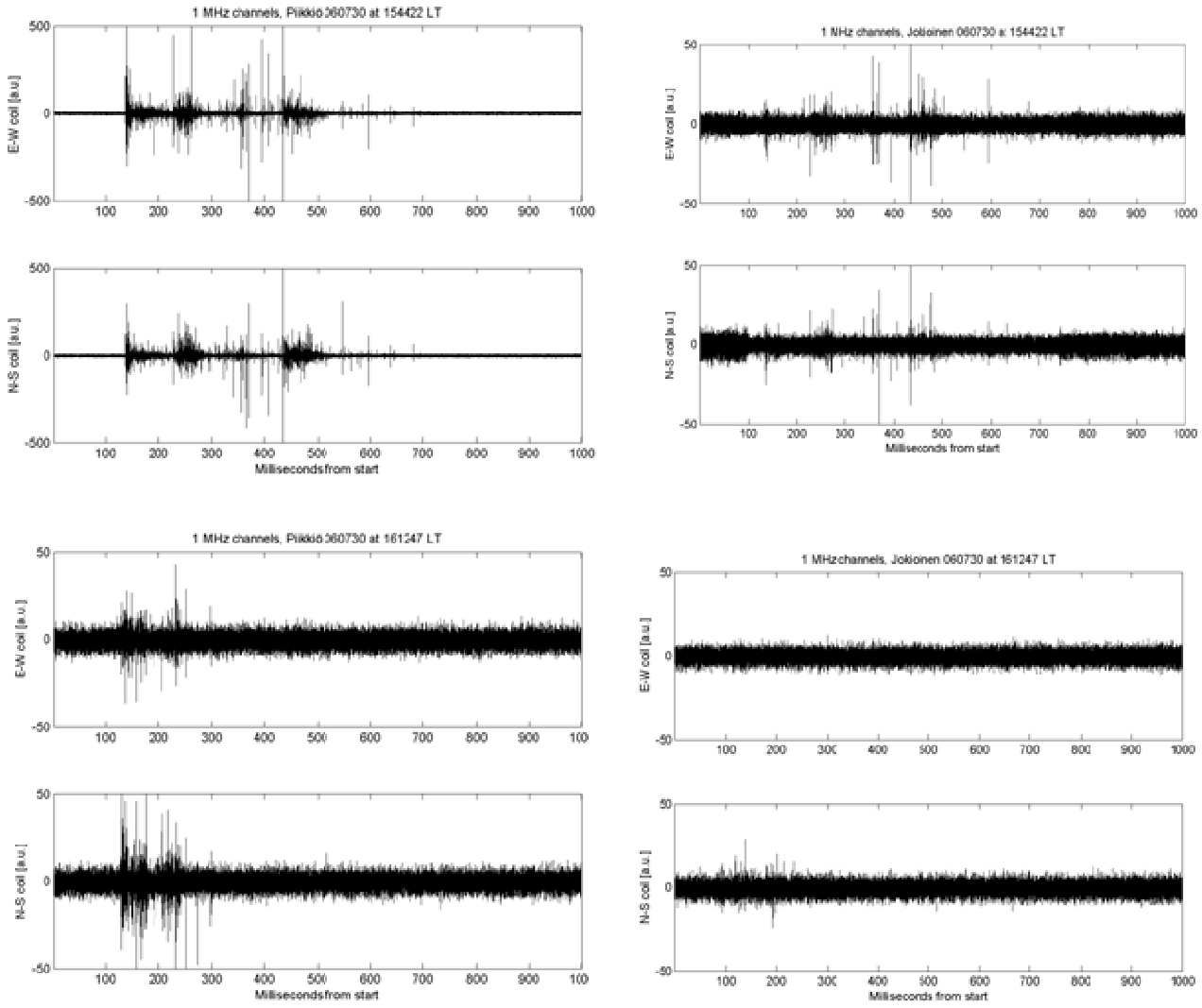


**Figure 8: Narrowband signals from four cloud-to-ground flashes, using the narrowband devices of papers II-IV. The signals from two orthogonal coils are shown in each plot. The x-axis has dimensions of millisecond; each capture lasted 1 second. The y-scale is in arbitrary units; the top left flash has a scale that is ten times larger than the others, and is from a very close flash. The directionality is again particularly apparent in the bottom right flash, in which the distant flash is not seen at all in one of the channels.**

Figure 9 shows the response of the narrowband magnetic antenna and the narrowband flat-plate electric field antenna compared to the broadband signal.

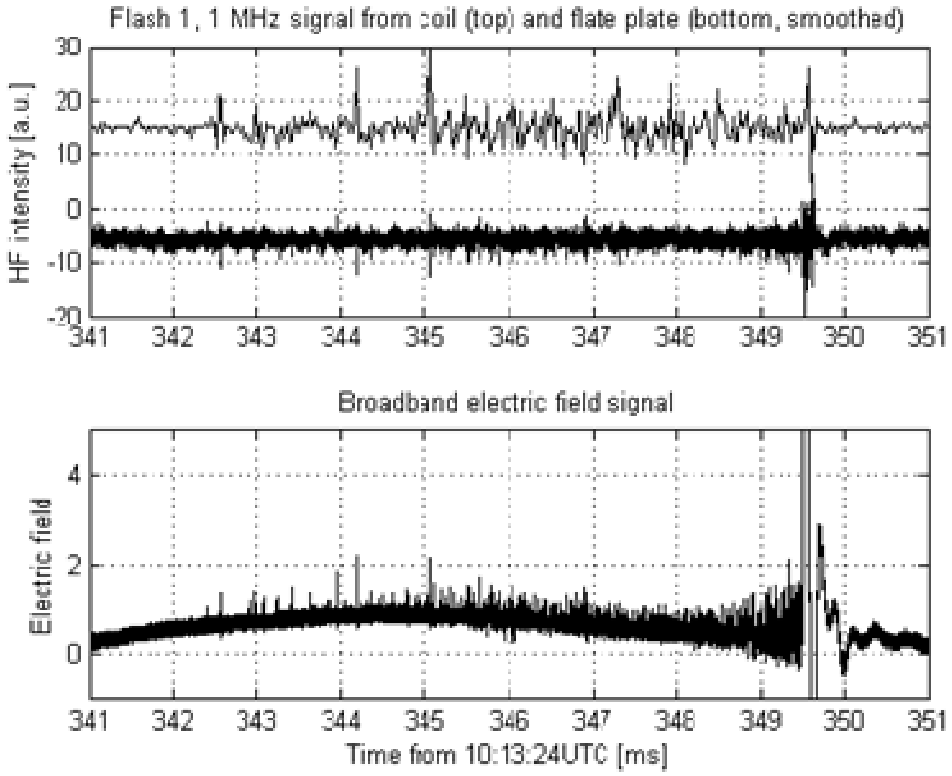


**Figure 9: Close-up comparison of magnetic field and narrowband electric field (top), and broadband (bottom)**

The analysis of Le Vine (1987) discussed in Section 2.2 did not model the effect of downmixing the signal to a lower intermediate frequency, but noted that such downmixing is often done for practical reasons (for example, to simplify the audio processing in a radio). The devices of Papers II-IV performed such downmixing to decrease the data rate and storage requirements. The effect was therefore modeled in Paper III. The antenna resonates at a central frequency $f_c$, while the mixer (local oscillator) was preset to be within 10 kHz of $f_c$. The signal at the antenna response frequency is proportional to $exp(i\omega_c t)$, which is then multiplied by the mixer signal $exp(i\omega_{Lo} t)$ giving

$$s(t) = \exp\left[i(\omega_c \pm \omega_{LO})t\right] \quad \textbf{(20)}$$

The higher frequency is then filtered with a low-pass filter, and the resultant signal is digitized at a sampling frequency of 44.1 kHz. In other words, the resulting signal is an audio signal, and the data were processed and stored through an audio interface. A software was written which followed the baseline

noise level, and stored the signal in one-second clips whenever any peak exceeded a pre-defined threshold of 6 dB above the baseline noise. This system enabled the data collection to be automated. In Paper II, the effect of the mixer stage was not considered in detail since the full-flash energy was used. However, for close-up studies, it is crucial to consider its effect. Because the antenna response and mixer are not necessarily in phase, Equation (20) in fact includes an unknown phase difference $\varphi$, and the equation is

$$s(t) = \exp\left[i\left(\left(\omega_c \pm \omega_{LO}\right)t + \varphi\right)\right] \quad \textbf{(21)}$$

In effect, the phase difference randomizes any impulsive input, since the effect of Equation (21) is to multiply the input by an unknown factor $\exp(i\varphi)$. This is seen experimentally in Figure 10, where a train of identical pulses was fed into the front-end (bottom line). The output peak (upper line) has a random magnitude and sign.

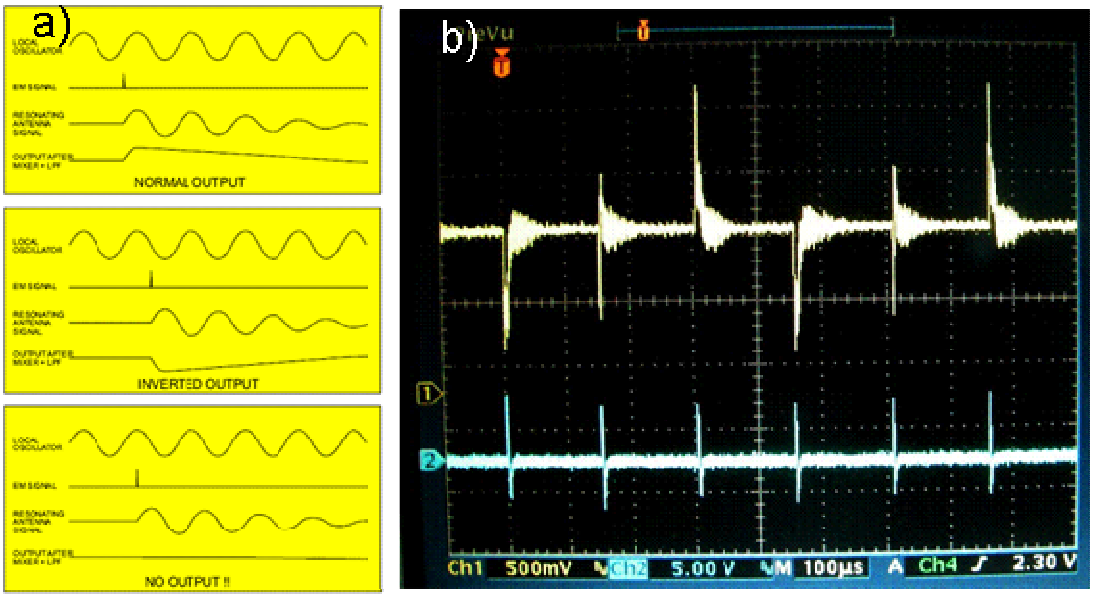


**Figure 10: a) Schematic of the effect of the unknown phase term. An impulsive input function can be output multiplied by any factor between -1 and 1. b) Experimental verification of the mixer effect. A train of identical sharp pulses was fed into the front-ends (bottom line). The output peaks (top line) are seen to be randomized. Picture courtesy of Tom Ahola and Joni Jantunen.**

In the general case, the signal consists of a series of pulses which are each multiplied separately by a random uncorrelated phase signal $S_i = x_i \sin(\phi_i)$. This is analytically solvable in the case of a rectangle function of height $x$ and large length $N$:

$$< S >= \sum | x \sin(\phi_i) | = \frac{2}{\pi} Nx \Rightarrow \frac{< S >}{Nx} = \frac{2}{\pi} \approx 0.637 \quad \textbf{(22)}$$

$$< S_{RMS} >= < \sqrt{S^2} >= \sqrt{\sum x^2 \sin^2(\phi_i)} = x\sqrt{\frac{N}{2}} \Rightarrow \frac{< S_{rms} >}{x\sqrt{N}} = \frac{1}{\sqrt{2}} \approx 0.707 \quad \textbf{(23)}$$

In the case of constant and very long signal, both the direct sum and the RMS sum are proportional to the unmixed signal multiplied by a constant. In such a case, it makes little difference which definition is used to characterize the signal energy. However, since lightning signals are impulsive, the effect of the mixer has to be simulated for short signals. Figure 11 shows the simulation results for a rectangle function of length one (a single peak) and a rectangle function of length two. One hundred peaks of amplitude 1 were run through the mixer model, and the direct sum (top panel) and RMS sum (bottom panel) were calculated. Without the mixer, the sums would always be 100. Five thousand runs were made. Figure 12 and Figure 13 show the simulation results for longer rectangle functions.

Note that the mean values are always close to the ideal values given by Equations (22) and (23). The effect of the downmixing is that it can produce outputs that are very far from this mean. When the length of the rectangle is 50 units, the sum and RMS cluster closely around the ideal values given by Equations (22) and (23). When the length is 10 units, the distribution is still wide but begins to resemble a Gaussian. However, when *N=1*, there is a non-zero probability that the sum of the output pulses is almost zero (which happens if the phases are all near zero). At *N=1*, the sum and RMS are identical. At *N=2* to *N=4*, the RMS sum has a sharper peak. This means that the probability of a severely distorted output is smaller with the RMS sum. The simulation thus suggests that the RMS sum is preferable when the input signal is highly impulsive.

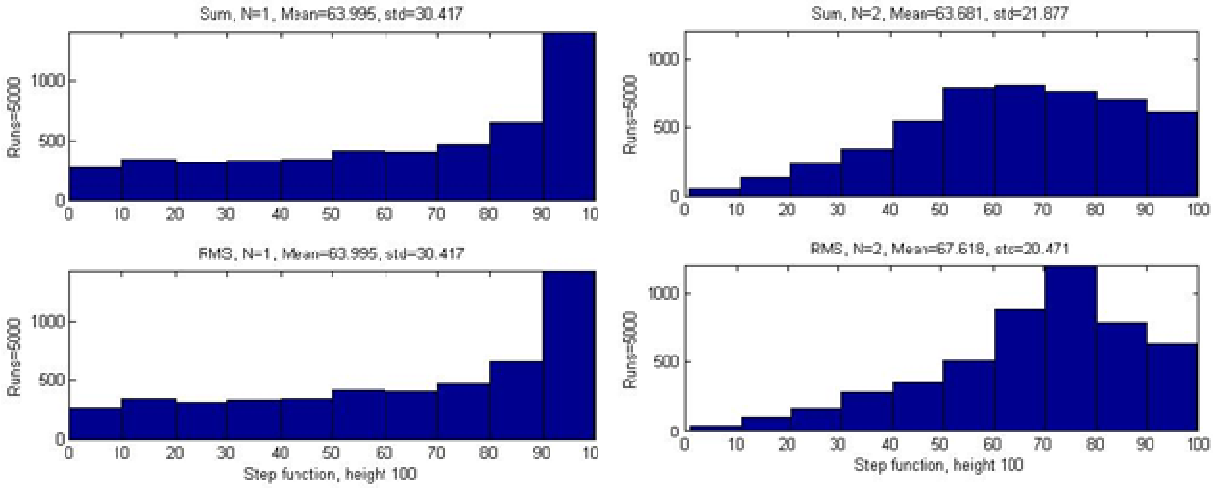


**Figure 11: Effect of downmixing on rectangle functions of lengths *N=1*, *N=2*. See text.**

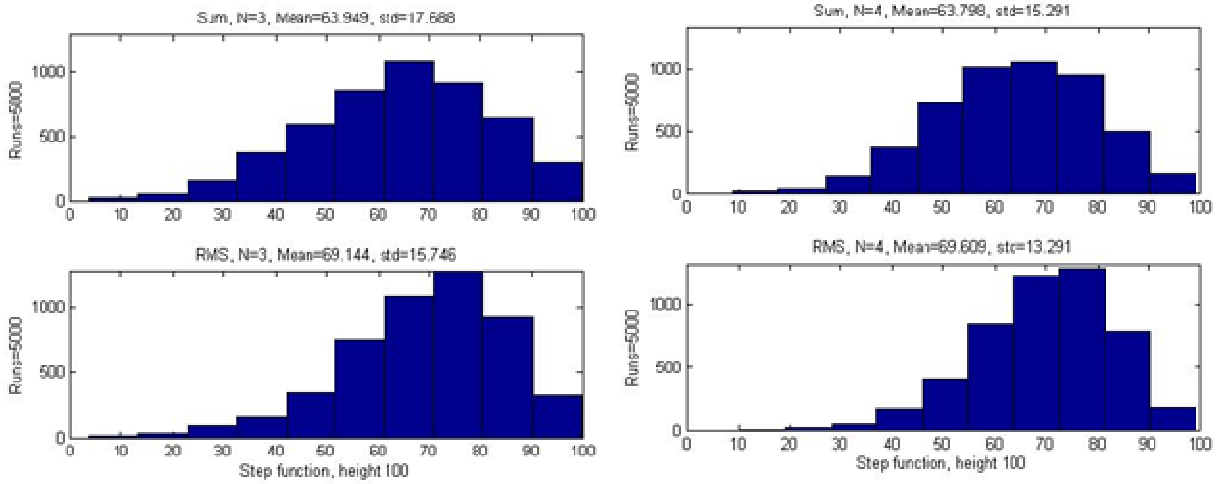


**Figure 12: Effect of downmixing on rectangle functions of lengths *N=3, N=4.* See text.**

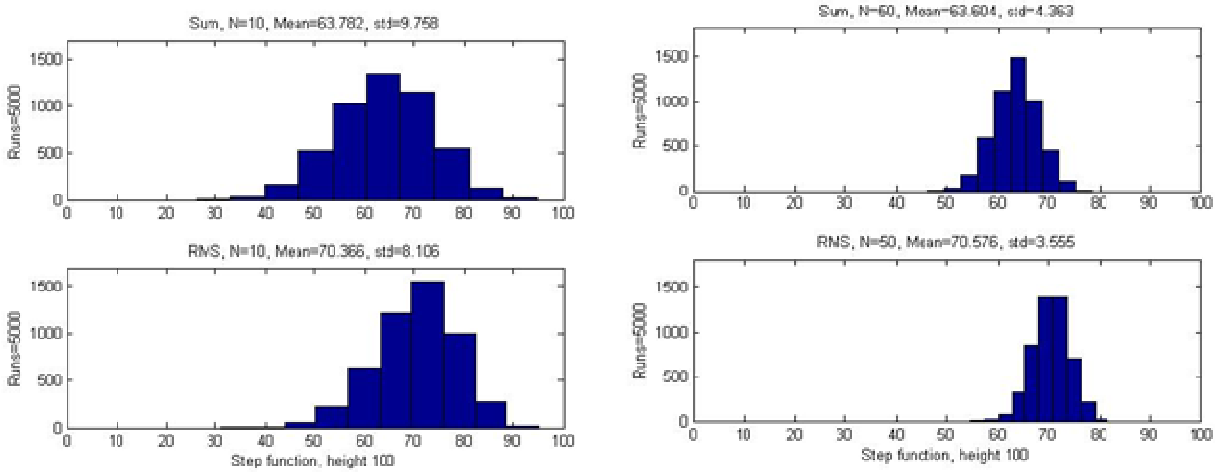


**Figure 13: Effect of downmixing on rectangle functions of lengths *N=10, N=50*. See text.**

Although a rectangle function is not likely to occur in natural lightning, the author has often observed it in man-made interference (see Section 9.3). The downmixing effect can also be simulated for other incoming wave shapes which are less ideal. The worst-case example is a completely random signal,

simulated in Figure 14 and Figure 15. In each simulation, the input consisted of 100 impulses of length *N*, with each input having an evenly distributed random value between 0 and 1. The sum of the unmixed input is shown in the bottom panel of each Figure. For *N=1*, the input is evenly distributed between 0 and 100. The RMS sum, however, is peaked near zero, meaning that the mixer has a high probability of producing anomalously low readings. For these random signals, the difference between the RMS and the normal sum is not as large as it is for a rectangle function. For longer input signals, the sums settle close to constant values.

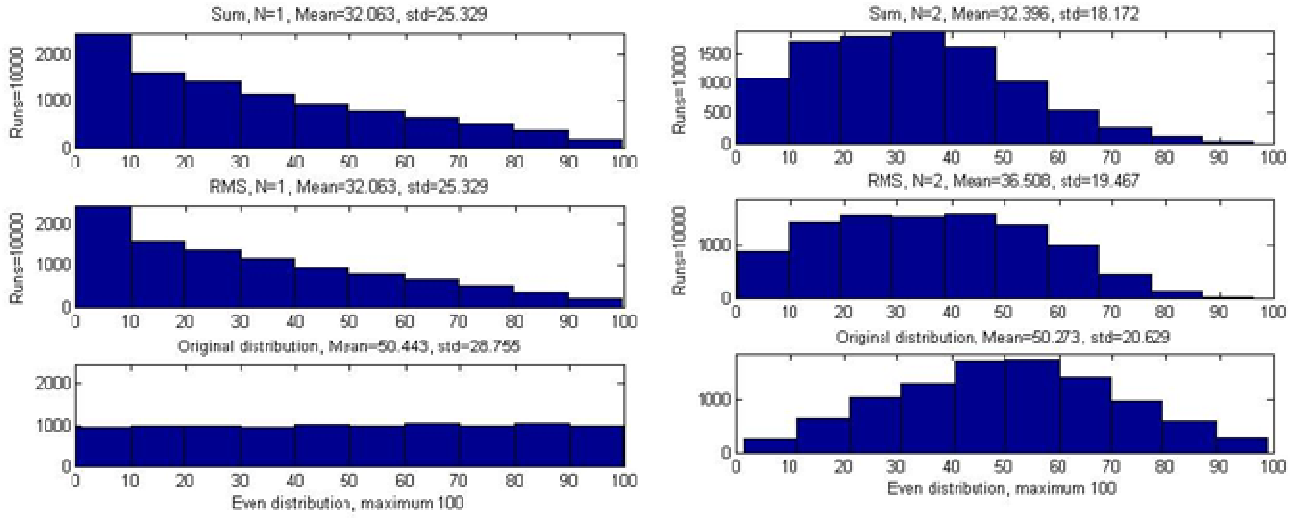


**Figure 14: Effect of downmixing on a random signal. The input (bottom panel) into the mixer consists of single peaks with random values between 0 and 100, resulting in the downmixed sum distributions in the top panel. The middle panels present the downmixed RMS energy. See text.**

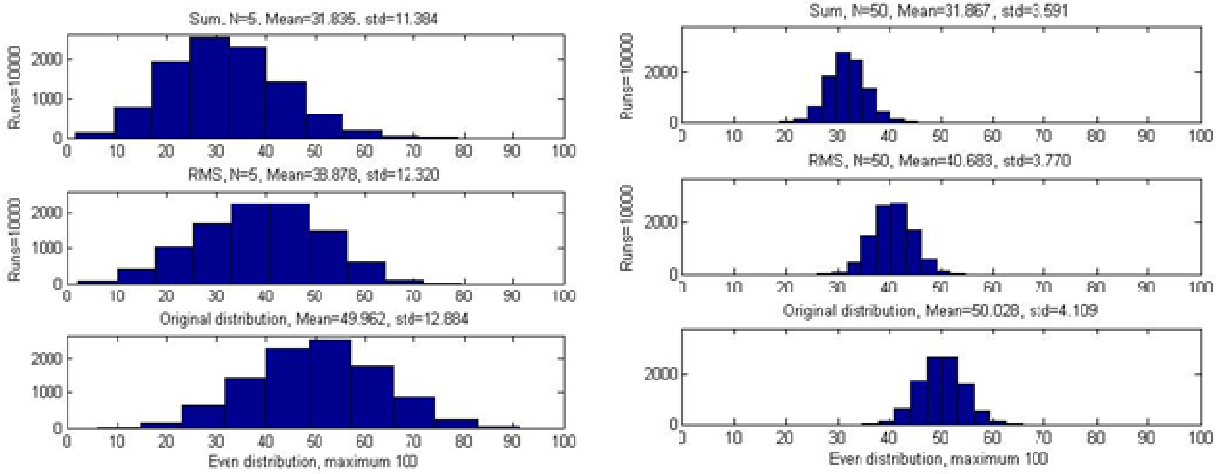


**Figure 15: Effect of downmixing on random signals of lengths 5 and 50. See text.**

The downmixing also affects system calibration. Due to the nonlinearity, there is no simple way to invert the measurements to determine the absolute narrowband energy spectral densities. Calibration must therefore be done empirically. Even if absolute calibration could be made, it would be difficult to compare the result to earlier measurements. Although absolute measurements have been made (see e.g. Le Vine (1987) and Nanevicz et al (1987)), they are average results for a large number of flashes, using a wide variety of techniques and normalizations. The calibrations used in existing commercial narrowband devices have not been published in the open literature, and in any case are likely to be highly dependent on the specific system characteristics. There have been direct narrowband measurements using parallel-plate antennas (e.g. Cooray and Pérez (1994b), Jayaratne and Cooray (1994), Paper I), but the measurements were made without using any gain in the circuits. This makes it difficult to compare those results with the devices used in this thesis which did have gain; as seen in Figure 9, the relative ambient noise levels of the flat-plate antennas and the ferrite coils are quite different. The spectra of individual lightning processes have been transformed from broadband data e.g. by Willett et al (1990) and Weidman and Krider (1986), but again, the issue of noise has not been addressed in these studies. In addition, the measurements have typically not included the full flash, especially its in-cloud processes, which are a crucial part for narrowband detection. The literature therefore does not contain measurements which could be meaningfully used to check the calibration.

# 4 Hypothesis 1 (Papers I, III, IV)

Hypothesis 1 states that in-cloud contributions to the HF radiation can be at least as intensive as the radiation from return strokes. The literature on HF sources was described in Section 2 and is only briefly summarized here. Individual CG processes have been studied in detail, but there is no clear picture of the energy content in the composite flash. There is general agreement that in CG flashes, the return stroke produces an intense but brief HF pulse. Leader processes also emit but much more weakly, particularly the dart leaders that precede subsequent return strokes. Paper I adds the new observation that the presence of a ”chaotic” component (most likely related to in-cloud processes) can increase the intensity of radiation due to a subsequent leader so that it is nearly equal to that of the return stroke. Preliminary breakdowns emit strongly at high latitudes but less at tropical latitudes. Paper III shows that in Scandinavia, the preliminary breakdown can at times have an energy that is comparable to the return stroke energy.

IC flashes have been studied less extensively than CG flashes, as have the continuous signals in CG flashes between subsequent strokes. Although these signals have relatively small intensities, their long durations mean that they can contribute significantly to the composite flash. Paper IV appears to contain the first direct measurements of the electromagnetic radiation from CG and IC flashes at the same distance, albeit only from one storm. The composite energies of IC and CG flashes were seen to be comparable. The paper did not specifically break down the flashes into sub-processes or calculate the intensities of the continua. It is qualitatively clear e.g. in Figure 7 and Figure 8 that even though the return stroke peak can be very intense, the overall effect of the continuous processes is large.

Therefore, the literature is inconclusive on this hypothesis. In general, return strokes cause the most intensive individual peaks in the narrowband HF signal. However, Paper I showed that a chaotic leader can cause an impulse that is nearly as intense as the return stroke. If the composite flash is considered, the low-amplitude continua may well contribute at least as much energy as the higher-amplitude impulsive processes, as are suggested by the results of Paper IV (see also Section 6). The available information therefore does not contradict this hypothesis.

# 5 Hypothesis 2 (Paper II).

Hypothesis 2 states that the distance to a given ground flash can be statistically estimated from the flash energies alone, as long as the sample is large enough.

The simplest possible way to describe the intensity of a lightning signal is to measure the highest peak voltage of the signal. This was expected to produce a very poor energy estimate for the reasons discussed above: the lack of physical interpretation of the highest peak, worsened by the randomization. Therefore, the "glitch energy" (defined in signal processing as the area under the curve of a time-voltage plot) was used. Due to the relatively high ambient noise levels, the glitch energy must be normalized so that pure Gaussian noise gives a value of zero. One way to do this is to calculate the standard deviation σ of the one-second sample. In Paper II, the 3σ level was used as a threshold; i.e. any part of the signal that had intensity was below 3σ was considered to be noise. The glitch energy was then defined to be the RMS sum of all values which exceeded 3σ. This is effectively equal to the RMS energy of the signal minus the RMS energy of the noise, and was used in Paper II.

For Paper IV, the threshold was changed to 4σ, since for one flash digitized into 44100 samples, using a 3σ criterion means that the measured energy for pure Gaussian noise does not quite tend to zero. The difference is negligible for close flashes and does not affect the conclusions made in Paper II. However, since Paper IV also analyzes flashes that are up to 70 km away, the change was explicitly made. Only 99.73% of the data points are within the 3σ level; a Gaussian data set with a record length of 44100 samples will still have 120 points that are above that level. Using a 4σ level (99.994%) means that a Gaussian signal with record length 44100 will have at most 3 points above that level and hence the energy will in fact tend to zero.

In practice, both the peak value and the glitch energy give rapidly decreasing results that could be usable for ranging (Figure 16). Note, however, that the peak value is at least 10 dB weaker than the glitch energy at any given distance; thus, the glitch energy is preferable. It was shown in Paper II that to a first approximation, the energy-distance relationship can be approximated by a simple equation of the form

$$E = a + b / R^k \quad \textbf{(24)}$$

where a and b are empirical constants, and k is approximately 3. Physically, *a* corresponds to the background noise level. The approximation is only piecewise valid, as seen in Figure 17, but is a good approximation for flashes within about 50 km.

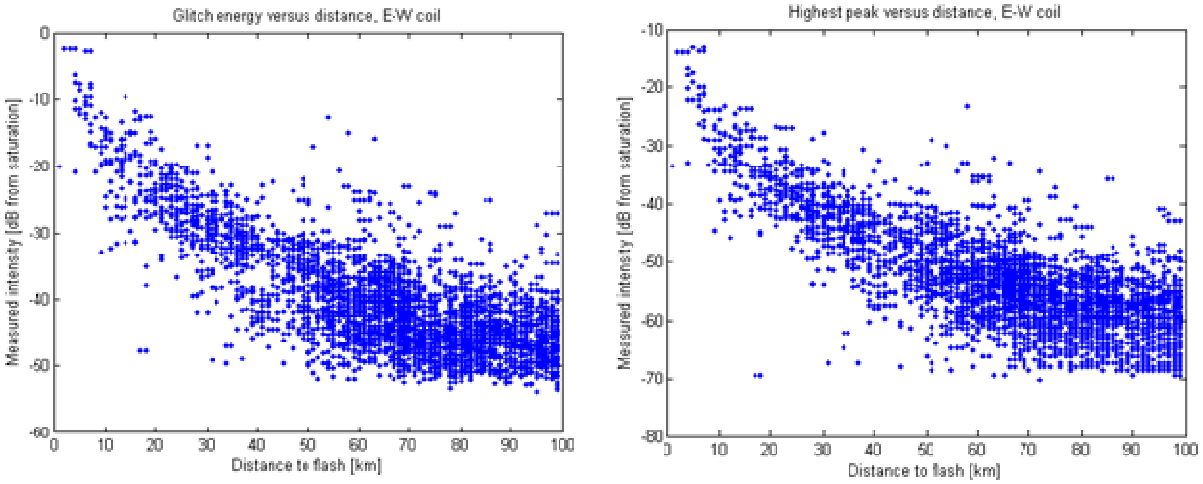


**Figure 16: Two methods of calculating intensity: glitch energy (left), highest peak (right). The highest peak gives a relative amplitude that is at least 10 dB weaker than the glitch energy at the same distance; thus, the glitch energy is the preferable parameter.**

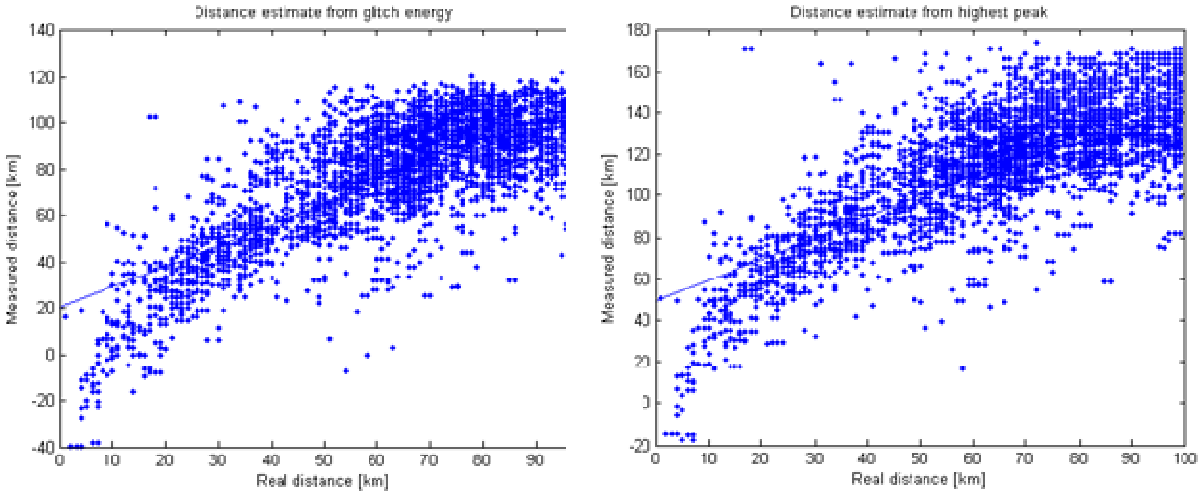


**Figure 17: Fitted least-squares distance estimate using the empirical formula $E=a+b/R^k$, using glitch energy (left) and highest peak (right). Note that accuracy decreases significantly after 50 km, and the approximation is only piecewise linear.**

Ranging can be improved by using two orthogonal coils; this was done in Papers III and IV. A theoretically ideal coil antenna would have an angular response

$$G(\varphi) = \cos^2(\varphi)G_0 \quad \textbf{(25)}$$

where $G_0$ is the gain along the main axis. The idealized approximation was used even though the actual antennas were not quite ideal (see Appendix). Direction-finding was not possible with the setup because the downsampling loses any phase information. Assume now that an ideal vertical current source is located at point *(x,y)* from the orthogonal pair and that the measured signal intensity for an omnidirectional antenna would be *E*. Then the measured intensities will then be

$$E_x = \cos^2(\varphi)E,\ E_y = \sin^2(\varphi)E \quad \textbf{(26)}$$

from which the angle can be solved as

$$\varphi = \arctan\left(\sqrt{\frac{E_y}{E_x}}\right) \quad \textbf{(27)}$$

Since there is no phase information, the angle is projected into the first quadrant. Since the positions of flashes are known from the lightning network data, the values of $\varphi$ can be plotted against the known values of angle $\theta$ to see how valid the estimate is (Figure 18). When the full-flash energy was used, the correlation was strongly statistically significant (r=0.88). Only intense flashes (within 50 km) were used.

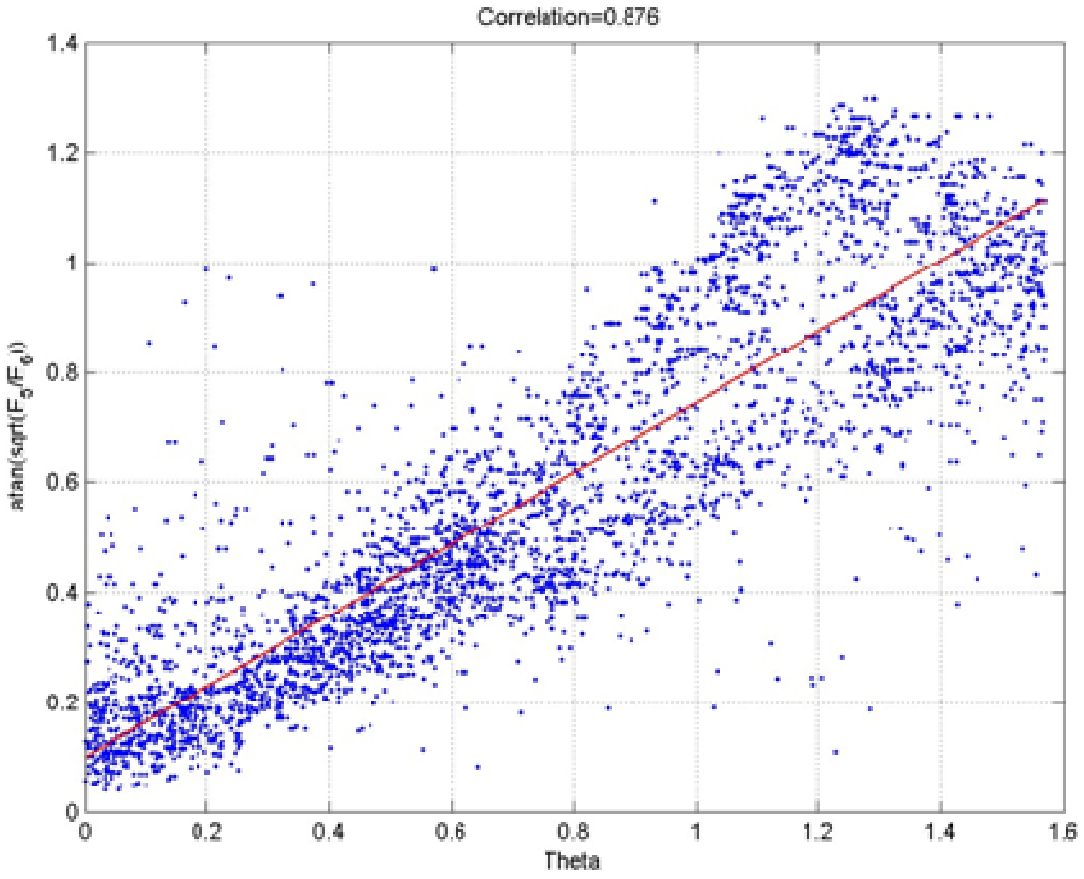


**Figure 18: Correlation between real angle to flash (radians from east-west direction) and angle calculated from the energy ratios. Only flashes up to 50 km were used.**

Orthogonal antennas could therefore, in principle, be used for direction-finding but only projected to a single quadrant. Such information has little practical value, although it could be used to help assess the motion of a given storm cell. More practically, two coils improve ranging accuracy, because for an ideal coil the source energy is simply the sum of the two individual energies. (However, see Appendix for a description of the non-idealities in the system). This eliminates the extra scatter due to the unknown orientation of the coil. The improvement (using glitch energy) is shown in Figure 19, where the light dots show the measurements from a single coil, and the dark dots show the energy estimate from the sum of the coils. The effect on ranging accuracy is shown in Figure 20. Although the result is still only piecewise linear, the scatter decreases significantly, especially at large distances. The useful range of the system could now, at least in principle, be extended up to 100 km.

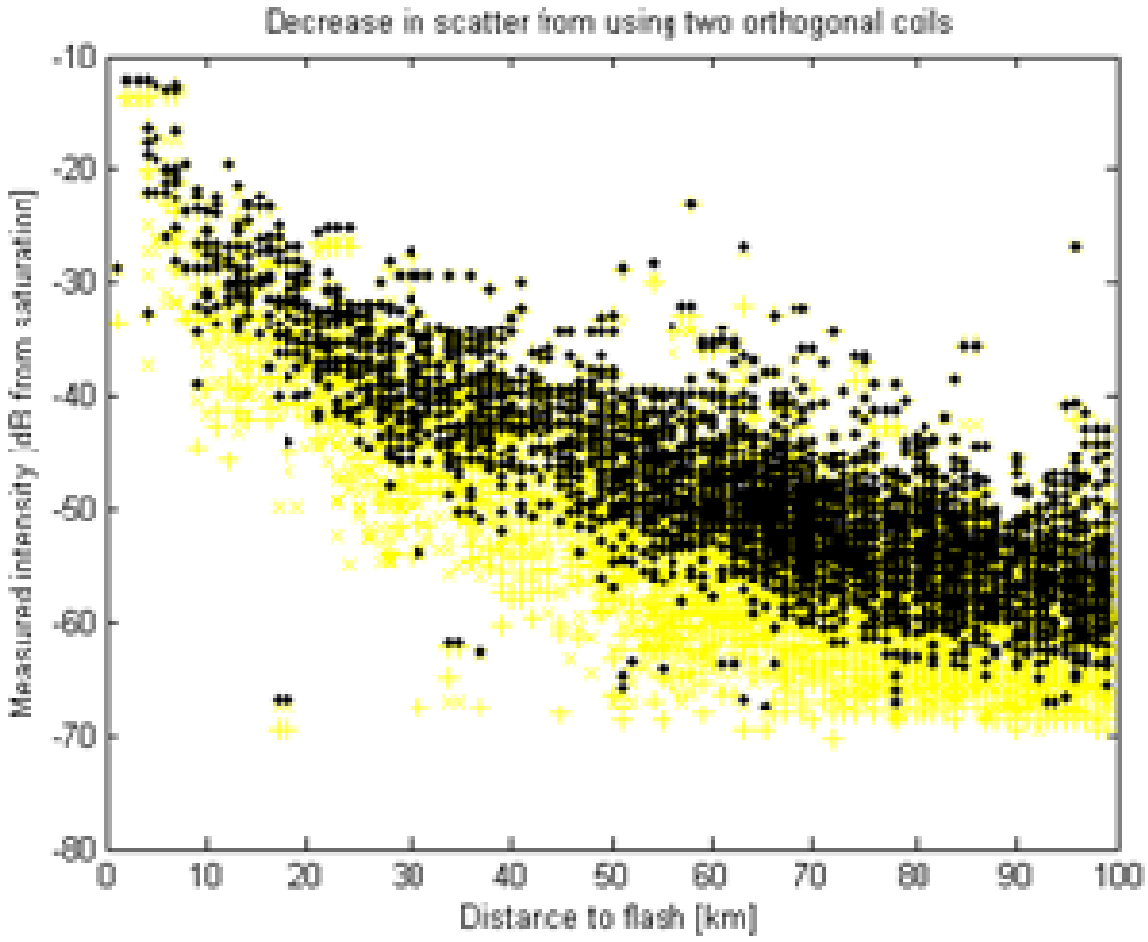


**Figure 19: Decrease in energy scatter from using two orthogonal coils (glitch energy). Light dots: single coil. Dark dots: orthogonal coils.**

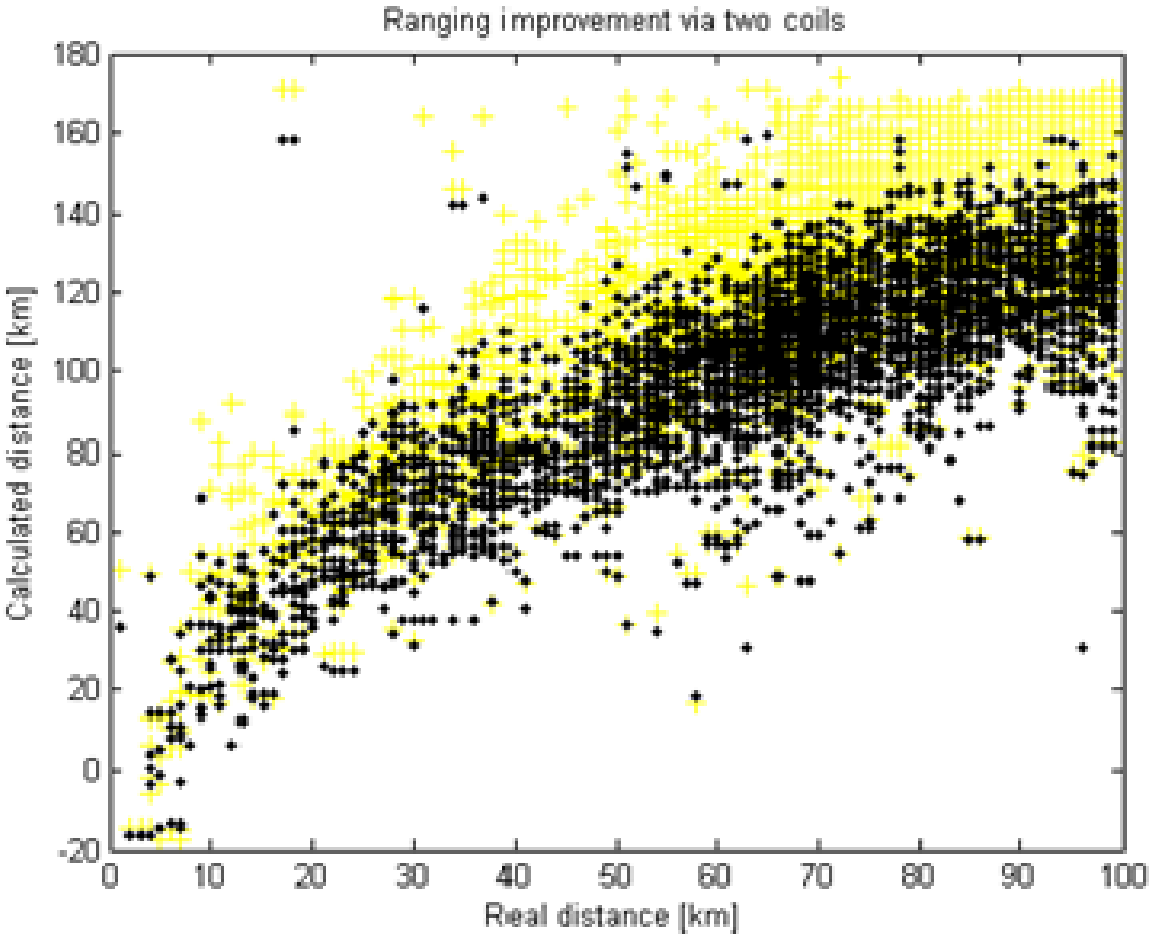


**Figure 20: Improvement in ranging accuracy using two coils. Light dots: single coil. Dark dots: orthogonal coils. Useful range can be up to 100 km (although the basic $1/R^k$ approximation is not valid for full distance).**

The directionality effect brings up a subtle effect which has not been discussed in Papers II-IV. It has a negative effect on the ranging accuracy, but on the other hand, it increases the detection probability with a single coil. Proctor (1997) showed that almost all flashes have a significant horizontal in-cloud component, up to 20 km in some cases but typically 4-8 km in South Africa. For Finland, the typical horizontal extent is approximately 10 km (Tapio Tuomi, personal communication). If the ideal equation $G(\varphi) = \cos^2(\varphi) G_0$ is correct, then there will be a null direction at which a point source is not observed at all. If, however, the channel has a horizontal extent, then part of the channel will still be observed. As a very rough schematic diagram, see Figure 21. The response at the very tip of the channel will then be approximately $G_{\max} \approx (H/R)^2 G_0$. For a channel length of 4-8 km, the value is 4-16% of the maximum value at 20 km, falling to a few percent at 40 km. In addition, a real antenna does not have a perfect null angle. This means that even with just one antenna, there is, in practice, no risk of missing a storm completely.

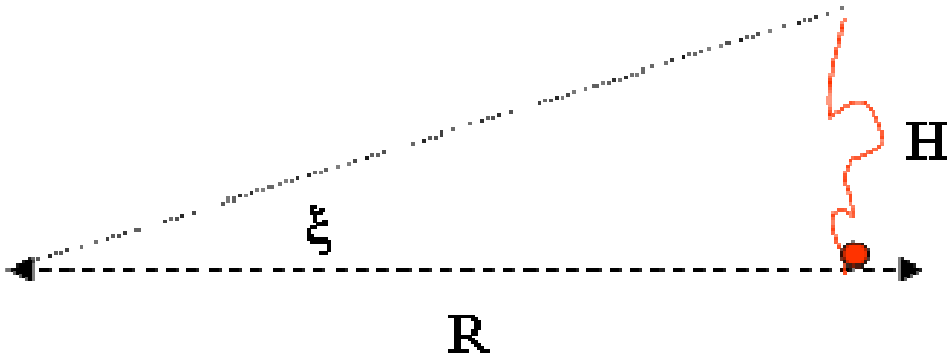


**Figure 21: Schematic diagram of effect of horizontal channel on detection probability. The dot shows the CG location, which is at the null direction of the coil. Part of the horizontal channel H is seen in the coil even if the coil has a perfect null in the direction of the CG location.**

# 6 Hypothesis 3 (Papers III, IV)

Hypothesis 3 states that if the full-flash energetics are considered, the signals from CG and IC flashes do not differ significantly at any given distance. This means that there is no need for to differentiate between CG and IC flashes.

Based on Paper III, in-cloud processes dominate the narrowband energy of CG flashes. However, this in itself does not prove that IC and CG flashes are similar; in fact, the measured data (Figure 7-Figure 8) suggest that they are not. Although the differences are clear to the eye, it was found that no simple metric can be used to adequately differentiate between IC and CG flashes. In Paper II, it is suggested that there are differences between the CG and IC signals, with IC flashes having longer duration and smoother energy envelope than CG flashes. Rather than making the differentiation using a waveform analysis, we evaluated whether such differences could be found by reducing each flash to a few statistical parameters. As discussed in Paper II, the antennas have a directional gain, which was avoided by adding the signals from two orthogonal coils (see Appendix).

Results of such analyses are shown in Figure 22 to Figure 24, from Paper IV. They show the simplest parameters that can be determined from flash data. To reiterate, a "glitch" was defined to be a discrete impulse during which the signal intensity remained above the threshold level; this level was defined to be $4\sigma$ in paper IV. This definition is expected to reveal whether the visually observed features are statistically genuine; the CG flashes should have a small number of glitches with relatively high energy, while IC flashes should have a larger number of glitches, often with lower energy.

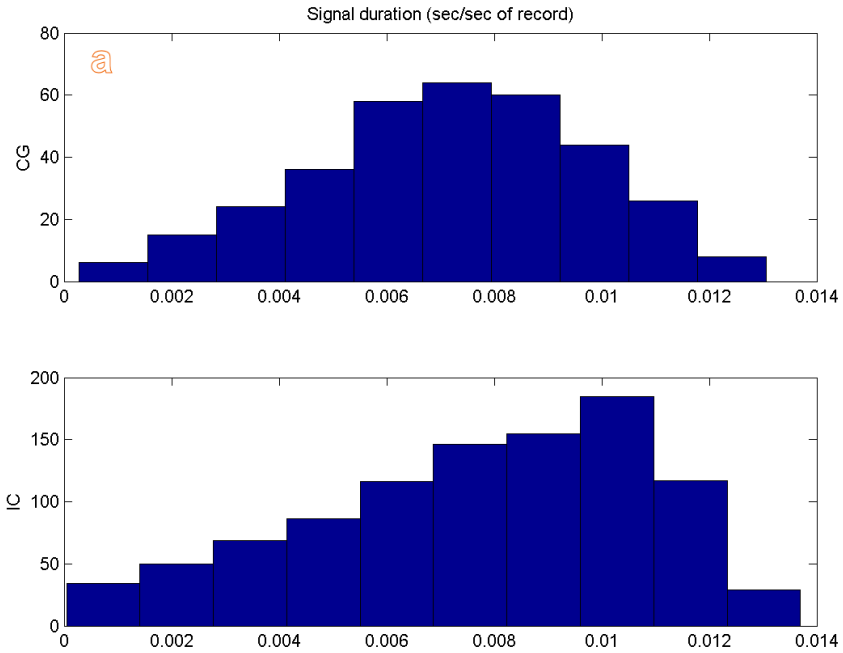


**Figure 22: CG/IC comparison: Average time during which the signal is above the ambient noise level, in seconds/second. From Paper IV.**

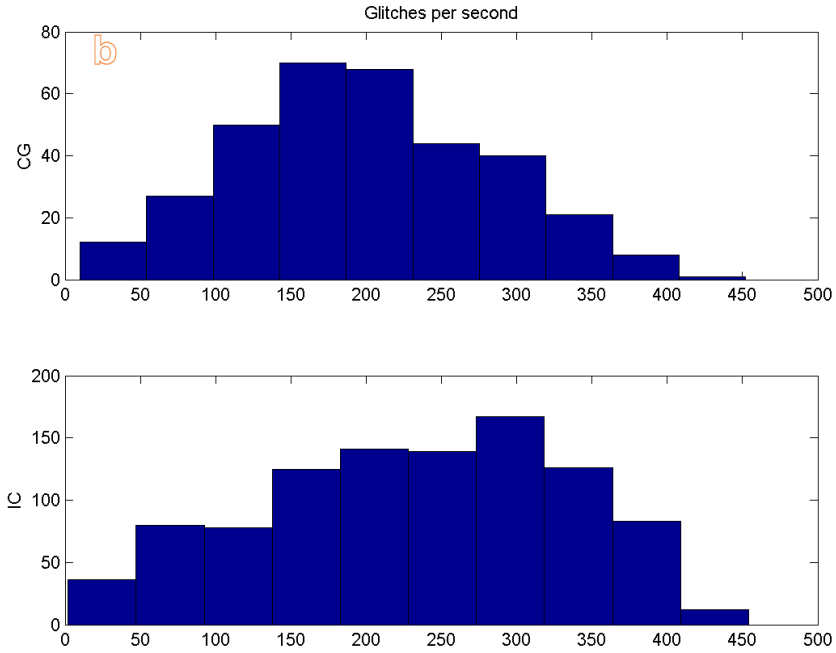


**Figure 23: CG/IC comparison: Number of glitches per second. From Paper IV.**

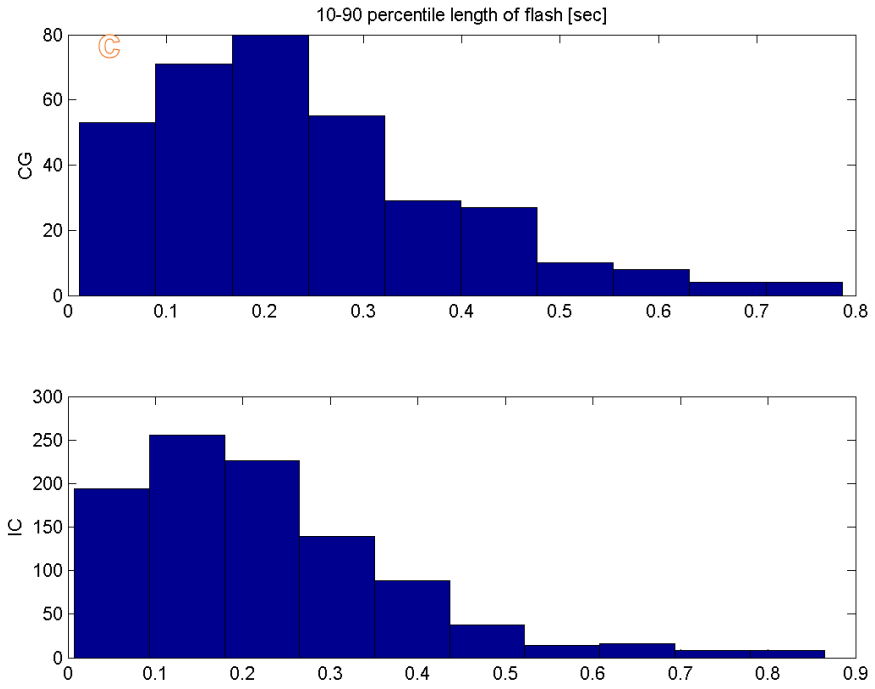


**Figure 24: CG/IC comparison: 10%-90% percentile duration of signal. From Paper IV.**

Figure **22** shows the time duration for which the signal is above the 4σ level. A small duration means that the signal has only a few peaks. The number of glitches (Figure 23) is a measure of the smoothness of the signal; a small value indicates that the signal is relatively smooth. The 10% to 90% cumulative energy distribution (Figure 24) is a robust estimate for the duration of the flash. There clearly are differences in the distributions, but they are not large enough to enable a reliable differentiation based on such simple metrics alone. Traditionally, the lack of such discrimination would be considered a weakness. However, when the statistical risk-based approach is used, such differentiation is not necessary. Every flash, whether IC or CG, means that electrical breakdown is possible, and, in principle, the next flash could be a CG flash.

The question could be conclusively answered by comparing large numbers of IC and CG flashes at similar distances. This is, however, not easy to do in practice, since the ground truth for IC flashes is difficult to determine with current measurement devices. High-resolution networks using VHF imagers are in principle capable of doing this, but the VHF lightning-location system of the Finnish Meteorological Institute was not sufficiently accurate in 2006. A direct comparison is possible if a lightning cell is very small in horizontal extent and travels toward the measurement location; in this case, it can be estimated that the CG and IC flashes are co-located within the horizontal extent of the cell. In such a case, the accuracy is not necessarily much inferior to a direct measurement with a VHF imager;

note that even with a VHF imager, the large horizontal extent of a typical IC flash makes it impossible to define a single unambiguous value for distance.

Such ideal cells are very rare, at least in Finland. The analysis of Paper IV was based on a single intense storm with well-defined cells, occurring on July 30, 2006, between 1430-2000 local time (UTC+3). Several well-defined individual cells were formed close to the Piikkiö site, and moved to the northwest, and there was no other significant activity within several hundred kilometers. A total of 412 CG flashes were identified within 30 km by the lightning detection network during the storm. In the same time period, 1473 narrowband signals were triggered. Of these records, 341 could be unambiguously tied to a CG flash. This implies rather a low detection efficiency, but it is, at least in part, due to the automatization of the measurements. A relatively high triggering level of 6dB above the baseline level was used to limit the number of spurious signals. At this level, weaker flashes may be missed. Of the remaining records, 43 were due to a known instrumental anomaly which recorded very long flashes twice. In 102 cases, the signal was either an interference signal similar to those discussed in Section 9.3 (most likely due to light switches), or single peaks, which may be due to very distant lightning over the sea. This left 987 flashes consistent with IC flashes within the same distance range as the CG flashes. There is a 3:1 ratio between IC and CG occurrences.

The results are shown in Figure 25. Qualitatively, the energies measured for IC flashes and CG flashes were comparable at any given moment. To quantify the connection, each CG flash was compared to all IC flashes that occurred within five minutes of the CG flash (the value was chosen arbitrarily, but the results are not sensitive to variations in the time chosen). The result is shown in Figure 26, where the CG energies have been sorted for clarity. There is considerable scatter, and for the very highest CG energies, the IC energies appear to be systematically lower. The implication therefore is that overhead CG flashes would tend to radiate more intensively than overhead IC flashes. No further discussion of this was made in Paper IV, but there may, in fact, be a simple geometric explanation: the closest part of a CG return stroke can be arbitrarily close to the measurement point, while the closest part of an IC flash is located at the altitude of the flash (several kilometers). In the storm used in this analysis, there were 42 flashes that were within 3 km of the measurements site (Figure 27). It is seen that the number of very intense CG flashes is indeed approximately 40; for the rest of the flashes, the IC energies become comparable to the CG energies. There was correlation of 0.5 between IC and CG flash energies (Figure 28) which is significant at $p=0.01$. The implication is that the source intensities of IC and CG flashes do not differ significantly.

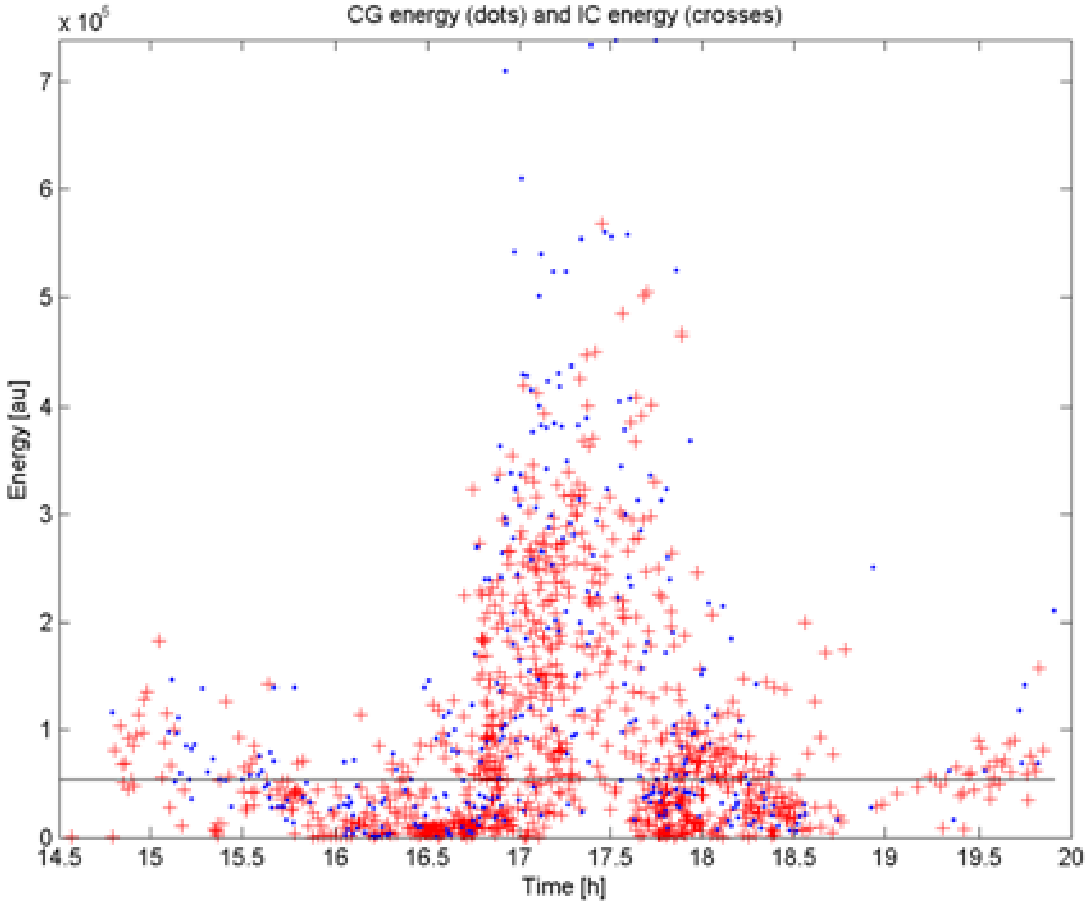


**Figure 25: Comparison of measured CG and IC energies for June 30, 2006 storm event. Dots are CG flashes, crosses are CG flashes. The x-axis is UTC hours from midnight. From Paper IV.**

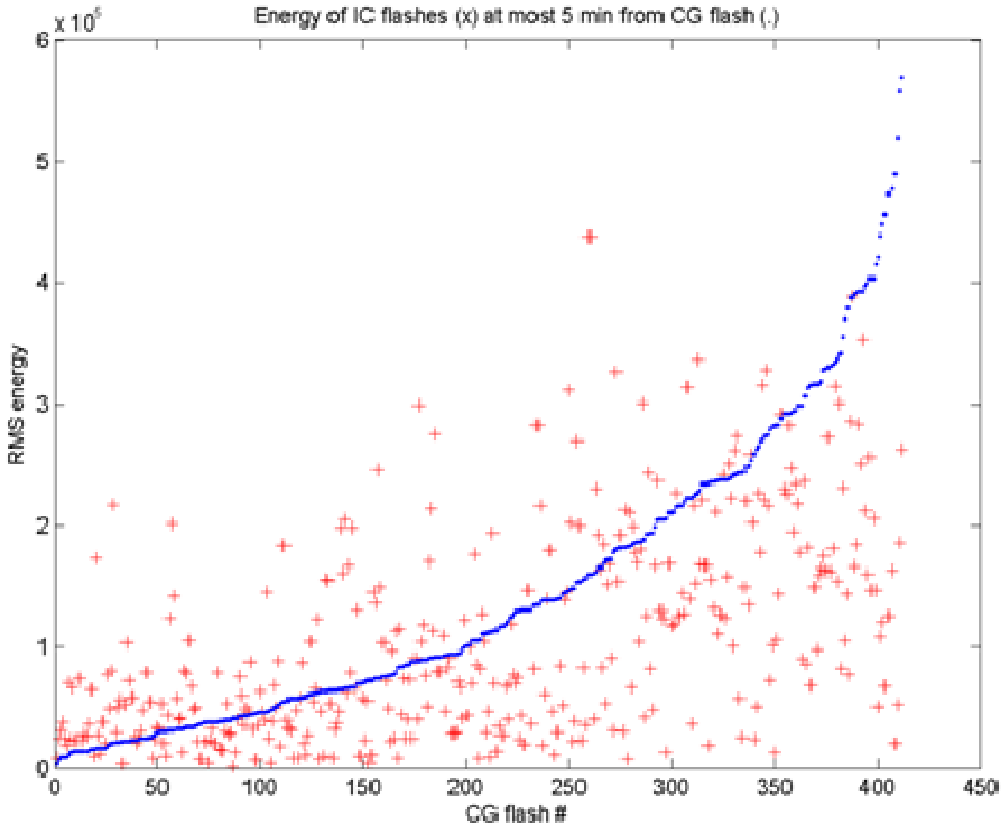


**Figure 26: Spread of energies of IC flashes that are temporally collocated with CG flashes. The CG flashes (dots) are numbered on the abscissa in order of increasing energy. From Paper IV.**

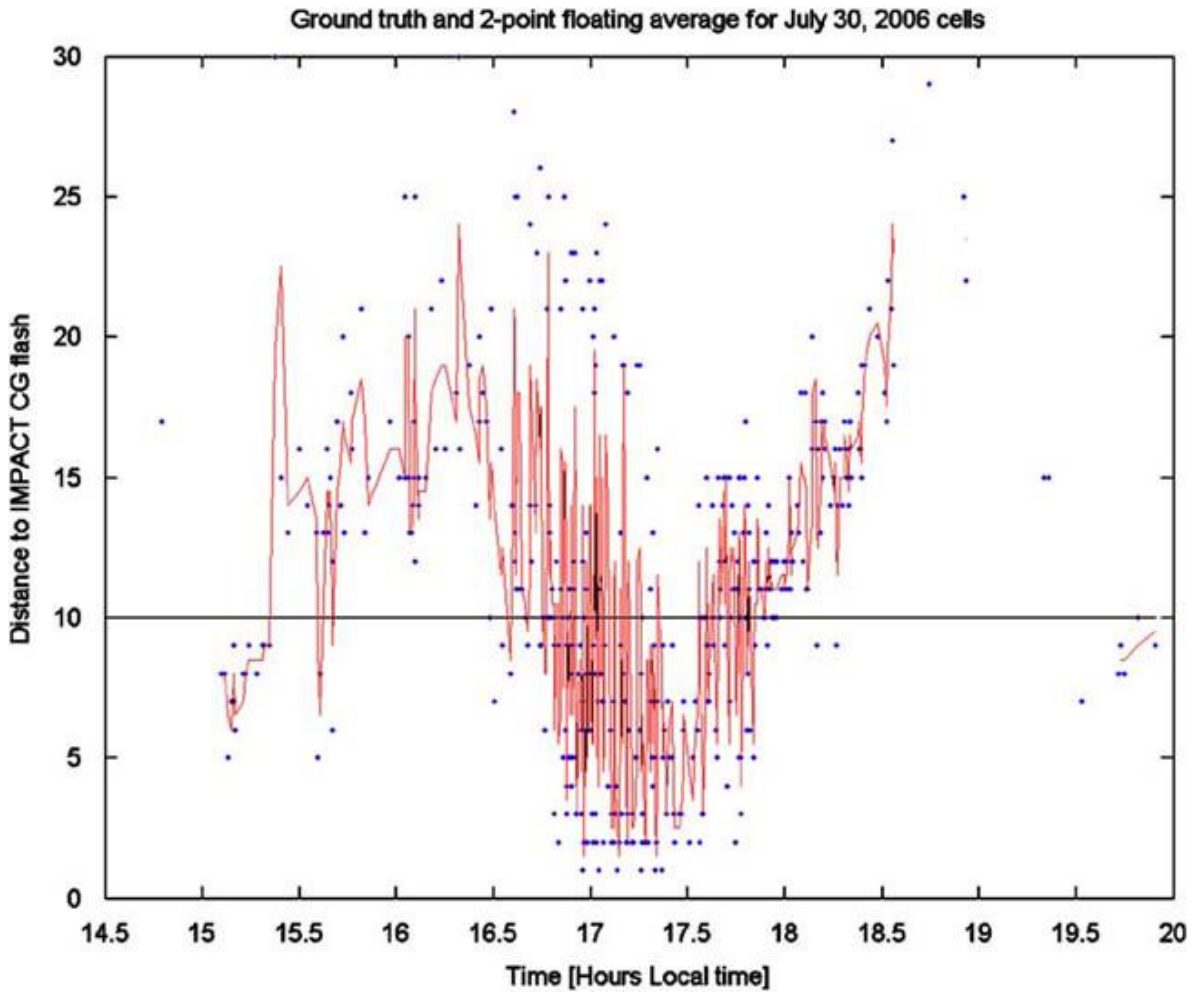


**Figure 27: Distances to the CG flashes of the storm analyzed in Paper IV. The x-axis is local time in hours. The dots are distances to each flash; the line is a two-point floating average to aid the eye. A total of 42 flashes were within 3 km of the measurement site. From Paper IV.**

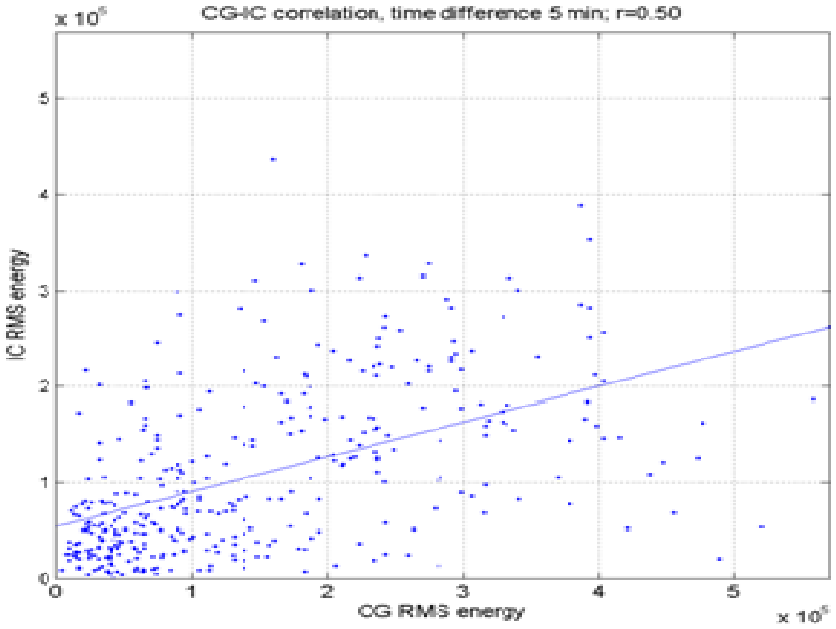


**Figure 28: Correlation of CG and IC flash energies. From Paper IV.**

In the general case, it is not clear whether this approach of using CG location as a proxy for IC location is valid. In the specific data set of Paper IV, the horizontal extent of the cell was small (as seen in the CG location data as well as visual observation of the storms), which means the CG and IC flashes will have been collocated within a small area. It is known that CG flashes as well as IC flashes may have significant horizontal extent. Furthermore, Proctor (1997) made observations with a VHF imager in South Africa, and showed that most IC flashes have a horizontal extent between 4 and 8 km with extents of more than 20 km observed but uncommon. Proctor (1997) also noted that especially when the IC source altitude is low (less than 7 km), there is no a priori way to determine from the stepped leader phase whether a given flash will continue as an IC flash or become a CG flash (this is some contrast to the earlier results of Kitagawa and Brook (1960), who found that IC and CG flashes have distinct types of preliminary breakdowns). In combination, these factors justify the use of the CG locations as a proxy for the IC locations in this particular case.

It is less clear whether this is a valid assumption globally. Much larger horizontal extents for IC flashes in the tropics have been suggested e.g. by Mazur et al (1998) in the case of "spider" lightning; however, there are no statistics on the horizontal extent of these flashes, nor is it really known whether they are common or anomalous. There is no quantitative way to define an exact "distance" to such a flash. However, with the risk-based approach, Paper IV points out that the parameter of interest is the distance to the closest part of the flash. Since the intensity drops rapidly as a function of distance, this closest part dominates the signals. For a channel oriented radially to the observer, the distant parts contribute little. However, if the channel is tangential to the observer, most of the channel contributes to the composite signal.

At present, there is no model to account for this exactly. However, Figure 29 shows the result of an (unpublished) simulation of an extreme case in which the flash is assumed to have a horizontal extent H

of 10 km, and the closest location R is at 10 km. In addition, all the in-cloud activity in the flash is assumed to occur along this channel. Each channel segment is assumed to contribute an energy that is related to the distance $R$ as $R^s$, where $s$ is an unknown exponent. Since the exact value is not known, the plots are shown for different possible values of $s$. The plots are normalized so that the intensity is 1 in the case where the channel is radial to the observation point. Figure 30 shows the resulting scatter in intensities for $s=-1$. The distribution has a long tail, but the median is 1.08 and the 90$^{th}$ percentile is 1.32. Crucially, the error is always on the side of caution: the closest position of the flash may be ranged to be too close, but, in principle, never too distant. According to this simulation, the median error in the intensity is 8%, and the error is essentially always less than 30%. This results in a median distance error of 3% and the 90$^{th}$ percentile error is 10% in the direction of a smaller distance. In the worse case of $s=-3$, the median error is 1.2 and the 90$^{th}$ percentile is 2.3, corresponding to a median distance underestimate of 6% and 90$^{th}$ percentile error of 32%.

The simulated channel length of 10 km may be a slightly pessimistic value, given the smaller extents observed by Proctor (1997), but when the channel length is shortened to 4 km in the simulation (not shown), the maximum error only drops by about 0.1 units. Unlike other errors discussed in Section 8, this systematic error will not disappear in the floating average, but the systematic error will tend to the median and hence cause only a few percent of error.

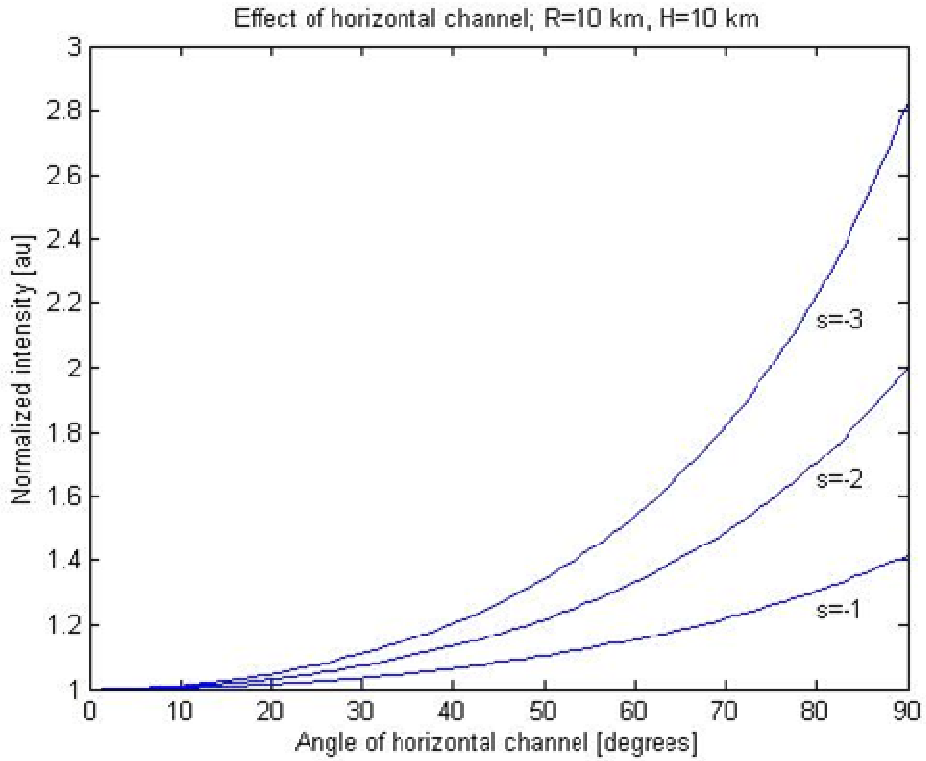


**Figure 29: Simulated effect of horizontal channel orientation on measured intensity. The modeled flash is an extreme case, with horizontal extent 10 km and located 10 km from observer. Results shown for three possible values of distance-attenuation exponent *s*.**

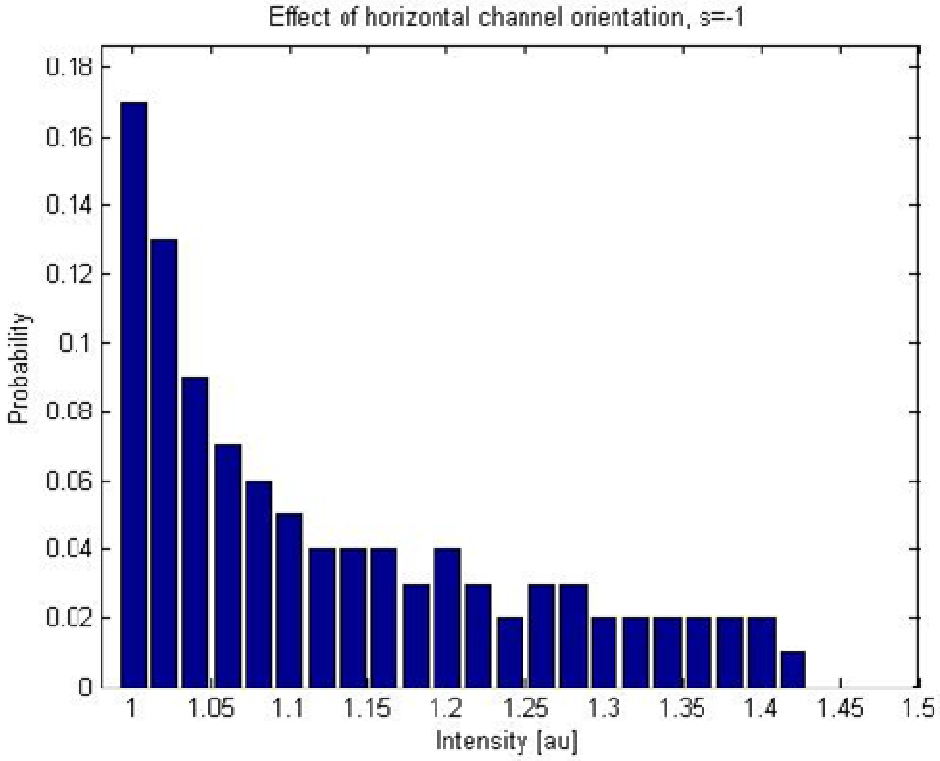


**Figure 30: Simulated effect of channel orientation when the distance-attenuation exponent *s* has value -1. Median intensity is 1.08; 90th percentile is 1.32.**

# 7 Hypothesis 4 (Papers III,IV)

Hypothesis 4 states that although ground conductivity affects the results, its effects can be neglected in the first approximation. There is, at present, only a qualitative model to explain the distance dependence of the HF intensity. The model cannot take into account variations in the ground conductivity. No quantitative modeling is made in Paper III, but empirically, the results are consistent with the propagation effect described by Cooray (2007). The signal from the lowest part of the return stroke propagates predominantly as a ground-wave even at close distances, with no significant change in the propagation regime as distance grows. However, the signal from the preliminary breakdown propagates as a space-wave at very close distances (with little attenuation), but as the distance increases a larger part of the signal propagates as a ground-wave (with faster attenuation).

This change in the propagation regime qualitatively explains the fast drop in intensity observed in Paper II, compared to the peak electric field which drops as *1/R*. Most of the narrowband energy is emitted by in-cloud processes; these undergo a change in the propagation regime from pure space-wave to pure ground-wave. The end result is that the drop in intensity is expected to be non-linear; within the limits of this thesis, the exact form of the distance dependence cannot be theoretically determined. The data points in Paper III have a large scatter, and thus it is not possible from this data set to derive more than a qualitative agreement with the simulations of Cooray (2007).

If the theory above is valid, it implies that there is a ”break-even” distance at which the ground-wave contribution can no longer be ignored. Within the break-even distance, the detector would be ”universal” in that there is no need to consider the ground conditions. Beyond the break-even distance, the ground characteristics would need to be factored in. In the worst case, the system would become unreliable for example at the coast (with over-the-sea lightning appearing to be much closer than ground-based lightning). The “break-even” distance could not be theoretically determined in the scope of this thesis.

The results in this section are therefore based on the measurements shown in Paper IV. The data set includes flashes that were located within 70 km of both stations; this is an approximately oval shape between the stations in Figure 6, and avoids flashes that would be directly overhead one of the stations. This area contains no major bodies of water or cities and consists mainly of flat clay-based ground. Equation (24) be simplified, if is assumed that the background noise (the constant $a$ in the equation) is negligible. Then, if the ground conductivity is assumed to be constant as a first approximation,the equation has a particularly simple form. (Note that in Paper IV, the variable $E$ of Equation (24) was named $I$. For the sake of consistency, the equations of Paper IV have here been written using $E$). To keep the equations dimensionally correct, $E_0$ can be defined as the intensity at distance 1 km. Then

$$E_i = E_0 / R_i^k \,. \quad \textbf{(28)}$$

With two stations and known distances, there are two equations and two unknowns. The solutions are

$$k = -\frac{\ln(E_2 / E_1)}{\ln(R_2 / R_1)} \qquad \textbf{(29)}$$

$$E_0 = \sqrt{E_1 E_2 R_1^{\,k} R_2^{\,k}} \qquad \textbf{(30)}$$

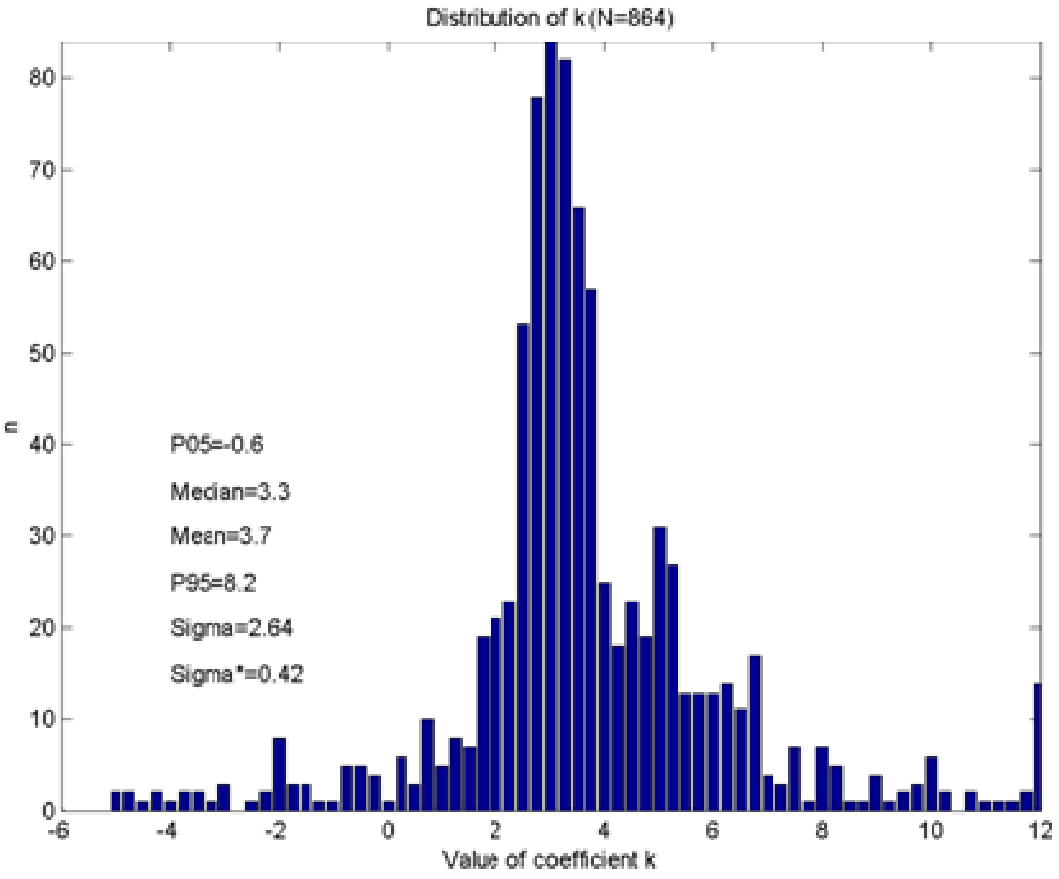


**Figure 31: Distribution of values of exponent *k*. From Paper IV.**

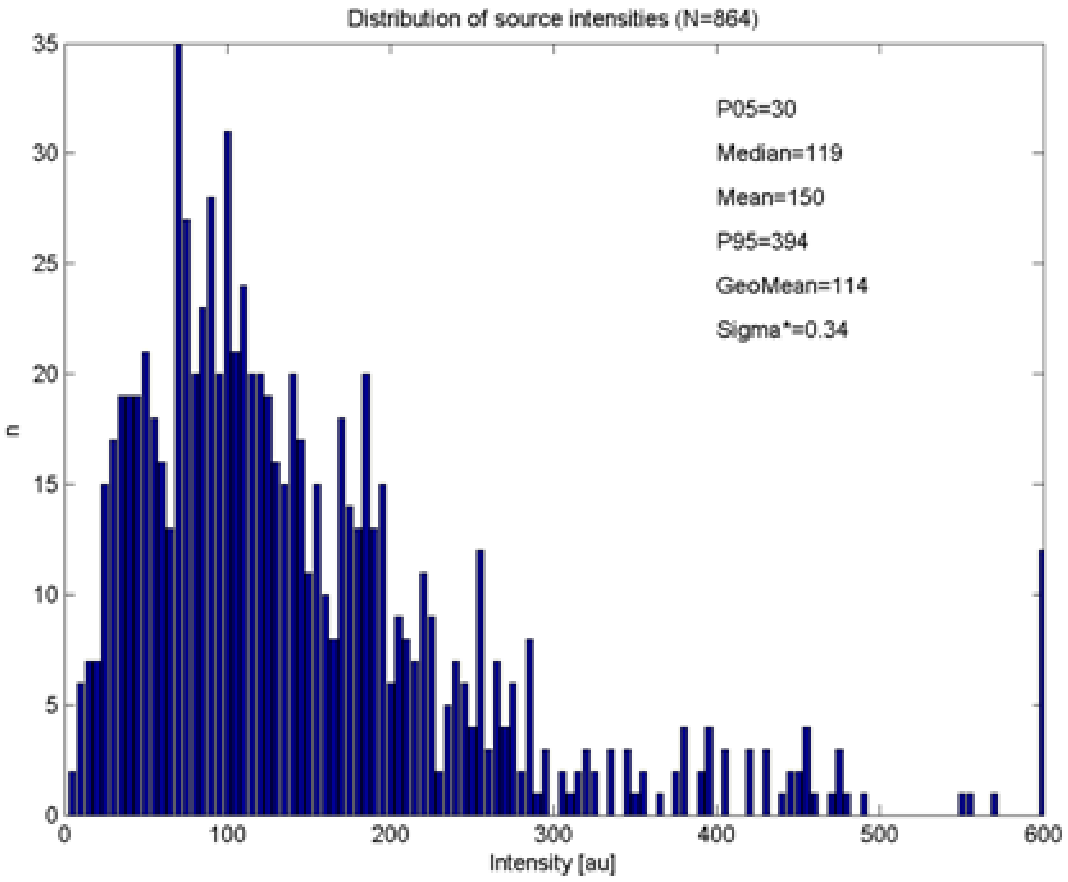


**Figure 32: Distribution of source intensities. From Paper IV.**

The distribution of the measured values for $k$ is shown in Figure 31. Although there is some scatter, the median value is 3.3, consistent with the value determined in Paper II. The very large values of $k$ are due to the numerical instability of Equation (29) is when $R_1 \approx R_2$; i.e. when the flash is equidistant from both stations, any small variations will cause significant variations in the calculated value of $k$.

The calculated source intensities are shown in Figure 32. The distribution is long-tailed and reasonably modeled by a log-normal distribution with $\sigma^* = 0.36$. This is consistent with the results of Pierce (1977), who also suggested a log-normal distribution in the absolute intensities (at $R$=100 km the median is 4 V/m, but 10% exceed 12 V/m) and the intensities of HF/VHF pulses (with a standard deviation around the median of 6 dB). Additionally, Pierce (1977) noted that the average intensities for different storms may vary by up to a factor of two. Based on the information available, it is not possible to determine what the values of $\sigma^*$ would have been, and thus a quantitative comparison to the results of Paper IV is not possible.

However, two additional factors must be considered. Equation (28) ignores background noise, and is at best piecewise valid; with only two stations, it is not possible to include more terms in the approximation. Also, the propagation characteristics of the ground are likely to be non-uniform. The only analytically tractable model is to use empirical attenuation parameters $\alpha$ and $\beta$, which depend on the ground conductivity of the propagation path from the flash to the given station, so that the pair of equations is written as

$$E_1 = \alpha E_0 / R_1^{\,k} \qquad E_2 = \beta E_0 / R_2^{k} \quad \textbf{(31)}$$

Unless the ground is completely homogeneous, the values of $\alpha$ and $\beta$ will vary from flash to flash. Ground conductivities can vary from $10^{-2}$ to $10^{-5}$ S/m as discussed by Master and Uman (1984), while the attenuation constant at 1 MHz can drop by close to 30 dB when the conductivity drops by 10 dB (Cooray (1994)). The solutions for each individual flash are then

$$k = -\frac{\ln(E_2 / E_1) - \ln(\beta / \alpha)}{\ln(R_2 / R_1)} \qquad \textbf{(32)}$$

$$E_0 = \sqrt{1/\alpha\beta}\,\sqrt{E_1 E_2 R_1^{\,k} R_2^{\,k}} \qquad \textbf{(32)}$$

Note that Equation (6) in paper IV erroneously had the term $\sqrt{\alpha\beta}$ in the numerator. This does not, however, affect the results of paper IV. The error introduced in *k* can be analyzed as a function of the distance ratio $D = |(R_2 - R_1)/(R_2 + R_1)|$. For small values of D, Equation (32) will be dominated by the *ln(β/α)* term, in addition to being numerically unstable.

However, a simple argument suggests that the value of $\beta/\alpha$ will be symmetrically distributed around the value 1, at least in the case of the particular measurements of Papers II-IV. Consider the ground as a mesh in which individual cells can have random values of ground conductivity, but there are no large conductive areas such as lakes. The attenuation of a signal will depend, in the first approximation, on the average conductivity along the line connecting the flash and the station. With these assumptions, for a large number of flashes, the statistical distributions of $\alpha$ and $\beta$ will be identical. The mean value of $\beta/\alpha$ therefore tends to 1, and *ln(β/α)* tends to zero. Thus, the extra term in Equation (32) is distributed around zero, and simply causes more spread in the calculated values of *k*. The spread should be most severe for small *D*.

This is, in fact, observed in Figure 33 where the calculated values of *k* are plotted as a function of *D*. The mean and 1σ lines are drawn as horizontal dashed lines; as is seen, the equation is indeed unstable for small *D*, that is for flashes which are equidistant from both stations. The analysis was, therefore, redone for data where *D* was large enough for Equation (32) to be well-behaved; $D > 0.4$ was chosen. The results (Figure 34 and Figure 35) show that this reduces the outliers but does not change average values. The average value of *k* approaches 3.1, while the source intensity distribution is not essentially changed. In other words, the errors cancel out for a large enough data set.

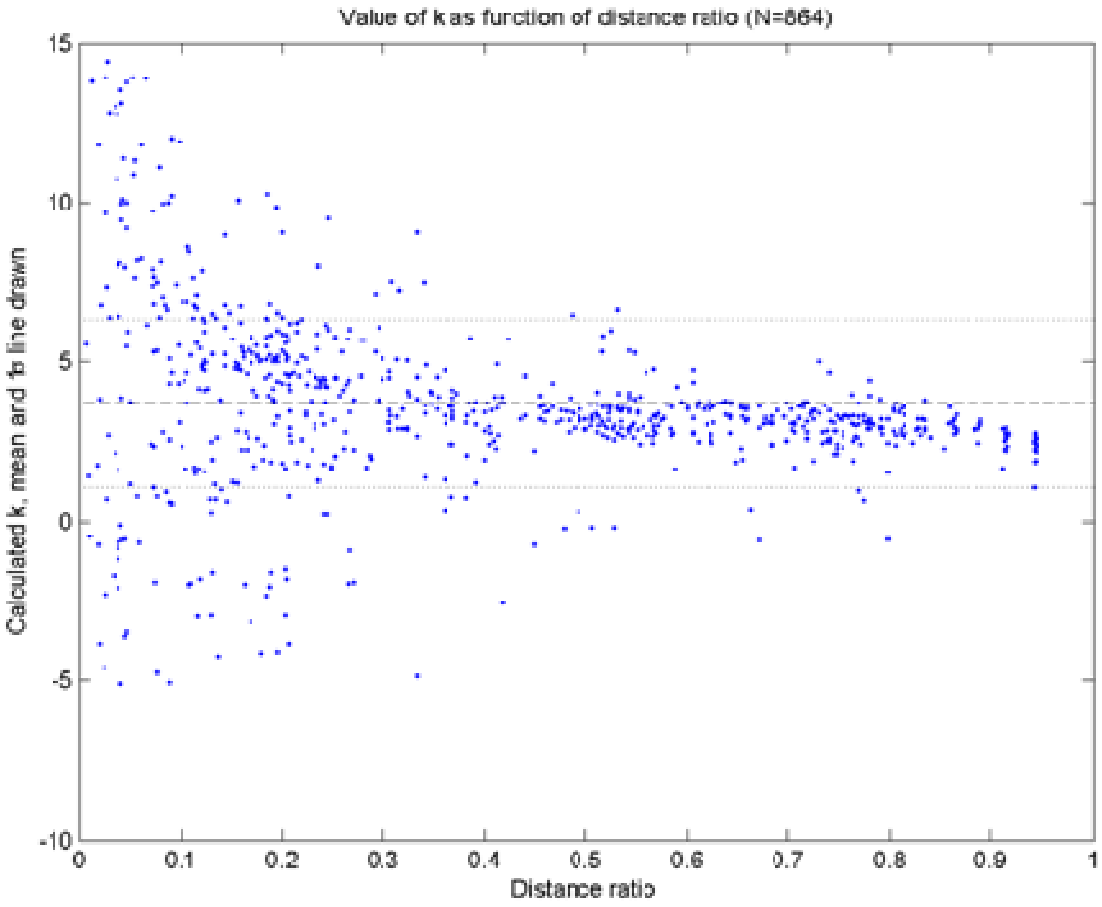


**Figure 33: Exponent *k* as a function of distance ratio *D*. The dashed lines are at 1 standard deviation from the mean. From Paper IV.**

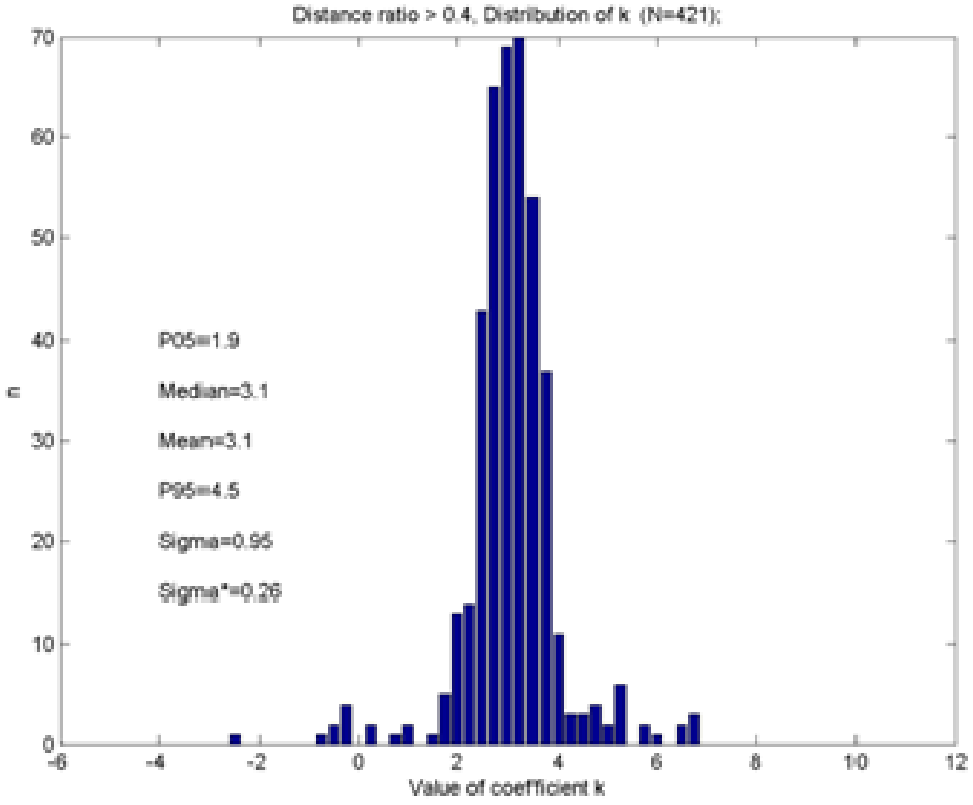


**Figure 34: Values of exponent *k* for numerically stable data set. From Paper IV.**

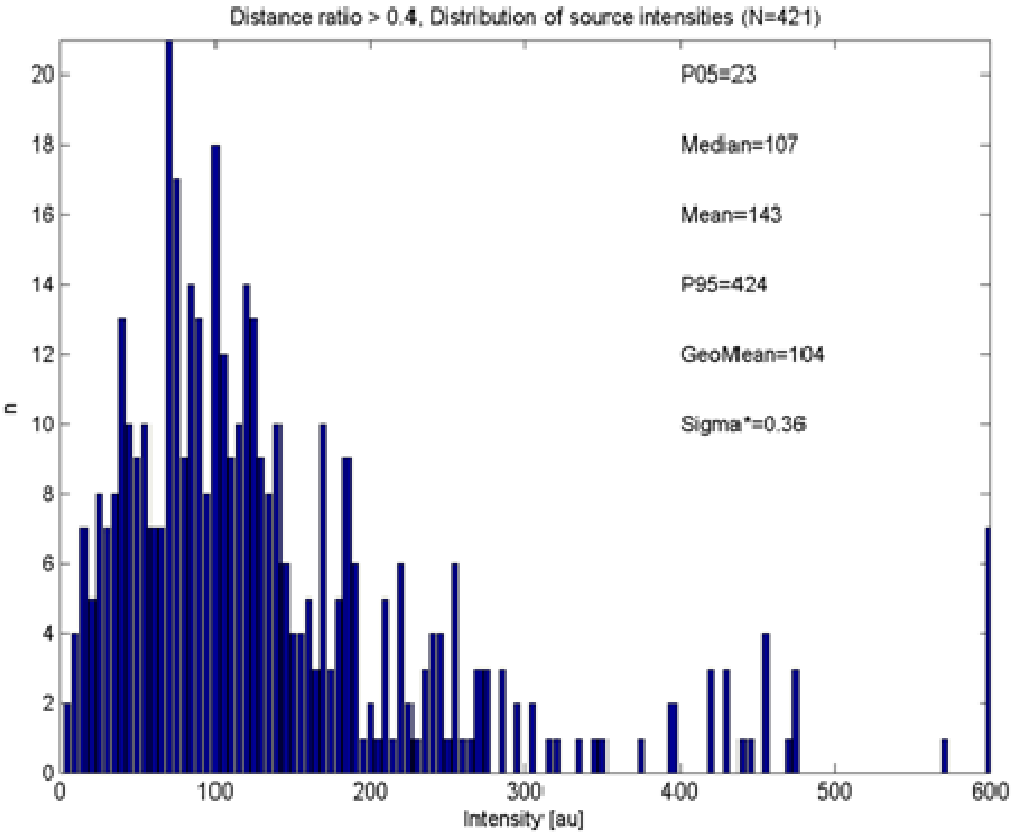


**Figure 35: Distribution of source intensities for numerically stable data. From Paper IV.**

Assume now that the equation is indeed of the form $E = E_0 / R^{3.1}$, with the mean value of $E_0$ known, so that a flash measured to have intensity $E_{meas}$ will be ranged to the distance $R_{meas} = (E_0 / E_{meas})^{0.32}$. Any scatter in the source intensity will cause proportionately less scatter in $R_{meas}$ because of the approximate cube root. Since the distribution of source intensities (Figure 32) is log-normal, it is necessary to evaluate the effect by simulation. Simulating the $E_0$ distribution as log-normal, with $\mu$=ln(2000) and $\sigma$*=0.36, gives the distribution in the top panel of Figure 36, which is close to a Gaussian distribution with mean 10 km and standard deviation 1.1 km; that is, 95% of the measured values will be within 2.2 km of the true distance. Better accuracy can be achieved by averaging more than one flash. With just two flashes, the standard deviation drops to 0.79 km; with three it is 0.64; and with 4 it is 0.56. This means that to achieve an accuracy of 1 km at a distance of 10 km, it is necessary to average over four flashes. This information is needed in Section 8.

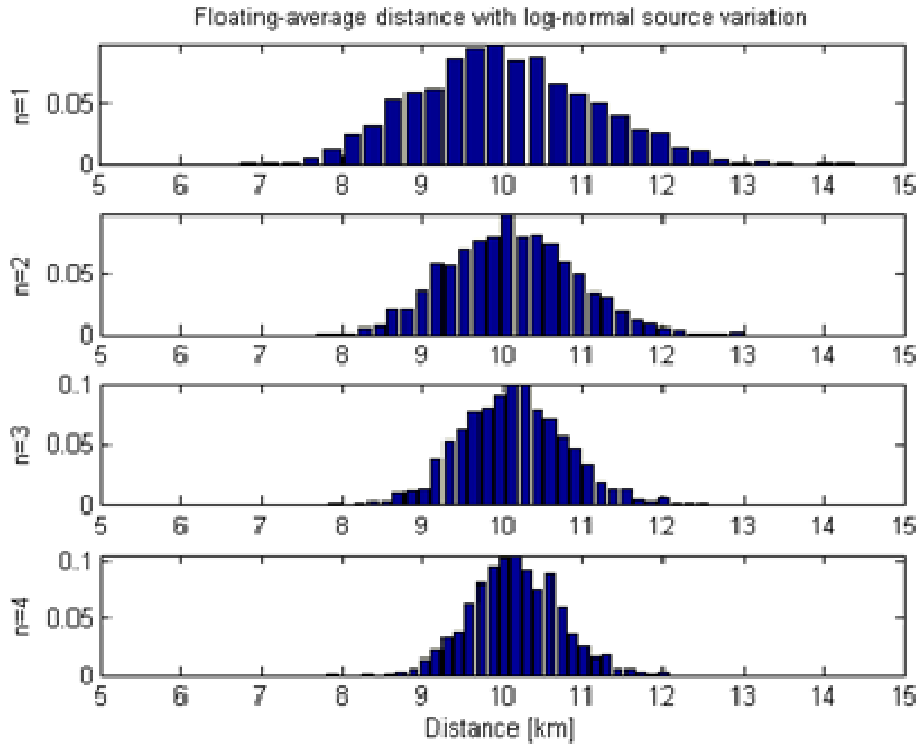


**Figure 36: Simulated distance scatter from log-normally distributed flash intensities. From Paper IV.**

# 8 Hypothesis 5 (Paper IV)

Hypothesis 5 states that the distance to the closest edge of a storm cell can be statistically estimated from the full-flash energy of all lightning flashes (both CG and IC). A floating average should be used.

Based on Hypotheses 1-4, the principle for ranging the edge of a cell becomes simple. The desired parameter is the distance to the closest observed flash; however, because of all the phenomena that cause scatter, several flashes must be averaged. The edge of the cell may also move during this time; this motion must be tracked as faithfully and quickly as possible. A simple floating average over time $T$ is therefore not suitable, since it will overestimate the distance to the edge. An additional parameter $M$ must be introduced: only the $M$ most intense flashes during the time period $T$ should be used in the averaging. Optimal values of $M$ and $T$ can be estimated based on the literature as well as the results of Papers II and IV.

The effect of parameterizing $T$ and $M$ is shown in Figure 37 for the storm on July 30, 2006 used as a reference in both Papers II and IV. The measured intensities were empirically calibrated using $R = (b/E)^{0.3}$ and defining $b$ so that the accuracy is best at a distance of 12 km. This distance was chosen to be consistent with the zoning principle described later in Section 9.2. The source variations discussed in Section 7 imply that even if all flashes are exactly at the edge, using a single flash ($M=1$) results in a 20% distance uncertainty.

This is clearly seen in Figure 37a, where the estimate for the edge fluctuates widely. If several flashes are used, the uncertainty decreases. Thus, $M$ should have a value of at least 2. On the other hand, if $M$ is too large, the distance will be systematically overestimated, since some of the flashes will be from the center of the cell. A large value of $M$ also causes a time lag: an approaching storm will not be detected fast enough since the older, more distant flashes will keep the average lagging, while a receding cell will be estimated to be within warning distance for too long. This is clearly seen in Figure 37d, where a choice of $T=10$ and $M=10$ results in the tracking of the "average location" of the cell rather than its edge, and response to the approach is delayed badly. The optimal value of $M$ therefore is more or less the same regardless of the storm type. It was shown in Section 7 that four flashes are needed to achieve an accuracy of 1 km. Based on these arguments, it is suggested that an optimal value for $M$ would be 3 or 4.

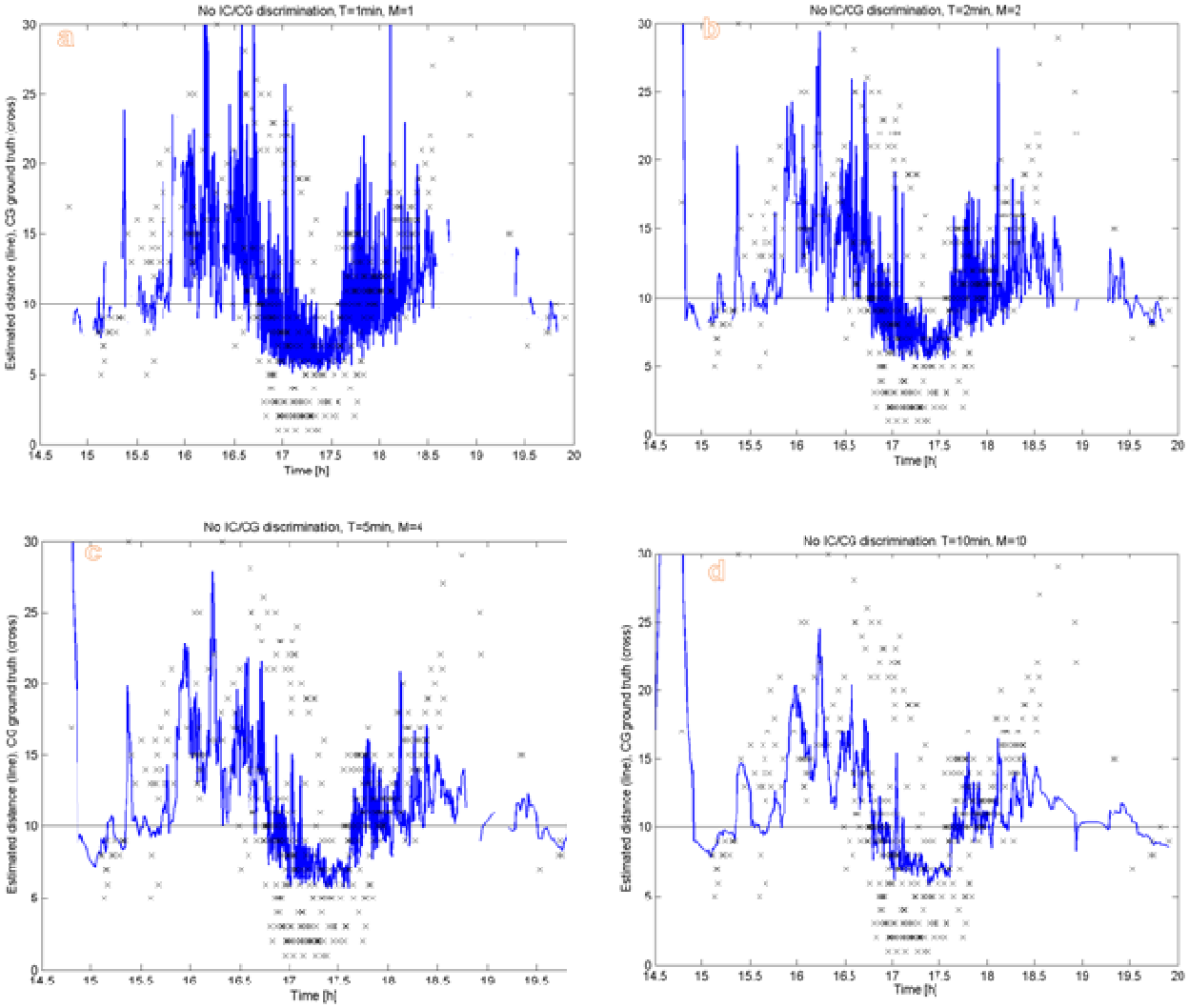


**Figure 37: Four parameterizations of the distance to the storm. The black crosses are known distances to ground flashes; the blue line is the distance calculated from the energy. A) Top left: Using T=1 min, M=1 (that is, distance is defined to be the closest measured distance during the last minute) means that the system responds immediately when the storm approaches, but fluctuates widely. It also responds when the storm moves away. B) Top right: Using T=2 min, M=2 (distance is the floating average of the two closest flashes in the last 2 minutes) fluctuates less but is also slow to respond to a storm moving away. C) Bottom left: Using T= 5 min, M=4 (distance is average of 4 closest flashes in the last 5 minutes) gives a reasonable compromise between fluctuation and response speed to changes in the storm distance; however, when the storm approach is rapid, as at about 16.5 h, it is slow to respond. D) Bottom right: With T= 10 min and M=10, the "average location" of a cell is tracked well, but the response to an approaching storm is very slow, making this an impractical choice. There is no quantitative way to determine the "best" parameterization of T and M, but the values used in B and C represent good possible compromises.**

The optimal value of $T$ depends more closely on the climatology. The known statistical flash rates of storms are of some use. Boccippio et al (2000), using global satellite data, have measured the flash rate to be 4 flashes/min or less for about 80% of all storms. For storms in Florida, Peckham et al (1984) report maximum flash rates between 4 and 14 flashes/min. However, these figures are maximum rates; for our application, low-flash-rate storms and the initial phases of storms are the more difficult and important cases. In the case of the July 30, 2006 cell the CG flash rate rarely exceeded 1 flash/minute. Even with the higher IC rate, the number of usable flashes was typically 3/minute or less, scattered throughout the cell. For typical storms, the averaging time $T$ therefore should be between 5 and 10 minutes.

More advanced algorithms could of course be adaptive; in particular, the value of $T$ can be lower if the flash rate is very high. However, such algorithms have not been studied in the context of this thesis because of the difficulty in proving their validity. In keeping with the proposed validation methodology (Section 9.4), the method should be as simple and unambiguous as possible if it is to be compared meaningfully with other techniques.

# 9 Discussion

## 9.1 Validation of the hypotheses

The results discussed above were based on one summer of measurements in a single country, and partly on measurements from one single storm. Therefore, the claims have not actually been globally verified, and it is not possible to claim that the hypotheses 1-5 would have been proven. However, it is suggested that the hypotheses provide a framework against which future narrowband devices can be verified.

Such a framework is necessary because of the present lack of clarity about the parameters that mobile narrowband devices can measure. Without adequate definitions, it is not possible even in principle to verify or discard such devices. The framework presented here is not limited to the devices that were used in Papers II-IV, but to any device operating by a similar principle. The propagation issue in particular is one which is fundamental to a single-station system. In addition, the large scatter in source intensities means that any narrowband system by definition has to be statistical in nature.

It has been shown that narrowband ranging without CG/IC differentiation has the potential to be accurate, if some limitations are accepted. For Scandinavian CG flashes, the source intensities were consistent with a log-normal distribution, with the majority of flashes being within a factor of four of the median intensity. It was shown that due to the rapid drop as a function of distance, these source variations only cause variations of about 20% in the range estimate. Further, when the average of several flashes was used, the theoretical range uncertainty could be reduced to about 10%.

Ground propagation will significantly affect the results, especially for distant flashes. However, it is shown in Paper III that the fast increase in the intensity is largely due to the fact that a significant part of the narrowband energy is emitted by cloud processes. The radiation from these processes propagates as a space wave when distances are small, and ground propagation has a negligible effect. There is no exact cutoff at which the propagation regime changes, but based on geometrical considerations and the calculations of Cooray (2007), space-wave propagation is still significant at distances larger than 10 km. Beyond distances of about 20 km, variations in ground conductivity can dominate the measured intensities. At minimum, this will increase the scatter; in the worst case, it can lead to systematic or directional errors (in particular, underestimating the distance to flashes over the sea). The results of Paper II imply that the system used in this paper has reasonable ranging accuracy to over 50 kilometers, but this can in part be ascribed to the homogeneous terrain. In general, the accuracy will degrade faster unless the terrain conductivity is factored in.

## 9.2 Framework for validating narrowband detectors

For a practical system, it is necessary to evaluate whether a system can be reliable even with such large scatters. Paper IV presents a framework which is both practical and supported by the literature. The framework is based on the so-called 30-30 rule (e.g. Holle et al (1999)), which is a simple but widely used "rule-of-thumb". According to the rule, protective actions must begin when the time between the visual flash and its associated audible thunder is 30 seconds or less (in other words, the distance is 10 km or less), and the user should then stay in a protected area until 30 minutes have passed from the last audible thunder.

Although the "30/30 rule" is basically a useful mnemonic, the numbers are based on valid statistical measurements. It is also based on a philosophy which is at the core of this thesis. Implicitly, the rule understands that for any ordinary user, the distance as such need not be of interest; what matters is the risk that lightning will strike close enough to cause damage. The statistics behind the 30-30 rule support this principle. According to Krider (1988), the distance between consecutive flashes is 3-5 km, although Lopez and Holle (1999) found somewhat larger distances. Since there are large storm-to-storm variations (and possibly latitudinal effects, which have not been well studied), Holle et al (1999) do not define a single number for the minimum safe distance from a given flash, but consider 10 kilometers (30 seconds) a useful approximation.

This thesis suggests that to gain any acceptance in the scientific community, a risk-based warning should be designed around the 30-30 rule. In Paper IV, three zones are defined to correspond to different modes of operation. As in the case of Holle et al (1999), these values should not be considered exact. These are similar to the generalized danger zone (DZ) and warning zone (WZ) proposed by Gulyás et al (2008) . However, for a practical local detector, a slightly more nuanced definition is needed.

Zone 1 ("danger distance"). This is the zone in which the user is in immediate danger of being struck, according to the 30-30 rule. This is similar to the danger zone (DZ) of Gulyás et al (2008), but with a somewhat larger radius. For consistency with the 30-30 rule, this range can be taken to be 10 km. At this range, even a single lightning flash should, in principle, launch a warning. In contrast, ranging within the zone does not have to be exact; according to the philosophy of the 30-30-rule, it makes no difference to the risk level whether the storm is 6 or 8 kilometers away. From a risk-based point of view, it makes no difference whether the flash being detected is an IC or CG flash; if there is any kind of flash activity at a given location, it means that the potential for a ground flash also exists.

Zone 2 ("tracking distance"). This zone overlaps with the warning zone (WZ) of Gulyás et al (2008). If a remote detector is to have any practical value, it must range storms at significantly more distant ranges than zone 1. This allows lightning risk to be evaluated before the storm poses a real risk, mainly by tracking the approach speed of a storm, or the growth of a new cell. Ranging in this zone, therefore, must be reliable, and must respond quickly to changes in storm distance. A practical monitoring system has to alert the user of a possibly increased risk level without yet triggering the full alarm. In a practical application, the tracking distance should not be too large; a storm at 50 km distance poses no real and immediate risk to the user, and giving a warning would lead to too many false positives, which eventually would lead to the warnings being ignored. There is no physical reason to suggest a specific value of the tracking distance. In principle, a value could be derived from the average speeds of storm cells, but in practice, lightning activity does not always move as well-defined cells. The propagation phenomena,

described in more detail in Section 7, suggest that ground characteristics begin to significantly affect the ranging at some break-even distance which is most likely to be between 10 and 20 km. As a first approximation, Zone 2 should probably end at approximately at a distance of 20 km.

Zone 3 ("monitoring distance"). At distances larger than the tracking distance, a practical system needs to monitor for the presence of lightning activity, but the user should normally not be alerted. The ranging must be accurate enough to establish whether a storm is approaching the tracking distance, but high accuracy is not required. On the other hand, any practical system will have a minimum usable signal intensity, set both by the expected signal intensities and the receiver sensitivity. For the particular detector used in Papers II-IV, the maximum confident ranging distance is about 50 km. Again, at the practical level, there is also an upper distance limit after which a storm is irrelevant to any user; this distance is certainly less than 50 km. In practice, a narrowband detector would therefore not need to have a range as large as the device used in this thesis.

Using the zoning principle loosens ranging accuracy requirement. A detection system should be calibrated so that it has maximum accuracy within the tracking range. The crucial variable, and a quantitative metric for the detection accuracy, is the accuracy in determining when the storm edge crosses the border between the tracking zone and the danger zone. Within the danger zone, ranging does not need to be accurate as long as the flashes are correctly measured to be within the danger zone. From a design viewpoint, saturation of the receiver would therefore be acceptable, which in turn allows a higher sensitivity to be used.

On the other hand, any statistical technique has difficulty dealing with the case of convective storms developing almost overhead; since the statistical approach requires several flashes to be ranged, there is a risk that the detector would not react to the first few flashes of an isolated overhead storm. A system which raises an alarm on every signal above the threshold level would be impractically sensitive to interference sources. However, the proposed method also utilizes IC flashes, which are usually more numerous than CG flashes. Although not perfect, a method that utilizes both CG and IC is therefore more robust against this problem than one detecting only CG flashes.

## 9.3 Interference sources

The issue of manmade interference is outside the scope of this thesis, but is clearly a problem in any practical detection system. A general solution to the interference problem is difficult to find due to the wide variety of artificial noise sources. However, a brief overview of some unpublished preliminary results is given here. The author of the thesis has framed a hypothesis which will be either validated or falsified in future research: what differentiates lightning from manmade noise is a combination of impulsiveness and long duration. Physically, this would be due to the fact that they are both wideband, non-periodic, and have long durations; no manmade interference has all these characteristics.

It appears that external noise sources can be classified very loosely into four categories, although this classification has so far not been submitted for peer review. Light switches and similar devices tend to result in "short-peak" noise, i.e. peaks with a very sharp rise and fall time (Figure 38). There are many "quasi-periodic" noise sources, such as motors, which produce a strong signal with partially periodic

structure (Figure 39). “Impulsive” noises may for example occur near light switches (Figure 40). “Steady” interference is emitted, for example, by LCD displays (Figure 41).

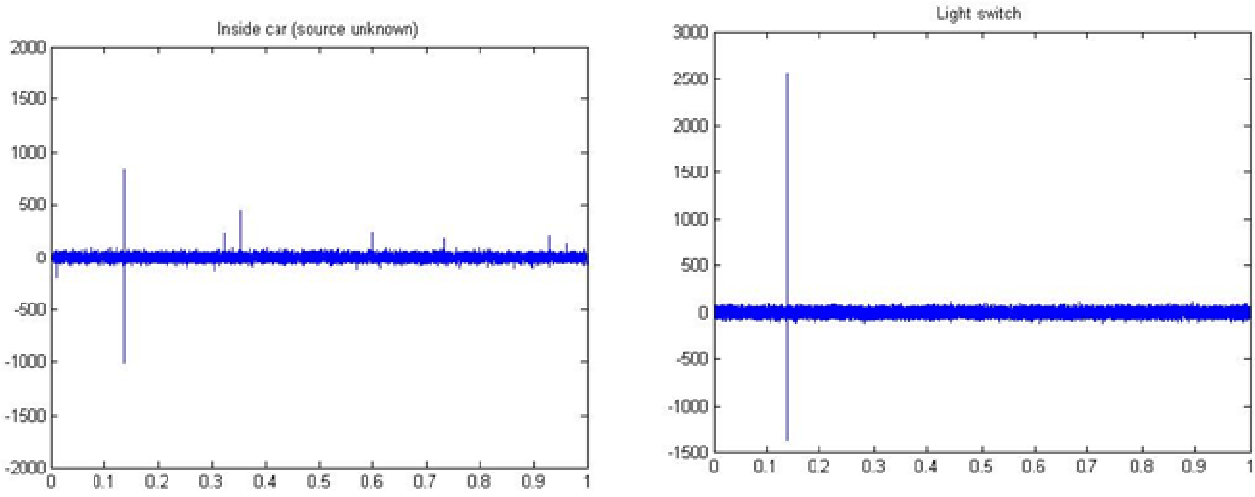


**Figure 38: "Short-peak" noise measured with the devices used in Papers II-IV. The duration of each plot is one second. The left figure shows noise of unknown origin inside a car; the right figure shows the signal from an ordinary light switch.**

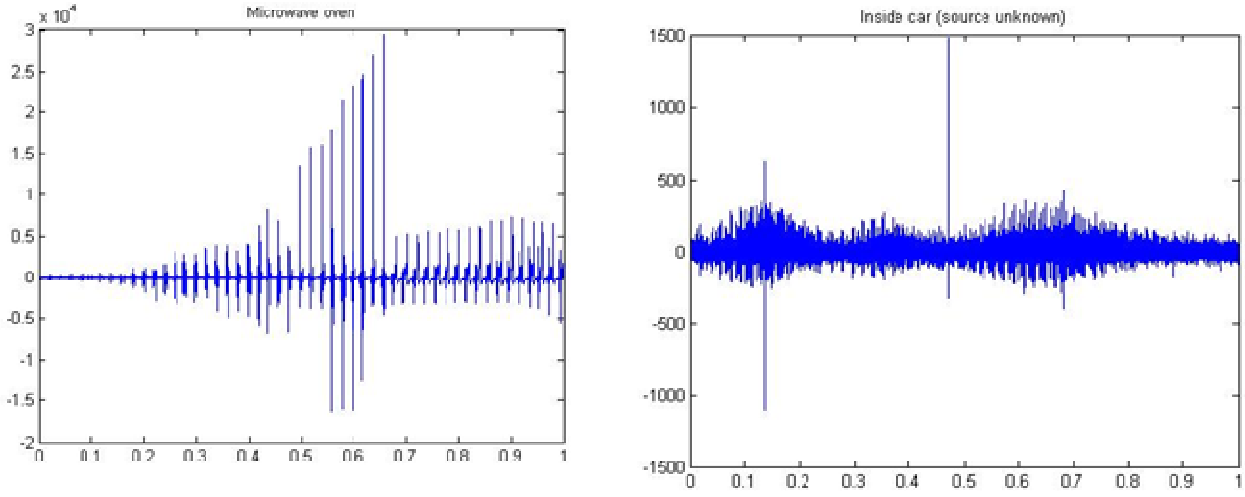


**Figure 39: "Quasi-periodic" interference. The left plot is a signal from a microwave oven. The right plot is from inside a car; the source is probably a windshield wiper engine.**

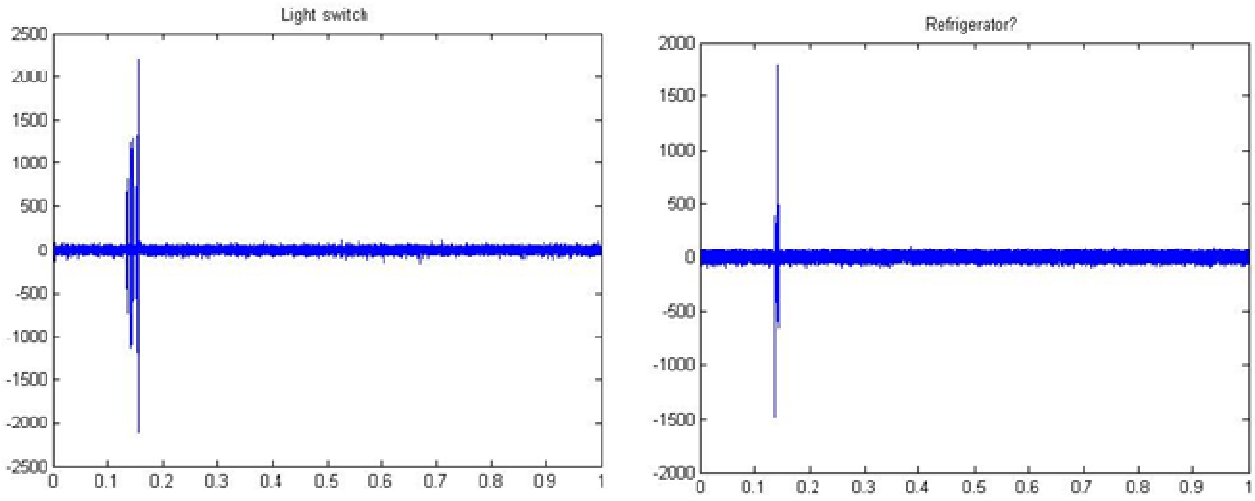


**Figure 40: "Impulsive" interference. The left plot is the signal from switching on fluorescent light tube. The right plot is from a compressor on a refrigerator.**

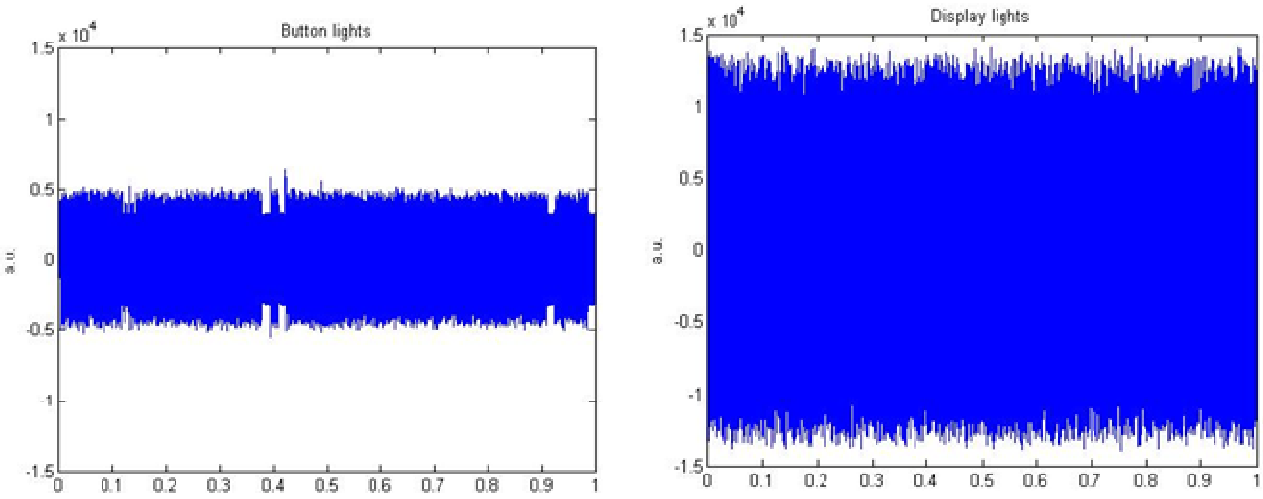


**Figure 41: "Steady" interference. The left plot shows the noise from the button lights of a mobile phone (which are driven by LED's). The right plot shows the emission from an active mobile phone LCD display. Most other components in a mobile phone do not appear to cause significant interference at 1 MHz.**

If this classification is valid, there are several ways to deal with or eliminate the various types of interference. The short-peak interference can be distinguished by its short duration, and possibly eliminated with a very simple filter, as suggested in the patent application by Mäkelä et al (2008a). For quasi-periodic noise, a more advanced signal processing tool, such as FFT or autocorrelation, may be

needed. Impulsive interference is the most problematic type to distinguish from lightning, but the duration is typically shorter than for most lightning flashes. A high level of steady interference cannot be compensated or eliminated, and will always lead to ranging being seriously degraded, or even made impossible. However, if this baseline hiss level is monitored continuously, it is at least possible to determine when ranging cannot be done.

Another matter of major practical importance is the ambient background noise due to manmade and atmospheric sources. Pierce (1977) shows a curve of the variations expressed in dB above the thermal noise level (Figure 42). At 1 MHz, the atmospheric noise level at noon (the lowest level) is about 40 dB; at midnight (the highest level) it is up to 100 dB. Above 1 MHz, the daytime noise level begins to flatten out until dropping sharply at about 20 MHz; the nighttime curve drops steadily, and becomes equal to the daytime curve at 20 MHz. Figure 42 also shows the difference in man-made noise between rural and urban areas. The difference between the two is about 20 dB throughout; at 1 MHz the rural noise level is about 60 dB and the urban is 80 dB, while at 15 MHz the corresponding values are 20 dB and 40 dB.

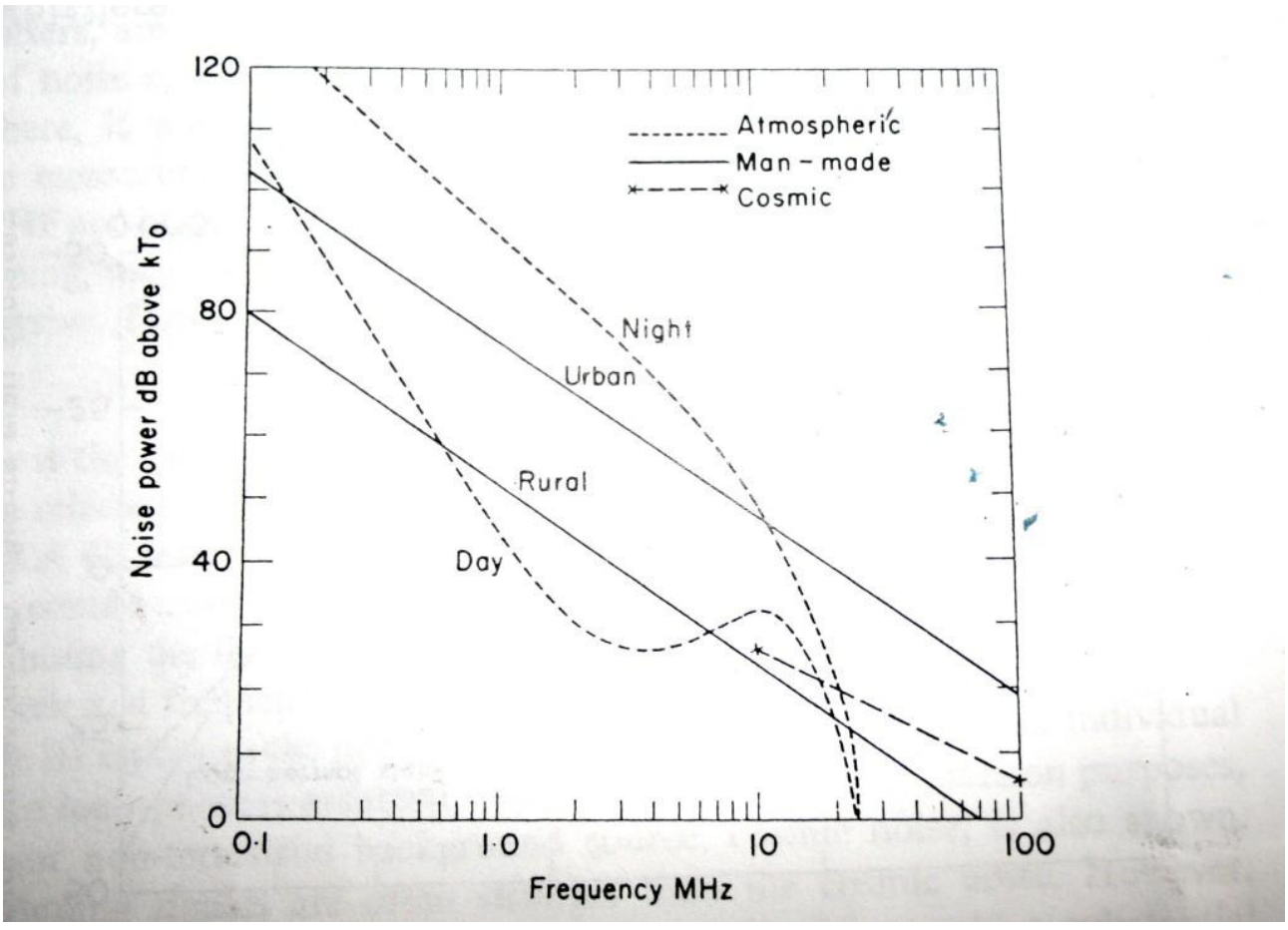


**Figure 42: Ambient noise as a function of frequency for day/night and rural/urban conditions. From Pierce (1977).**

These noise variations must be considered in any practical detection system. In principle, the lightning atmospherics are independent of the ambient noise, and the atmospheric noise can be subtracted away as has been done in Papers II-IV. The measurements of Papers II-IV were however done in Finland, which receives very few audible AM transmissions in the daytime. There were both day and night flashes in the data set, and no difference was seen. The effects of heavy manmade interference (mainly strong AM radio transmissions) have not been formally tested so far. If a transmission occurs within the bandwidth of the detector, it will add to the baseline noise level. If necessary, the problem can be avoided by moving the center frequency to e.g. 2 MHz, which is outside of the MW transmission band; the tradeoff is that the lightning signal is weaker at the higher frequency.

## 9.4 Proposed methodology for validation of narrowband devices

One aim of this thesis is to present a methodology which could be used to fairly compare simple narrowband devices to more advanced reference devices. The American Meteorological Society (2002) calls for such peer-reviewed measurements to be made before any recommendations can be made for or against these devices. There may well be practical business issues which have prevented such measurements (the device manufacturers seem to be very small industries for the most part), but there is also a valid question about what would constitute a fair comparison. Much of the difficulty lies in the fact that there is no general agreement on what these devices exactly measure, or indeed should measure.

Johnson et al (1982) made a field comparison of several early devices, which is one of the few published studies of this type. The performance of the devices was tied to a specific application: the risk of premature detonation of blast caps in an open-pit mine blasting operation due to lighting. The detonation can be caused by direct or very close strikes (unlikely), the induction of current impulses in the blast cap due to lightning transients (most likely scenario, even for fairly distant flashes), or by large static buildups leading to flashovers in the cap (a less likely scenario, except for very close clouds). A simulated and instrumented blast system was used to measure the detonation risk. A risk situation was also defined to exist when lightning was within 18 km of the site, or when an experienced operator heuristically determined a risk to exist. The devices tested included a sferics counter to detect the presence of lightning (closest to the device used in this thesis); a corona point sensor, radioactive sensor, and a field mill to detect high electric fields; and an azimuth/range locator and triangulation locator to measure the locations of the flashes. In addition, radar as well as visual and thunder observations were used. Since the risk scenario was thus unambiguously defined, alarm reliability and false alarm rates could then be determined. This philosophy allowed different technologies to be compared in a fair way, at least for the particular application (open-pit mining).

This thesis suggests that a fair comparison could be made if narrowband devices of this type are considered to measure risk levels rather than exact distances. Accurate flash-by-flash ranging of CG flashes is not possible with this simple method. However, such accuracy may not be necessary for a practical application. Any given location is “at risk” when the conditions overhead are such that a breakdown leading to a CG or IC flash has a possibility of occurring. Such a condition could be more accurately observed with an electric field mill. However, in compliance with the 30-30 rule, it would be preferable to estimate whether such conditions prevail anywhere within a 10 km range of the point of observation.

Qualitatively, the performance of any local-warning device can be boiled down to three questions.

a) Does the device warn accurately and promptly when the user is at immediate risk: that is, in a situation where electrical breakdown can occur within Zone 1?

b) Does it accurately and promptly determine and warn the user when the risk is becoming imminent (that is, electrical activity passes from Zone 2 into Zone 1)?

c) Does it accurately and promptly inform the user when the risk is over (i.e. the electrical activity is in Zone 2 and is receding)?

Although the parameter that is truly of interest is the electric field intensity in the cloud, breakdown conditions can only be truly quantitatively measured by observing an actual breakdown. This allows comparisons to other reference devices. These qualitative questions can be transformed into exact quantitative measures, if there is an absolute reference measurement to compare to. In practice, such a reference does not exist, but there are multiple proxies that can be used.

The devices to be tested must be set up so that their performance can be monitored and recorded. In existing devices, the user interfaces are highly variable and alerts may occur at a variety of distances; for example, LED lights may blink when a flash has been ranged to a given distance. Alternately, exact distances may not be given, but warnings may be given when the storm is local. Therefore, it may not be possible to directly compare the reading to the zoning principle. However, any useful device will have to determine the Zone 1 – Zone 2 transition. It is strictly speaking not necessary for the device to alert in any way to individual flashes; however, unless at least some indication is given of when the device has been triggered, it is difficult to estimate the detection efficiency.

Reference devices should include the following whenever possible.

1) A lightning detection network for locating CG flashes. These systems are the de facto standard used in lightning research, and can have accuracies better than a kilometer. However, it must be realized that the location of a CG flash may not be sufficient to estimate the risk level at other locations. In particular, storms may have IC activity long before any CG activity. Also, since even CG flashes have a large horizontal component, the CG location is not really at the "edge" of the storm, which is the parameter that the narrowband devices are tracking. A narrowband device should ideally respond to every CG flash at least within Zone 2. However, the narrowband device would also be expected to give a range which is smaller than the range implied by the CG flashes.

2) A VHF detection network. A high-quality imager would be able to measure exactly the parameter that the narrowband device measures: the closest part of any given horizontal flash. Because of the inherent scatter, the response to any individual flash will be uncertain; however, for a large enough set of flashes, there should be a one-to-one correspondence between the edge given by the VHF network and the edge given by the narrowband device. In practice, the accuracy of existing VHF imagers may not be sufficient to act as a perfect reference device.

3) Weather radar reflectivity data can measure where the icing occurs in the cloud, and hence find the location where lightning initiation is likely. Typical radar accuracies may not be sufficient.

4) Optionally, an electric field mill or optimally a network of mills to calculate where the vertical electric field is capable of initiating an electrical breakdown.

5) Optionally, visual and audible thunder observations. An advantage with including these measurements is that the 30-30 rule is originally based on thunder observations. This gives an unambiguous measure of failure: if there is a visual and thunder observation corresponding to the 30-30 rule, and the device fails to give an alarm, it has failed. Such occasional failures are however unavoidable in a statistical approach, as discussed below.

There will be cases in which a simple narrowband device of this type simply fails. If there is a large jump between two flashes (for example a flash at 13 km followed by a flash at 8 km), then the first flash

within Zone 1 will not be measured because a floating average is used. There will also be some cases where the very first flash in a storm is initiated within Zone 1 (but it must be noted that most of the reference devices, except perhaps the field mill, would also fail to give a pre-warning in this case). Since false positives must be kept to a minimum, the system cannot in practice be allowed to alert immediately on the first such flash, and there is no perfect way to eliminate this problem. The number of such failures should be documented, and over time compared to the number of storms for which the alert was done successfully. This will give a failure probability. There is no scientific rationale for determining what would be an "acceptable" failure rate; this depends entirely on the application. However, a zero failure rate is not a realistic with this method (or with any of the reference methods either).

Aside from such pathological cases, a fair comparison can be made by overlaying several of the reference measurements to arrive at an estimate for the edge of the cell. This can then be compared to the edge distance given by the narrowband device. The quantitative analysis should be done within approximately five kilometers of the Zone 1 – Zone 2 boundary, since the ranging of the narrowband device does not need to be accurate outside this range. The distance estimate given by the narrowband device should be compared to the edge estimate from the reference devices approximately once a minute, since the narrowband devices are not capable of faster responses due to the low flash rates in most storms (Section 8). There will be fluctuations, but if the narrowband device is valid, the differences should tend to zero over many storms.

Even if the narrowband device does not give out exact distance estimates, it must be able to alert when the Zone 1 – Zone 2 boundary is crossed. Because both the narrowband device and the reference system have uncertainties, small variations in the transition times can be allowed. The narrowband device may alert slightly before or slightly after the transition time determined from the reference devices, but if the edge moves clearly from one zone to another, it will have to alert eventually. The time difference should tend to zero for a large number of storms. The more serious time delay occurs when the narrowband device does not react in an acceptable amount of time when the edge continues deeper into Zone 1. Because the response time of the narrowband device is limited by the flash rate in the storm, a delay of two or three minutes can be unavoidable. Again, there is no scientific rationale to define any delay time as "unacceptable"; these delay times must simply be tabulated, and it is up to the application designer to decide what is acceptable.

There will however be problematic storms in which the edge fluctuates around the Zone 1 – Zone 2 transition without clearly passing into either zone for an extended period. Both the reference devices and the narrowband device may then give more or less random transition times. In such cases, no fair comparison can be made, since the reference devices also have inherent uncertainty. For this reason, it would be much preferable that the narrowband device give an estimated distance, even if that distance is not shown to the actual end user.

A measurement campaign of the type described above has significant costs associated with it. However, the experience from the work done for this thesis is that narrowband tests could quite realistically be run as a "piggy-back" of other measurement campaigns. The specific advantage of narrowband devices, in this respect, is that they are so simple that full automation is possible. The equipment setup used in papers II to IV was complicated to design, and somewhat bulky, but the actual operation was simple and automated over the whole summer. As long as care is taken to keep the data time stamps accurate (ideally with a GPS clock), the measurements need little or no attention, and the analysis can be done offline. In the simplest case, data could simply be streamed directly to the PC, at

least if downmixed data are used (in which case the data rates and storage needs are small). It would thus not be unreasonable to expect device manufacturers to provide this type of verification in the future.

A much simpler approach would be to collect a standard set of flash signals at known distances, which could then be used to generate the same signal in a laboratory. This would allow narrowband measurements to be calibrated much faster in the laboratory. In principle, it is simple to take recorded narrowband signals, and feed them into an antenna which then simulates the original lightning. In practice, the signal is strictly valid only for the specific antenna that was used to measure it, and may or may not be correct for other devices, even if they were to operate at exactly the same frequency. No such standard data set exists at present, and collecting such a set is problematic due to equipment differences. Absolute spectral measurements have been made (see e.g. Le Vine (1987); Nanevicz et al (1987)), but they are average results for a large number of flashes, using a wide variety of techniques and normalizations. The spectra from individual lightning processes have been transformed from broadband data e.g. by Willett et al (1990) and Weidman and Krider (1986), but the issue of noise has not really been addressed in these studies (Fernando and Cooray (2008)). There have been direct narrowband measurements using parallel-plate antennas (e.g. Cooray and Pérez (1994b), Jayaratne and Cooray (1994)), but these have very high noise levels, and it would be difficult to generate a realistic signal from them directly. In addition, the measurements have typically not measured the full flash, especially its in-cloud processes, which are a crucial phenomenon for narrowband detection. Thus, at present no general laboratory tests can be defined.

# 10 Summary and future work

This thesis presents results from measurements made by what may be the simplest possible device which could still be considered a lightning detector: a modified AM radio. Based on comparisons with reference devices, it was shown that such a device can extract useful scientific information. It was also shown that a device of this type can be used to range thunderstorms statistically. The measurements were made for a limited data set, in one country, and over one summer. It is known that the HF signatures of lightning differ at different locations on the globe, and, therefore, the device has not been validated globally. The core content of the thesis is, however, not in validating this particular instrument. Rather, the core point is to note that there are fundamental limitations to the accuracy of such ranging, and based on a detailed analysis of these limitations, to arrive at an understanding of what such a technique can and cannot realistically claim to do.

A major objection against narrowband devices of this type is that they have not been validated and peer-reviewed. This thesis raised an even more fundamental issue: it is not necessarily clear what such devices even claim to measure, which means that they cannot be compared to references in any meaningful way. The thesis clarifies the terminology and defines a framework against which a meaningful comparison would be possible. Devices of this type are not suited to accurate flash-by-flash ranging of lightning strikes. Rather, they can be used to statistically estimate the distance to the closest edge of a thunderstorm. The ranging uncertainty grows rapidly at distances of more than 20 km. However, this range is sufficient to provide a warning in compliance with the so-called 30-30 rule, which is a practical mnemonic used to train ordinary people to thunderstorm risk.

Fundamentally, a device of this type could provide a warning of increased thunderstorm risk at a range that is longer than the typical range of the human senses, and in real time. It is possible to quantify the performance of such a device with field tests by using several instruments as references.

Several directions of inquiry can be seen which should be covered in the future. Little original work has been done in this thesis to create a theoretical model for the radiation signatures. It is possible to design a working detection system based on empirical measurements only; however, it would add to the credibility of the system if there was a stronger theoretical understanding of the processes that cause the signal. Specifically, the role of propagation needs more analysis. Due to the lack of an exact model, the system at present is strictly verified only for locations where the ground conductivity does not change dramatically. Conductivity variations, for example at the seashore, start to affect the results after a certain break-even distance. As shown in Section 7, if the break-even distance is close to the zone 2 – zone 3 boundary (about 20 km), the reliability of the system is not dependent on knowing the ground characteristics. This break-even distance needs to be determined theoretically before it is possible to ascertain whether the system is “universal” or always requires some knowledge of the terrain.

A crucial practical issue with this type of detector is that manmade interference will cause false alarms, especially if the device is portable. The danger of such false positives means that ranging cannot take every flash into account, which in turn leads to a slower response when a storm moves quickly towards the user. Research work into this issue is ongoing, but nothing has been published at the time of this thesis. Because field tests are relatively costly and time-consuming, it would be advantageous to find a good method to validate and calibrate narrowband devices in the laboratory. So far, no adequate solution has been found.

# References

American Meteorological Society. 2002. Updated recommendations for Lightning Safety -- 2002

Beasley, W., Uman, M.A. and Rustan, P.L., 1982. Electric fields preceding cloud-to-ground lightning flashes. Journal of Geophysical Research 87 (C7), 4883-4902.

Boccippio, D.J., Goodman, S.J. and Heckman, S., 2000. Regional differences in tropical lightning distributions. Journal of Applied Meteorology 39, 2231-2248.

Breitmeier, J.W., Clubb, S.B. and Shaver, E.F., 1993. Hand-held lightning detection and ranging device, US patent 5,263,368.

Brook, M. and Kitagawa, N., 1960. Electric-field changes and the design of lightning-flash counters. Journal of Geophysical Research 65 (7), 1927-1931.

Clegg, R.J. and Thomson, E.M., 1979. Some properties of EM radiation from lightning. Journal of Geophysical Research 84 (C2), 719-724.

Cooray, V. and Lundquist, S., 1985. Characteristics of the radiation fields from lightning in Sri Lanka in the tropics. Journal of Geophysical Research 90, 6099-6109.

Cooray, V., 1986a. Temporal behaviour of lightning HF radiation at 3 MHz near the time of first return strokes. Journal of Atmospheric and Solar-Terrestrial Physics 48, 73-78.

Cooray, V., 1986b. Response of CIGRE and CCIR lightning flash counters to the electric field changes from lightning: A theoretical study. Journal of Geophysical Research 91 (D2), 2835-2842.

Cooray, V. and Orville, R.E., 1990. The Effects of Variation of Current Amplitude, Current Risetime, and Return Stroke Velocity Along the Return Stroke Channel on the Electromagnetic Fields Generated by Return Strokes. Journal of Geophysical Research 95 (D11), 18,617-618,630.

Cooray, V. and Jayaratne, K.P.S.C., 1994. Characteristics of lightning flashes observed in Sri Lanka in the tropics. Journal of Geophysical Research 99 (D10), 21,051-021,056.

Cooray, V. and Pérez, H., 1994a. Some features of lightning flashes observed in Sweden. Journal of Geophysical Research 99 (D5), 10,683-610,688.

Cooray, V. and Pérez, H., 1994b. HF radiation at 3 MHz associated with positive and negative return strokes. Journal of Geophysical Research 99 (D5), 10,633-610,640.

Cooray, V., 2007. Propagation effects on radiation field pulses generated by cloud lightning flashes. Journal of Atmospheric and Solar-Terrestrial Physics 69, 1397-1406.

Cooray, V. and Fernando, M.,2008. Effects of branches, charge irregularities and tortuosity of the stepped leader channel on the current, electromagnetic fields and HF radiation of return strokes, 29th International Conference on Lightning Protection, Uppsala, Sweden.

Cooray, V., and Y. Ming, 1994. Propagation effects on the lightning-generated electromagnetic fields for homogeneous and mixed sea-land paths. Journal of Geophysical Research 99 (D5), 10,643-610.652.

Cummins, K.L., Murphy, M.J., Bardo, E.A., Hiscox, W.L., Pyle, R.B. and Pifer, A.E., 1998. A combined TOA/MDF technology upgrade of the US National Lightning Detection Network. Journal of Geophysical Research 103 (D8), 9035-9044.

Curran, E.B., Holle, R.L. and Lopez, E.R., 2000. Lightning casualties and damages in the United States from 1959 to 1994. Journal of Climate 13, 3448-3464.

Edirisinghe, M., Mäkelä, J.S., Montaño, R., Fernando, M. and Cooray, V.,2006. Signatures of the lightning HF radiation at 10 MHz, 5 MHz, and 3 MHz associated with leader and return stroke process, Proc. of the 28th International Conference on Lightning Protection, Kanazawa, Japan.

Fernando, M. and Cooray, V.,2008. Narrowband radiation associated with lightning ground and cloud flashes: a review, 29th International Conference on Lightning Protection, Uppsala, Sweden.

Gomes, C., Cooray, V. and Jayaratne, C., 1998. Comparison of preliminary breakdown pulses observed in Sweden and Sri Lanka. Journal of Atmospheric and Solar-Terrestrial Physics 60, 975-979.

Gomes, C., Cooray, V., Fernando, M., Montaño, R. and Sonnadara, U., 2004. Characteristics of chaotic pulse trains generated by lightning flashes. Journal of Atmospheric and Solar-Terrestrial Physics 66, 1733-1743.

Gratz, J. and Noble, E., 2006. Lightning safety and large stadiums. Bulletin of the American Meteorological Society (September), 1188-1194.

Gulyás, A., Németh, B., Kiss, I. and Berta, I.,2008. Theoretical framework of preventive lightning protection, 29th International Conference on Lightning Protection, Uppsala, Sweden.

Hed, A.Z., Pavelle, R., Aisenberg, S. and Freedman, G., 2001. Warning system and method for detection of tornadoes, US patent 6,232,882.

Heitkemper, L., Price, R.F. and Johnson, D.B., 2008. Lightning-warning systems for use by airports. Transportation Research Board, Washington, D.C.

Holle, R.L., López, R.E., Arnold, L.J. and Endres, J., 1996. Insured lightning-caused property damage in three Western states. Journal of Applied Meteorology 35, 1344-1351.

Holle, R.L., Lopez, R.E. and Zimmerman, C., 1999. Updated recommendations for lightning safety -- 1998. Bulletin of the American Meteorological Society 80 (10), 2035-2041.

Holle, R.L., López, R.E. and Navarro, B.C., 2005. Deaths, injuries, and damages from lightning in the United States in the 1890s in comparison with the 1990s. Journal of Applied Meteorology 44, 1563-1573.

Idone, V.P. and Orville, R.E., 1990. Delimiting "thunderstorm watch" periods by real-time lightning location for a power utility company Weather and Forecasting 5, 139-147.

Idone, V.P., Davis, D.A., Moore, P.K., Wang, Y., Henderson, R.W., Ries, M. and Jamason, P.F., 1998a. Performance evaluation of the US National Lightning Detection Network in eastern New York: 1. Detection efficiency. Journal of Geophysical Research 103 (D8), 9045-9055.

Idone, V.P., Davis, D.A., Moore, P.K., Wang, Y., Henderson, R.W., Ries, M. and Jamason, P.F., 1998b. Performance evaluation of the US National Lightning Detection Network in eastern New York: 2. Location accuracy. Journal of Geophysical Research 103 (D8), 9057-9069.

Jayaratne, K.P.S.C. and Cooray, V., 1994. The lightning HF radiation at 3MHz during leader and return stroke processes. Journal of Atmopsheric and Solar-Terrestrial Physics 56 (4), 493-501.

Jeyanthiran, V., Edirisinghe, M., Fernando, M. and Cooray, V.,2006. The lightning HF radiation at 10MHz, 5MHz, and 3MHz associated with cloud flashes, 28th International Conference on Lightning Protection Kanazawa, Japan.

Jeyanthiran, V., Edirisinghe, M., Fernando, M. and Cooray, V.,2008a. HF radiation pertinent to cloud flashes observed in Swedish thunderstorms, 29th International Conference on Lightning Protection, Uppsala, Sweden.

Jeyanthiran, V., Edirisinghe, M., Fernando, M., Gomes, C. and Cooray, V.,2008b. HF radiation at 3 MHz, 5 MHz and 10 MHz associated with preliminary breakdown pulses observed in Sri Lanka, 29th International Conference on Lightning Protection, Uppsala, Sweden.

Johnson, H.L., Hart, R.D., Lind, M.A., Powell, R.E. and Stanford, J.L., 1977. Measurements of radio frequency noise from severe and nonsevere thunderstorms. Monthly Weather Review 105, 734-747.

Johnson, R.L., Janota, D.E. and Hay, J.E., 1982. An operational comparison of lightning warning systems. Journal of Applied Meteorology 21 (703-707).

Kitagawa, N. and Brook, M., 1960. A comparison of intracloud and cloud-to-ground lightning discharges. Journal of Geophysical Research 65 (4), 1189-1201.

Kohl, D.A. and Miller, J.E., 1963. 500 kc/sec sferics analysis of severe weather events. Monthly Weather Review (May), 207-214.

Kohl, D.A., 1964. The Relation of Polarization of Sferics at 500
Kilocycles per Second to Lightning-Stroke Orientation. Journal of Geophysical Research 69 (19), 4184-4185.

Kohl, D.A., 1966. Comments on Paper by K. L. Zonge and W. H. Evans,
'Prestroke Radiation from Thunderclouds'. Journal of Geophysical Research 71 (20), 5005-5006.

Kohl, D.A., 1969. A 500-kHz sferics range detector. Journal of Applied Meteorology 8, 610-617.

Kohl, D.A., 1980. An evaluation of the Area Thunderstorm Monitor in an operational application. Bulletin of the American Meteorological Society 61 (9), 993-997.

Krider, E.P., Noggle, R.C. and Uman, M.A., 1976. A gated, wide-band magnetic direction finder for lightning return strokes. Journal of Applied Meteorology 15, 301-306.

Krider, E.P., Weidman, C.D. and Le Vine, D.M., 1979. The temporal structure of the HF and VHF radiation produced
by intracloud lightning discharges. Journal of Geophysical Research 84 (C9), 5760-5762.

Krider, E.P., Pifer, A.E. and Vance, D.L., 1980. Lightning direction finding systems for forest fire detection. Bulletin of the American Meteorological Society 61, 980-986.

Krider, E.P.,1988. Spatial distribution of lightning strikes to ground during small thunderstorms in Florida, Proceedings of 1988 International Aerospace and Ground Conference on Lightning and Static Electricity, Oklahoma City, OK, USA.

Kuleshov, Y., Mackerras, D. and Darveniza, M., 2006. Spatial distribution and frequency of lightning activity and lightning flash density maps for Australia. Journal of Geophysical Research 111 (D19105).

Le Vine, D.M., 1977. The effect of pulse interval statistics on the spectrum of radiation from lightning. Journal of Geophysical Research 82 (12), 1773-1777.

Le Vine, D.M. and Krider, E.P., 1977. The temporal structure of HF and VHF radiation during Florida lightning return strokes. Geophysical Research Letters 4, 13-16.

Le Vine, D.M., 1980. Sources of the strongest RF radiation from lightning. Journal of Geophysical Research 85 (C7), 4091-4095.

Le Vine, D.M., Gesell, L. and Kao, M., 1986. Radiation from lightning return strokes over a finitely conducting earth. Journal of Geophysical Research 91 (D11), 11,897-811,908.

Le Vine, D.M., 1987. Review of measurements of the RF spectrum of radiation from lightning. Meteorological and Atmospheric Physics 37, 195-204.

Loboda, M.,2008. Lightning deaths and injuries in Poland in period of 2001-2006, 29th International Conference on Lightning Protection, Uppsala, Sweden.

Lopez, E.R. and Holle, R.L., 1999. The distance between successive lightning flashes, NOAA Technical Memo ERL NSSL-1XX

Mackerras, D., 1985. Automatic short-range measurement of the cloud flash to ground flash ratio in thunderstorms. Journal of Geophysical Research 90 (D4), 6195-6201.

Mäkelä, J., Porjo, N., Jantunen, J. and Ahola, T., 2008a. Method and apparatus for staged approach transient RF detection and sensor power savings, European patent application EP 2082245 (pending).

Mäkelä, J.S., Edirisinghe, M., Fernando, M., Montaño, R. and Cooray, V., 2007. HF radiation emitted by chaotic leader processes. Journal of Atmospheric and Solar-Terrestrial Physics 69 (6), 707-720.

Mäkelä, J.S., Porjo, N., Jantunen, J., Ahola, T. and Hämäläinen, A., 2008b. Using full-flash narrowband energy for ranging of lightning ground strokes Journal of Atmospheric and Solar-Terrestrial Physics 70 (1), 156-168.

Mäkelä, J.S., Porjo, N., Mäkelä, A., Tuomi, T. and Cooray, V., 2008c. Properties of preliminary breakdown processes in Scandinavian lightning. Journal of Atmopsheric and Solar-Terrestrial Physics 70, 2041-2052.

Mäkelä, J.S., Porjo, N., Jantunen, J., Ahola, T., Mäkelä, A., Tuomi, T. and Cooray, V., 2009. Single-station narrowband ranging of active storm cells without lightning-type discrimination. Journal of Atmospheric and Solar-Terrestrial Physics 71 (8-9), 911-922.

Master, M.J. and Uman, M.A., 1984. Lightning induced voltages on power lines: Theory. IEEE Transactions on Power Apparatus and Systems PAS-103 (9), 2502-2518.

Mazur, V., Shao, X.M. and Krehbiel, P.R., 1998. "Spider" lightning in intracloud and positive cloud-to-ground flashes. Journal of Geophysical Research 103 (D16), 19,811-819,822.

McLain, D.K. and Uman, M.A., 1971. Exact expression and moment approximation for the electric field intensity of the lightning return stroke. Journal of Geophysical Research 76 (9), 2101-2105.

Murtha, J.B. and Skinner, W.H., 1999. Lightning detection apparatus and methodology, US patent 5.977,762.

Nanevicz, J.E., Vance, E.F. and Hamm, J.M., 1987. Observation of lightning in the frequency and time domains. Electromagnetics 7, 267-286.

Németh, B., Gulyás, A., Kiss, I. and Berta, I.,2008. Lightning protection of open air mass performances, 29th International Conference on Lightning Protection, Uppsala, Sweden.

Oh, L.L., 1969. Measured and calculated spectral amplitude distribution of lightning sferics. IEEE Transactions on Electromagnetic Compatibility EMC-11 (4), 125-130.

Ortéga, P., 2007. A three magnetic direction finder network for local warning device. Journal of Lightning Research 2, 18-27.

Ostrander, K.A., 1989. Multi-input lightning detection system, US patent 4,873,483.

Peckham, D.W., Uman, M.A. and Wilcox, C.E., 1984. Lightning phenomenology in the Tampa Bay area. Journal of Geophysical Research 89, 11,789-711,805.

Pierce, E.T., 1956. The influence of individual variations in field change due to lightning discharges upon design and performance of lightning flash counters. Archiv Meteirol. Geophys. Bioklimatol. A9, 78-86.

Pierce, E.T., 1977. Atmospherics and Radio Noise. In: Golde, R.H. (Ed.), Lightning. Volume 1. 351-384. Academic Press.

Popov, A.S., 1896. Instrument for detection and registration of electrical fluctuations. Journal or Russian Physics and Chemistry Society 28, 1-14.

Proctor, D.E., 1997. Lightning flashes with high origins. Journal of Geophysical Research 102 (D2), 1693-1706.

Rafalsky, V.A., Nickolaenko, A.P., Shvets, A.V. and Hayakawa, M., 1995. Location of lightning discharges from a single station. Journal of Geophysical Research 100 (D10), 20,829-820,838.

Sonnadara, U., Cooray, V. and Fernando, M., 2006. The lightning radiation field spectra of cloud flashes in the interval from 20 kHz to 20 MHz. IEEE Transactions on Electromagnetic Compatibility 48 (1), 234-239.

Stanford, J.L., 1971. Polarization of 500 kHz electromagnetic noise from thunderstorms: a new interpretation of existing data. Journal of the Atrmospheric Sciences 28, 116-119.

Taylor, W.L., 1973. Electromagnetic radiation from severe storms in Oklahoma during April 29-30, 1970. Journal of Geophysical Research 78, 8761-8777.

Thottappillil, R. and Rakov, V.A., 2001. On different approaches to calculating lightning electric fields. Journal of Geophysical Research 106 (D13), 14,191-114,205.

Tuomi, T.J. and Mäkelä, A., 2007. Lightning observations in Finland, 2007.

Weidman, C.D., Krider, E.P. and Uman, M.A., 1981. Lightning amplitude spectra in the interval from 100 kHz to 20 MHz. Geophysical Research Letters 8 (8), 931-934.

Weidman, C.D. and Krider, E.P., 1986. The amplitude spectra of lightning radioation fields in the interval from 1 to 20 MHz. Radio Science 21 (6), 964-970.

Willett, J.C., Bailey, J.C. and Krider, E.P., 1989. A class of unusual lightning electric field waveforms with very strong high-frequency radiation. Journal of Geophysical Research 94 (D13), 16,255-216,267.

Willett, J.C., Bailey, J.C., Leteinturier, C. and Krider, E.P., 1990. Lightning electromagnetic radiation field spectra in the interval from 0.2 to 20 MHz. Journal of Geophysical Research 95 (D12), 20,367-320,387.

Zonge, K.L. and Evans, W.H., 1966. Prestroke radiation from thunderclouds. Journal of Geophysical Research 71 (6), 1519-1523.

# APPENDIX: Detailed description of the narrowband devices

## Introduction

The text in this Appendix is based largely on design work done by co-authors Joni Jantunen, Tom Ahola, and Niko Porjo, with relatively minor input from the author. However, the details should be in the public domain, and therefore this information is included in summary form.

## Overall architecture

The measurement system design was driven by a need for (semi-)automated operation, high reliability, and reasonable data storage requirement. A schematic diagram is shown in Figure 1, and the location and physical setup of the measurements is shown in Figure 2.

Although the hardware setup was complex, the data output was relatively simple: the data capture computer (B) monitored the nine data channels continuously, calculating the long-term noise level. Data were only recorded on the PC when one of the channels received a signal whose intensity exceeded the baseline noise by a user-defined threshold (6 dB was empirically found to trigger on most flashes without triggering on man-made noise). The tenth channel received the pulse-per-second signal from the GPS (C), i.e. a pulse at the exact start of a UTC second. Since the PC was also kept synchronized with the GPS, and data files were time-stamped, it was possible with some manual effort to timestamp the signals with millisecond accuracy.

The tenth channel also received the trigger out from the wideband signal (E), so that any flash that triggered the oscilloscope could be directly compared to the narrowband signals and its UTC time recorded, again with millisecond accuracy. The electric field measurements (E) were stored separately. Because of long latency in storing the data due to the large file size, only a small fraction of occurring flashes were recorded. The system was kept running automatically throughout the summer, but it was operated manually during some storms.

The FireFace had the capability to include up to ten channels. In addition to the 1 MHz front-ends used in the thesis, the other channels were used to test different configurations of the hardware. In particular, operation at 100 kHz was tested. Qualitatively, at 100 kHz the return stroke dominated the signal more than at 1 MHz, and in-cloud contributions were weaker. However, the results have not yet been analyzed in detail and have not been published.

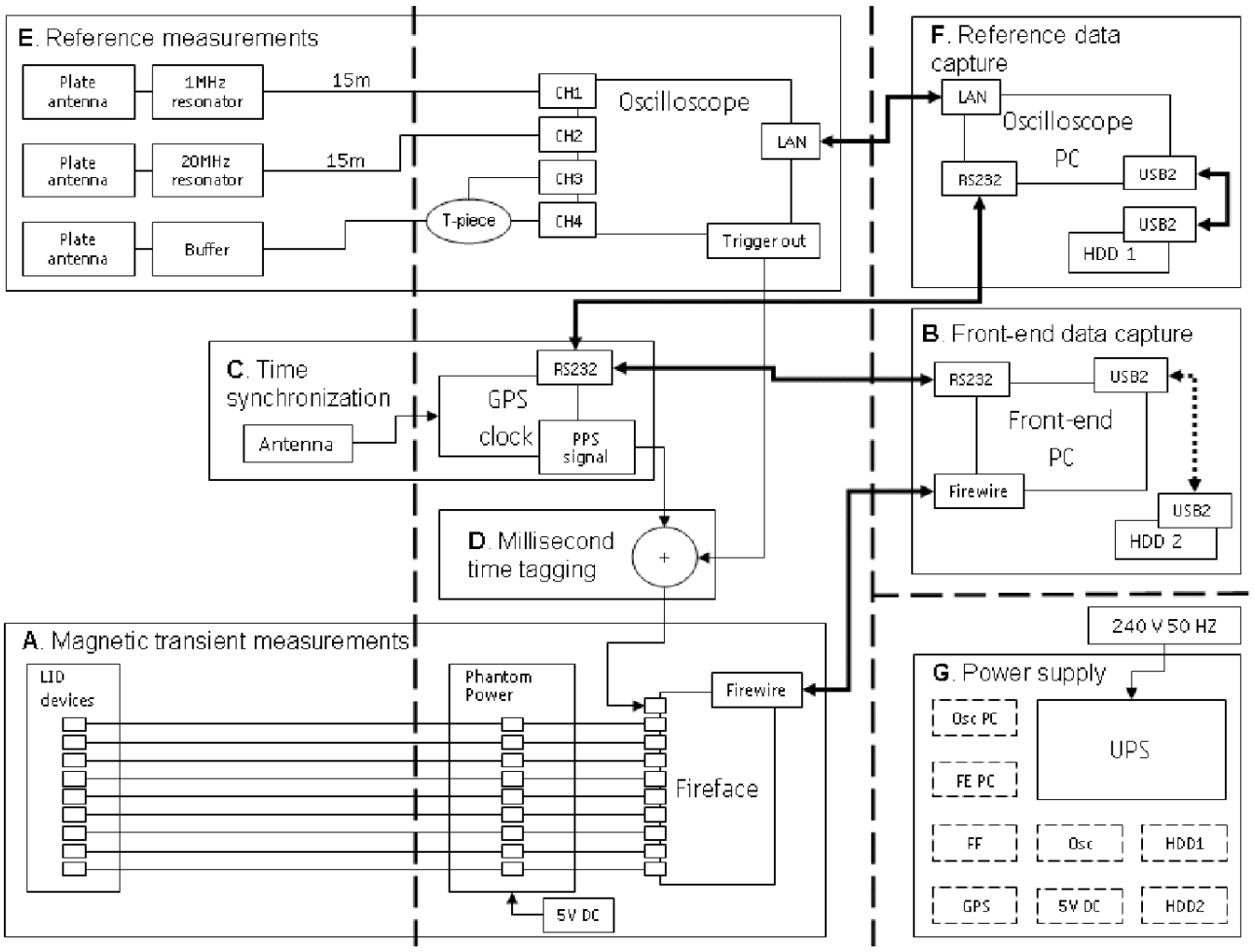


**Figure 1: Overall measurement setup for Papers II-IV. A) Nine front-end devices were attached to a FireFace sound card via a Phantom power system. The tenth channel received a GPS pulse-per-second signal overlaid on any trigger out signals from the oscilloscope. B) Data from the Fireface was stored an a PC; the PC clock was kept synchronized with the GPS. Software was written which only stored the data when the signal exceeded the noise floor by a user-defined relative threshold; in most of the measurements, the threshold was set to 6 dB. C) A GPS was used for the time synch, outputting a pulse-per-second signal on the start of every UTC second. D) The GPS signal and trigger out from the oscilloscope were summed. E) The reference measurements consisted of a broadband vertical electric field mesurement with flat plate antennas, as well as narrowband measurements of the electric field not used in this thesis due to high noise in the signal. The signals were captured by an Agilent oscilloscope set to trigger on rising edges in the broadband signal. The trigger out was then output via D. F) The broadband data were stored on a PC, with a latency time of several minutes due to a slow interface. G) The system was powered via a UPS. Diagram courtesy of Niko Porjo.**

**Figure 2: The setup in Jokioinen. The narrowband devices were kept in the large white box in the foreground. The electric field plate antennas are visible to the left. The electric field mill in the foreground was not used in the thesis. The hut in the background was an automated radiosonde sounding station of the Finnish Meteorological Institute, which did not cause measurable interference. No other potential sources of interference were located within at least 50 meters. Photo by author.**

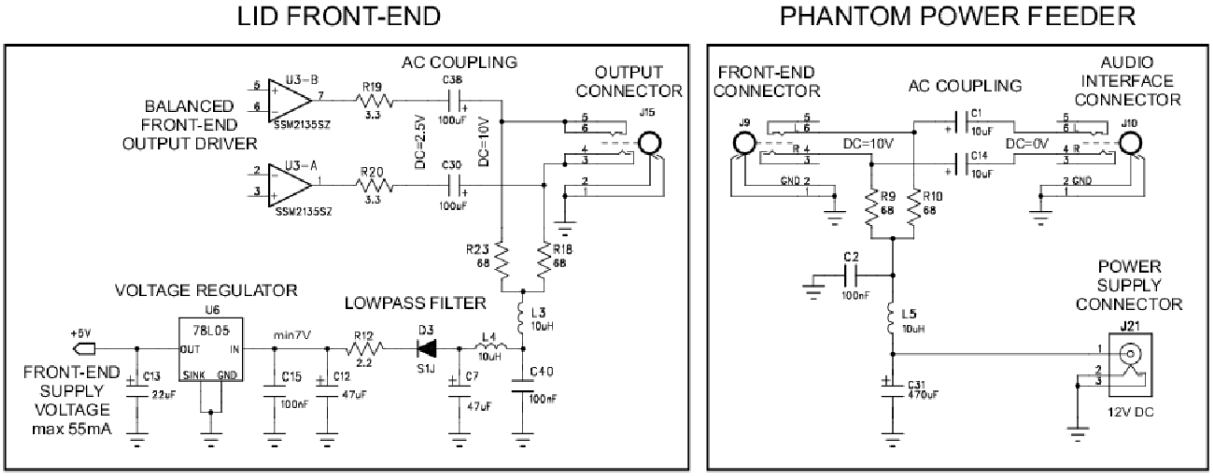


**Figure 3: Front-end and Phantom power feeder. LID (Lightning Detection) was the acronym used internally for the project.**

To avoid the need for separate power sources for the narrowband front-ends, the front-ends were powered by a Phantom circuit which fed the power to the boxes along the same lines as the data output (Figure 3). This is a commonly used technique for active microphones.

A schematic diagram of the narrowband front-ends is shown in Figure 4. Off-the-shelf standard components were used whenever possible (listed in Figure 4), except for the antennas which were manually made. The settings of the components were determined empirically.

The TLC082 low noise amplifier (LNA) was operated with a gain of $G=1$, i.e. no amplification at all. This was possible in part since the antennas were physically large in size (4 cm by 4 mm; see Figure 5) and therefore produced a sufficiently large voltage. The local oscillator frequency for the SA612A mixer was generated by using an AD9833 Direct Digital Synthesis (DDS) chip. The conversion gain of the SA612A mixer was about 16 dB.

The frequency of the local oscillator $f_{LO}$ was set to be about 20 kHz lower that the central frequency $f_c$ of the corresponding antenna. The antenna resonated as $exp(i\omega_c t)$, where $\omega=2\pi f$; when multiplied with the mixer signal it resonated as $exp[i(\omega_c \pm \omega_{LO})t]$. The signal was high-pass filtered and then low-pass filtered with the SSM2135 output buffer, filtering out the higher frequency. The effective bandwidth was then $f_c$-$f_{LO}$. The signal at this stage was still analog; the analog-digital (A/D) conversion was made in the FireFace. The data were then digitized at 44.1 kHz (a CD quality audio signal).

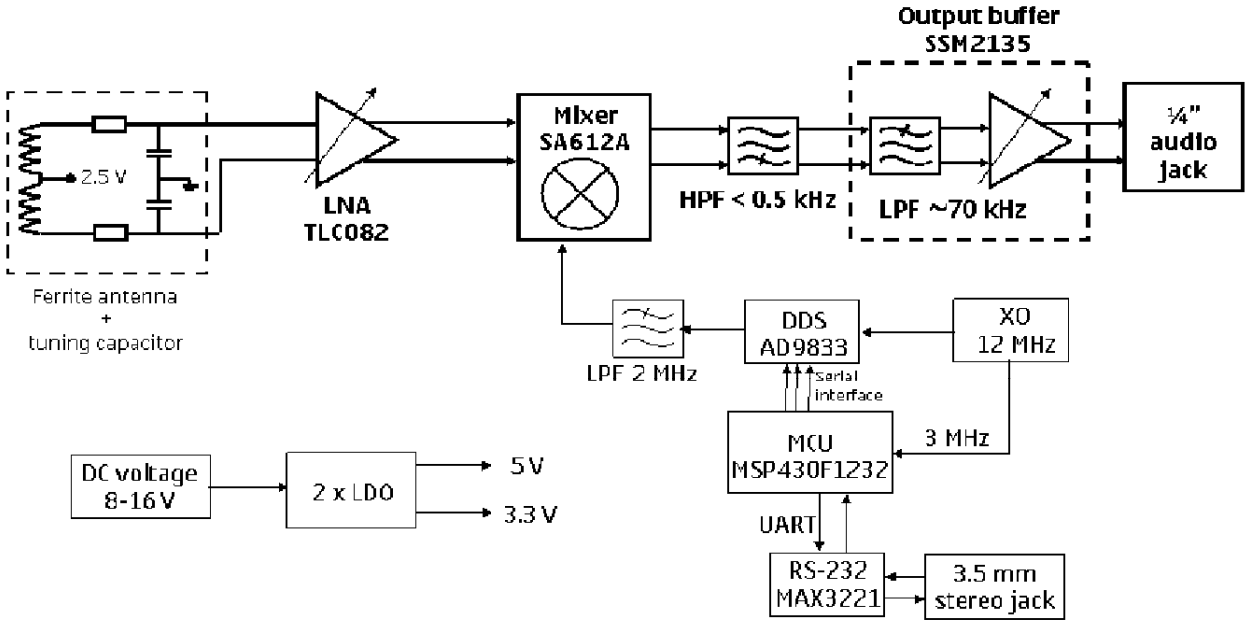


**Figure 4: Schematic of the front-end system. From Paper II.**

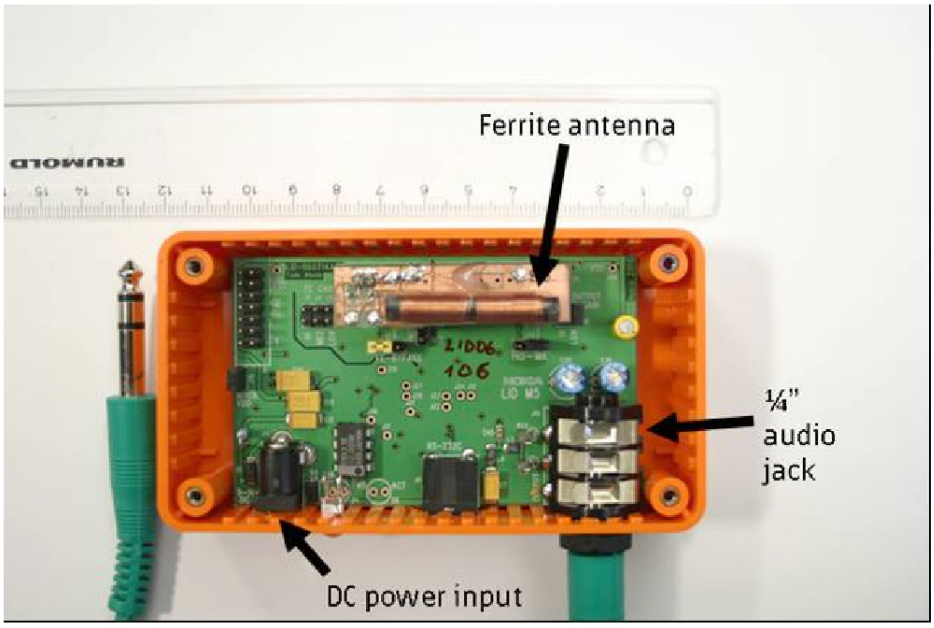


**Figure 5: Physical size of the narrowband devices. The antennas were 4 cm by 4 mm in size.**

## Antennae

The performance of the system was strongly affected by the antenna characteristics. The receiver coils were hand-wound around Fair-Rite ferrite cores. During the design phase, it was found that a center-tapped coil is much less sensitive to man-made interference than a dual-ended single coil. The exact reason for this is currently unclear, but is almost certainly related to the fact that a single coil can pick up electric field variations in the direction of the coil axis. In a center-tapped coil, any electric field contributions cancel out. Therefore a balanced antenna structure was used (Figure 6). The winding around the ferrite bar was split into two parts, and one end of each winding was connected to a 2.5 V bias voltage. Resonance capacitors were connected between ground and LNA inputs. Resistors were used to define the Q value of the whole antenna circuitry, and were located in the middle of the LC resonator branches.

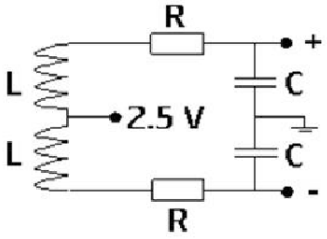


**Figure 6: Design of the center-tapped coil. The antennas of papers II-IV had center frequency of about 905 kHz, 100 turns per antenna (2x50), parallel capacitors 330 pF, and resistors 10 Ω. The resulting Q-value of the antennas was 30, equivalent to about 33 kHz bandwidth.**

There were a number of parameters which can be tuned to optimize the antenna. The resonance frequency $f_r$ for the coil antenna can be calculated from

$$f_r = \frac{1}{2\pi\sqrt{LC}} \qquad (1)$$

The inductance L for a ferrite-core coil is

$$L = \frac{10^{-4} 4\pi N^2 A \mu_{rod}}{l} \qquad (2)$$

where $N$ = number of turns, $A$ = cross-sectional area of ferrite core, $l$ = magnetic length of core, and $\mu_{rod}$ is the permeability of the ferrite material. As seen in Figure 5, the coils were wound only partway around the core, requiring a correction, where a and b are the length of the core and length of the coild respectively:

$$\mu' = \mu_{rod} * \sqrt[3]{a/b} \qquad (3)$$

The induced voltage by a en electric field E can then be calculated from

$$V = \frac{2\pi A N \mu' Q_L E}{\lambda} \qquad (4)$$

where $Q_L$ is the loaded Q value of the loop, $Q_L = f_r / W$, where $W$ in turn is the bandwidth. For a parallel resonant circuit, the loaded Q-value is given by $Q_L = \omega_r RC$. Thus, once the coil size and parameters were fixed, the bandwidth was adjusted by varying the resistance $R$ and capacitance $C$. The choice of bandwidth depended on the requirements of the rest of the system. As a practical design consideration, the bandwidth had to be wide enough to allow small variations in the local oscillator frequency due to e.g. temperature variations and other non-idealities. For the 1 MHz system, a Q-value of $Q_L = 30$ (equivalent to 33 kHz bandwidth) was empirically found to be a good compromise between the practical restrictions. (Note that the mixing stage narrowed this bandwidth further). The specific antennas used in papers II-IV had a center frequency of 905 kHz, 100 turns per antenna (2x50), parallel capacitors of 330 pF, and resistors of 10 Ω.

## System calibration and characterization

As discussed in the thesis, absolute calibration of the system was difficult because of non-linearities. In addition, creating a repeatable test signal was not trivial. The performance of the system without the antenna could be verified by feeding a known signal through the terminations of the coil with a signal generator. The front-end from the mixer stage onwards was characterized by measuring its response to a known signal. As seen in Figure 7, the mixer was very close to an ideal band-pass filter with bandwidth 40 kHz. The response was also consistent across all front-ends.

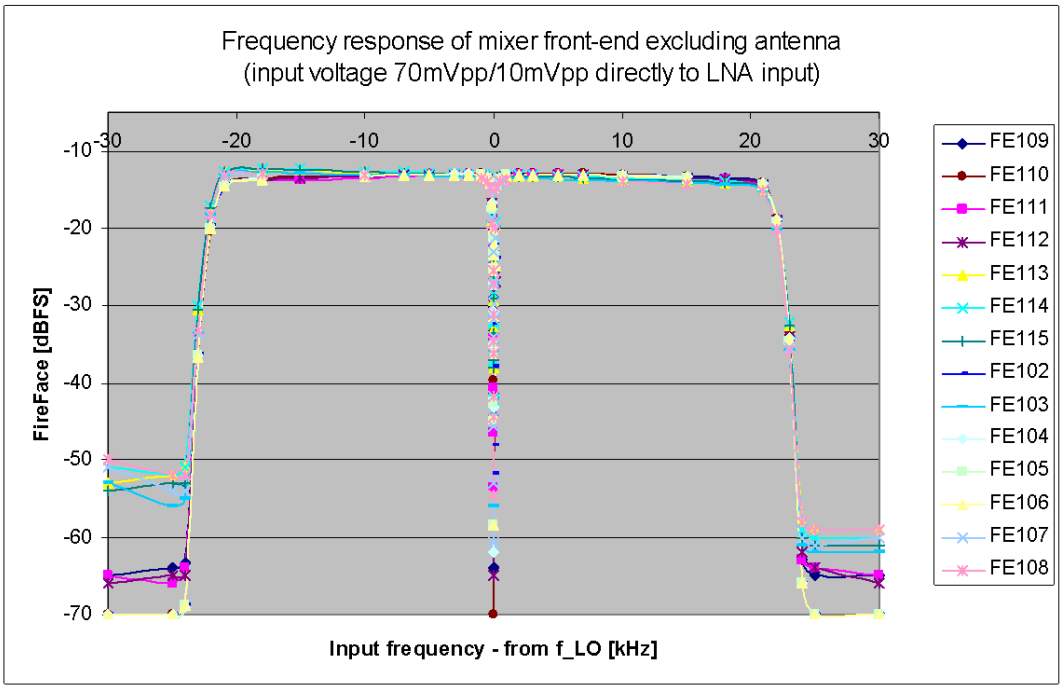


**Figure 7: Frequency response of the front-end, excluding effect of antenna. The local oscillator was set to oscillate at the center frequency of 1 MHz, and an input voltage of 70 mV peak-to-peak was fed into the terminations of the coil just before the LNA. The frequency of the input signal was then swept from 970 to 1030 MHz. The output from the Fireface was recorded and normalized to the maximum allowable output. The tests were repeated for a number of front-ends to ensure consistency and repeatability.**

The gain curve of the whole front-end and Fireface system is shown in Figure 8. Three different LNA gains were tested. Except for very large inputs, the gain was completely linear; since the lightning signals were never near saturation even for the closest flashes, no corrections had to be made. The final system response, with antenna included, is shown in Figure 10. The 3-dB bandwidth was approximately 30 kHz (with some asymmetry).

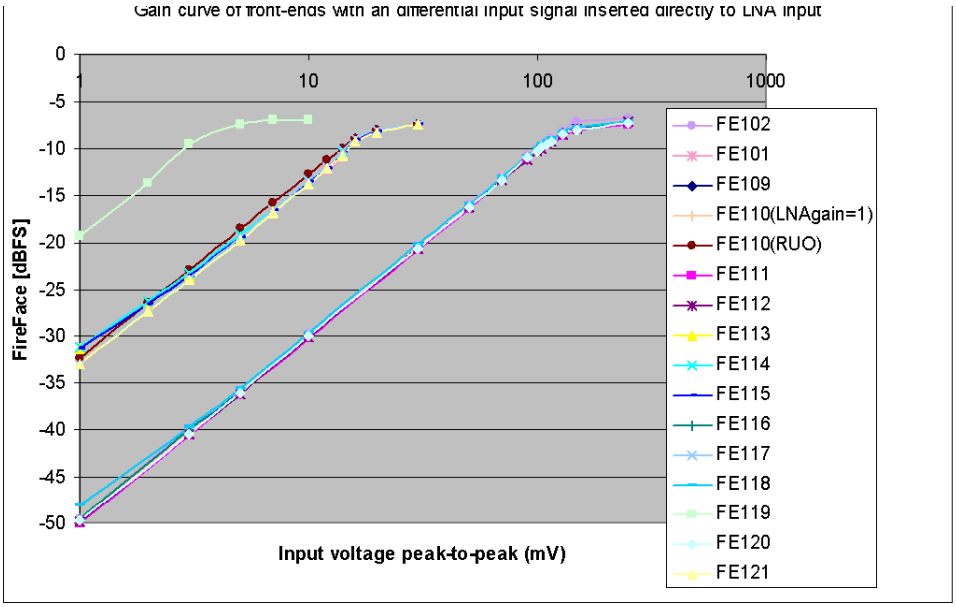


**Figure 8. Gain curves of front-ends for three gain settings, excluding the effect of the antenna. The local oscillator was set to oscillate at the center frequency of 1 MHz, and a 1MHz-signal was input through the terminations of the coil. The peak-to-peak voltage was then varied from 0 to 1000 mV. The output from the Fireface was recorded and normalized to the maximum allowable output. The tests were repeated for a number of front-ends to ensure consistency and repeatability, and for three different gain settings The output during the measurements almost never exceeded 300 mV, and therefore selecting the lowest gain setting (bottm curve) resulted in a linear response in all measurements.**

Verifying the performance of the system with the antenna included was not straightforward, as a repeatable magnetic field signal had to be generated. A one-off test system was therefore used by running a signal through a coil attached to a signal generator, with the front-ends held at a fixed distance from the coil (Figure 9). The same setup was used for all the measurements, and therefore the relative values are consistent.

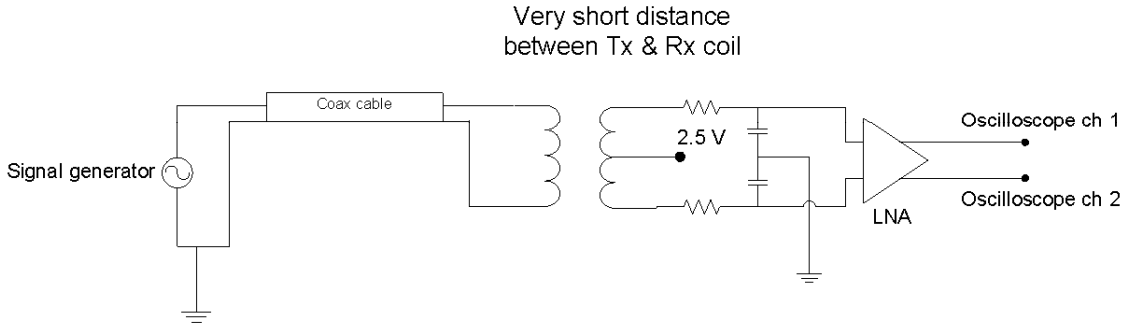


**Figure 9. Measurement set-up used for measuring resonance frequency of antenna and LNA.**

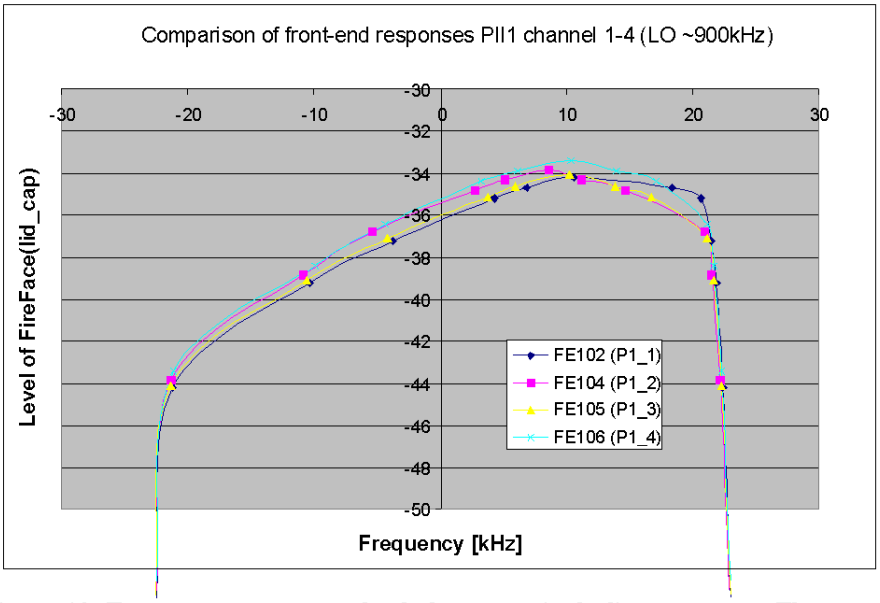


**Figure 10. Frequency response of whole system including antennas. The setup shown in Figure 7 was used to generate an identical magnetic field for all tests. The signal generator was swept from 970 to 1030 kHz, and the output from the Fireface was measured. The 3dB bandwidth was approximately 30 kHz for all fronet-ends.**

The directionality of the antennas was evaluated by driving a steady current through a large ferrite coil at a distance of 100 cm, turning the antenna around its axis, and measuring the output voltage. The curve is shown in Figure 11, overlaid on an ideal $cos^2(\theta)$ curve. The antennae displayed some distortion from the ideal. This is seen in Figure 12, where the sum of the two gains is shown as a function of angle. For an ideal pair antennas, the gain would be constant at any angle; obviously this is not so. The result could be empirically improved by e.g. using the RMS sum, but there is no theoretical justification for doing so. Thus, the direct sum was used in the thesis.

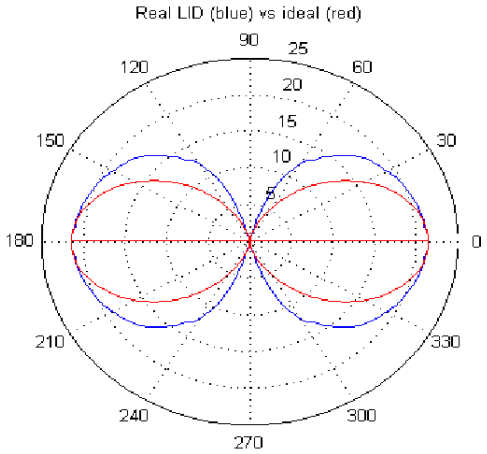


**Figure 11: Directionality curve of the antenna, shown in blue. The ideal $\cos^2(\theta)$ curve is shown in red, with the maximum of the ideal gain normalized to the maximum of the antenna gain. There is clearly some non-ideality in the used coils.**

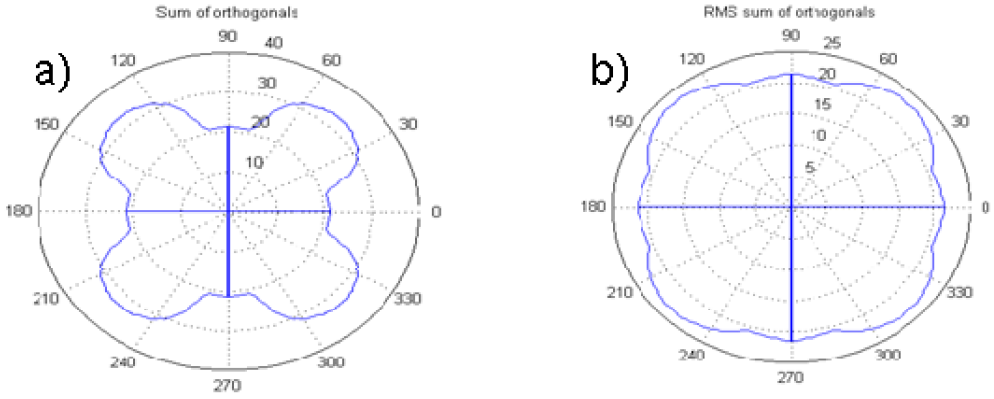


**Figure 12: Effect of non-ideality on gain curve of sum of two orthogonal coils. The radial values are in arbitrary units. A pair of ideal $\cos^2(\theta)$ coils would give a perfect circle. A) The direct sum gives a distorted gain curve. B) Using an RMS sum makes the gain more homogeneous. However, the direct sum was used in Papers II-IV.**